Laboratori per a la Innovació Tecnològica d'Estructures i Materials
UNIVERSITAT POLITÈCNICA DE CATALUNYA

Ph.D. Thesis

Analysis of unreinforced and TRM-strengthened brick masonry walls subjected to eccentric axial load

by

Ernest Bernat-Maso

Directed by:

Lluís Gil Espert
Pere Roca Fabregat

Tesi presentada per obtenir el títol de Doctor per la Universitat Politècnica de Catalunya

Programa de doctorat d'Anàlisis Estructural, Departament de Resistència de Materials i Estructures a l'Enginyeria

Escola Tècnica Superior d'Enginyeria Industrial i Aeronàutica de Terrassa. Universitat Politècnica de Catalunya, *BarcelonaTECH*

Terrassa, octubre de 2013

UNIVERSITAT POLITÈCNICA DE CATALUNYA
BARCELONATECH
Escola de Doctorat

Acta de qualificació de tesi doctoral

Curs acadèmic:

Nom i cognoms

Programa de doctorat

Unitat estructural responsable del programa

Resolució del Tribunal

Reunit el Tribunal designat a l'efecte, el doctorand / la doctoranda exposa el tema de la seva tesi doctoral titulada

_____

_____.

Acabada la lectura i després de donar resposta a les qüestions formulades pels membres titulars del tribunal, aquest atorga la qualificació:

☐ NO APTE ☐ APROVAT ☐ NOTABLE ☐ EXCEL·LENT

(Nom, cognoms i signatura) President/a	(Nom, cognoms i signatura) Secretari/ària

(Nom, cognoms i signatura) Vocal	(Nom, cognoms i signatura) Vocal	(Nom, cognoms i signatura) Vocal

_____, _____ d'/de _____ de _____

El resultat de l'escrutini dels vots emesos pels membres titulars del tribunal, efectuat per l'Escola de Doctorat, a instància de la Comissió de Doctorat de la UPC, atorga la MENCIÓ CUM LAUDE:

☐ SÍ ☐ NO

(Nom, cognoms i signatura) Presidenta de la Comissió de Doctorat	(Nom, cognoms i signatura) Secretària de la Comissió de Doctorat

Barcelona, _____ d'/de _____ de _____

Al meu fill Roc,

per posar aquest treball al seu lloc

Acknowledgements

I would like to thank all people who have helped in this research...

Firstly, special thanks to my parents without whose support this work would never had been possible to achieve, to my wife for her cheerful motivation and to the rest of my family who have been at my side along these years.

I wish to thanks my co-directors Professor Lluís Gil Espert and Professor Pere Roca Fabregat for their advice, insight and guide along the research process.

This work has been performed with the help of all my colleagues at the University. I would like to explicitly express my appreciation to Christian Escrig, Marco A. Pérez and Francesc Puigvert for their support and positivism.

Thanks to my friends for helping me to disconnect from this demanding job.

Finally, I would like to thanks the companies and institutions which have helped:

- Col·legi d'Enginyers de Camins Canals i Ports, for the economic support during the first research years.
- Ministerio de Ciencia e Innovación, for the economic support associated with the grant BIA. 2006-04127 which partially covered this research.
- Ruredil S.p.A. for providing the required material for the investigation.
- Mapei S.p.A. for providing the required material for the investigation.
- ETSEIAT for bringing the possibility of using the communal facilities during the experimental campaigns.

Abstract

A significant number of buildings are supported by load-bearing masonry walls. The preservation of these worldwide used structures is a sustainable alternative. However, there is little research about the structural response of these particular elements if compared with others like concrete or steels framed structures. Hence, a further study of the load-bearing masonry walls is necessary as a starting point for the preservation activities.

The load-bearing masonry walls are usually subjected to a vertical eccentric loading condition, which is related with their complex structural response. This response is characterised by the second-order bending effects due to the eccentricity of the load, the non-linear compressive response of the masonry and its almost negligible tensile strength. Thus, strengthening these walls, in order to increase their load-bearing capacity, is an interesting upgrading alternative to enhance their life-cycle.

In this thesis, an experimental campaign has been carried out. It consisted of hundreds of characterisation tests to obtain the mechanical properties of the component materials which have been used to build twenty-nine full-scale walls. Twenty of these walls were unreinforced and the other nine were TRM (Textile Reinforced Mortar) strengthened. All of them have been tested under eccentric compressive loading conditions. The analysis of the strengthened walls has allowed studying the influence of the strengthening mortar type on the load-bearing capacity. The effects using anchors or embedding different types of fibre grids have been also analysed.

A bidimensional (2D) simplified micro-model has been implemented to analyse these structural cases. This numerical tool has been validated using the data from the experimental campaign. Finally, analytical methodologies have been proposed to calculate the load-bearing capacity of unreinforced and TRM-strengthened brick masonry walls. Similarly, two current standards, Eurocode-6 and ACI-530 have been applied to the analysed cases and their results have been compared with the experimental ones.

The results show that the TRM provides a load-bearing capacity increase over 100% and homogenises the structural response, which becomes stiffer. Regarding the simulations, the proposed numerical model provides accurate results, which are better for the cases with larger slenderness or larger eccentricity of the applied load. Finally, the proposed analytical methods provide acceptable results, which are more accurate than the ones obtained by applying the formulations included in the analysed standards.

Keywords: Brick masonry walls; Second-order effects; Buckling; Textile Reinforced Mortar; Strengthening; Numerical simulation, Analytical study.

Resum

Un nombre significant d'edificis estan suportats per murs de càrrega d'obra de fàbrica. La preservació d'aquestes estructures que s'utilitzen arreu del món is una alternativa sostenible. No obstant això, hi ha molt poca recerca en relació a la resposta estructural d'aquests elements particulars si es compara amb altres com les estructures porticades d'acer o formigó. Per tant, és necessari un major estudi dels murs de càrrega d'obra de fàbrica com a punt de partida de les actuacions de preservació.

Normalment, els murs de càrrega estan subjectes a patrons de càrrega vertical excèntrica, cosa que està relacionada amb la seva resposta estructural complexa. Aquesta resposta es caracteritza pels efectes de flexió de segon ordre degut a l'excentricitat de la càrrega, per la resposta no linear a compressió de l'obra de fàbrica i per la seva, pràcticament negligible, resistència a tracció. Per tant, el reforç d'aquests murs, per tal d'augmentar-ne la seva capacitat resistent is una alternativa de millora interessant per allargar la seva vida útil.

En aquesta tesi s'ha dut a terme una campanya experimental. Aquesta ha consistit en centenars d'assaigs de caracterització de les propietats mecàniques dels materials components utilitzats per construir vint-i-nou murs. Nou d'aquests es van reforçar amb *Textile Reinforced Mortar*, TRM, i els altres vint van ser assajats sense reforç. Tots van ser sotmesos a compressió excèntrica. L'estudi dels murs reforçats ha permès analitzar la influència del tipus de morter de reforç, l'efecte de disposar ancoratges o la dependència de la capacitat resistent en el tipus de malla de fibra utilitzada.

S'ha implementat un micromodel simplificat bidimensional (2D) per analitzar els casos estructurals proposats. Aquesta eina numèrica ha estat validada utilitzant les dades de la campanya experimental. Finalment, s'han proposat mètodes analítics per calcular la capacitat portant dels murs sense reforç i dels reforçats amb TRM. De forma semblant, s'han aplicat dos normes actuals, l'Eurocodi-6 i l'ACI-530, als casos d'estudi per tal de comparar-ne els resultats amb els experimentals.

Els resultats mostren que el TRM aporta un augment de la capacitat resistent de més del 100% i homogeneïtza la resposta estructural que esdevé més rígida. En relació a les simulacions, el model numèric proposat obté resultats acurats, els quals són millors pels casos de major esveltesa o més excentricitat de la càrrega. Per acabar, els mètodes analítics que es proposen aporten resultats acceptables, els quals s'ajusten millor als experimentals que els obtinguts aplicant les formulacions de les normatives.

Paraules clau: Murs d'obra de fàbrica de maó; Efectes de segon ordre; Vinclament; Morter Reforçat amb teixits; Reforç; Simulació numèrica; Estudi analític.

LIST OF CONTENTS

LIST OF FIGURES

ANNEX A1

ANNEX A2

LIST OF TABLES

ANNEX A1

ANNEX A2

1

Introduction and objectives

1.1 Introduction

Masonry load-bearing walls are a common structural element which can be found in a large part of the buildings in-service nowadays. This essential structural member is characterised by its function and its material. Firstly, the main function is bearing vertical gravitational loads which are usually eccentrically applied on the thickness of the wall. This loading pattern causes lateral deformations due to the second order bending process which might be accentuated by the slenderness of the wall. Secondly, the constituent material, masonry, is characterised by its remarkable compressive strength, durability and isolation properties. However, the masonry shows an almost negligible tensile strength and a brittle failure.

In addition, most of the masonry load-bearing walls now in service were built before 1980's and need to be maintained, repaired or even strengthened to meet with the requirements of the current standards or to support new loads due to a change of the use of the building. The preservation of these structures, compared to their demolition and substitution, provides a more economical and environmentally sustainable alternative.

Thus, it is critical to understand the response of the load-bearing masonry walls, especially when these are eccentrically loaded with compressive loads. This loading case might cause a failure associated with mechanism formation because of the little tensile strength of the material and the expected lateral deformations due to the second order effects.

Strengthening the walls is a reasonable alternative for enhancing the life cycle of walls with insufficient load bearing capacity. Among all the strengthening alternatives, the Textile Reinforced Mortar (TRM) is the most promising system to retrofit and strengthen masonry structures because of its mechanical, chemical and physical compatibility with the substrate. However, TRM is a recent system and still needs

further structural characterisation oriented to test its applicability range and evaluate its performance. In addition, no national or international regulations have been yet produced on the use of TRM.

Looking at the researches carried out by other investigators it is noticed that masonry has not been studied to an extent comparable to other more modern materials like concrete or steel. Moreover, the available comprehensive research works on the load bearing capacity of masonry walls were performed around 50 years ago. An experimental investigation of the load-bearing capacity and response of the eccentrically loaded masonry walls using some of the now available experimental and numerical technologies is still to be carried out. This investigation would be oriented to update and complement the available data and to validate proposed numerical models.

Similarly to the case of the unreinforced masonry load-bearing walls, the TRM strengthened walls also need to be experimentally studied. Only a few experimental researches have been carried out on the application of this strengthening material and most of them were aimed to characterise the in-plane response against seismic or shear loading conditions. Finally, a calculation methodology for TRM strengthened masonry load-bearing walls is still lacking.

To sum up, masonry, as a material and structural typology, has not been comprehensively studied as others materials in spite of the large number of existing buildings having load-bearing masonry walls. In addition, new strengthening techniques are being used in these structures with no clear regulations and little experimental evidence. Therefore, it is necessary to update and improve the available information on the structural response of the load-bearing masonry walls. In particular, additional study and experimental evidence is needed for the case where the load is eccentrically applied because this case may provide the base for later on investigations on strengthening techniques and modelling approaches.

In the present research, an extensive experimental campaign is carried out to bring new information on the structural behaviour of unreinforced and TRM-strengthened load-bearing masonry walls. This new data, together with the exiting evidences in the bibliographic sources, is used to validate simple numerical models. These models are aimed to a sufficiently accurate characterization of the capacity of the walls. In addition, a simple approach based on the analytical formulations from the current standards and some generic formulae from the equilibrium and compatibility equations are used to estimate the capacity of the walls and compare the resulting values with those obtained experimentally and numerically.

1.2 Objectives

The main aim of this thesis is to contribute to the understanding of the structural response of unreinforced and strengthened masonry walls loaded with eccentrically applied compressive loads. This aim will be achieved by completing the following partial objectives.

1.2.1. Partial objectives

The following partial objectives are envisaged:

- Gathering information about
  - The experimental response of load-bearing unreinforced and strengthened masonry walls under eccentrically applied compressive loads.
  - The current formulation used in the codes to calculate the load-bearing capacity of masonry walls.
  - The numerical models developed in order to calculate the response of unreinforced and strengthened masonry load-bearing walls
- Proposing simplified analytical formulations to predict the response and the load-bearing capacity of unreinforced and TRM-strengthened masonry walls under eccentrically applied compressive loads. Comparing the results of these formulations with the experimental ones.
- Performing an experimental campaign on full-scale unreinforced and TRM-strengthened walls, consisting of:
  - Carrying out the required characterisation tests on the used materials in order to obtain the values of the main properties necessary to model this structural problem.
  - Defining the specimens to analyse different slenderness and eccentricities for the unreinforced walls.
  - Defining the TRM-strengthening configuration to analyse different types of fibres, types of mortars, number of fibre grids and the use of connectors.
  - Designing the test setup to accurately test the walls with no uncertainties about the boundary conditions.
  - Carrying out the tests to acquire information about the capacity and the vertical and horizontal deformation of the wall.
- Developing and validating a numerical model for the analysis of unreinforced masonry walls and TRM-strengthened walls.
- Comparing the experimental and numerical results with those from the current standards.

1.2.2. Scope and limitations

Although the aim of this thesis is to study the response of masonry walls under eccentric compressive loads, there are some limits to the scope of this work which should be mentioned. Only one loading patterns has been considered and a single masonry typology has been studied. Similarly, the TRM solutions tested are a part of the commercially available ones.

The analytical proposed method for calculating the unreinforced masonry walls is focused to accurately predict the load-bearing capacity of those walls which fails by mechanism formation associated to second

order bending effects. Similarly, the numerical models were developed using general purpose finite element software to ascertain wide availability to practitioners and other researchers resulting in a simple useful tool.

1.3 Methodology

The adopted research methodology has been determined, to large extent, by the experimental orientation of the thesis. The investigation procedure has consisted of the following aspects

a. Reviewing the relevant documentation regarding the experimental evidence on the structural response of load-bearing masonry walls under eccentrically applied compressive load. This review allowed noticing the knowledge gaps. The bibliographic research was carried out along all the investigation to detect the newest scientific publications in the field.

b. Taking into account the state of the knowledge at the beginning of the research and considering the available resources, the main objectives were defined, the research methodology was set out and the specific activities to achieve the particular goals were planned.

c. The experimental research was defined and planned. Two different campaigns were planned. The first one was oriented to the study of the effect of the slenderness and the eccentricity of the applied load on the load-bearing capacity of unreinforced brickwork walls. The second one focused on the analysis of the performance of different TRM-strengthening configurations to assess the influence of the type of fibres, the type of mortar, the number of fibre grids included and the use of connection elements.

d. For each experimental campaign, characterisation tests of the materials were planned.

e. The implementation of the numerical models and the theoretical formulations was done in parallel with the experimental campaign although its validation was performed using the obtained experimental evidences as comparison elements.

f. The calculation results obtained by applying some of the current standards were compared with all previous results in order to assess the accuracy of the methods proposed by the standards.

g. Finally, further research lines were defined. The data obtained during the research which actually pointed out the next knowledge gaps to be covered.

1.4 Contents

The thesis document is organised in six chapters and two annexes. The contents of each section is detailed next

Chapter 1. Introduction and objectives

This first chapter summarises the introductory elements of the thesis document. Firstly, a general introduction is included to present and justify the study topic taking into account the state of the knowledge. Then, the main aim is set to focus the investigation line. The partial objectives, which are used as a guide and checking elements of the progress of the research, are defined too. Finally, the used procedure to carry out the work is presented as a descriptive methodology and the contents of the document are detailed.

Chapter 2. State of the art

This second chapter presents the most significant researches that might help a better understanding of the structural response of load-bearing masonry walls and the strengthening possibilities. It is aimed to draw a general picture of the state of the art which provides the initial context for the reader of this thesis. A brief historical review of the use of masonry leads to present the main characteristics of its mechanical response, the load-bearing walls as a relevant structural element and the associated strengthening requirements. The main bibliographic references are divided in three parts: experimental evidences, standards and analytical formulations, and numerical tools. The unreinforced and strengthened cases are included in each part.

Chapter 3. Experimental campaign

This third chapter gathers all the experimental evidences of the current research. This key stone of the document is divided in two main parts. The first one is oriented to present the characterisation tests of the materials and their results whilst the second one is focused on the tests performed on full-scale walls. The samples production, the used test setups and the obtained results are briefly described. Special attention is paid to the application of TRM strengthening system and the design, production and testing procedure of the walls. There is not presented all obtained data which can be found in the first annex.

Chapter 4. Finite element analysis

The implemented numerical model is presented in the first section of this fourth chapter. To describe this calculation tool the following information is provided: the geometric modelling process, the material definition, the contacts definition, the meshing process, the loading procedure and boundary conditions and the general data post-processing procedure.

The second part of the chapter is focused on the validation of the model, the comparison with the experimental results and the application of this model to calculate theoretical cases enhancing the available information.

Chapter 5. Analytical approach

This part of the thesis presents some analytic methodologies to calculate the load bearing capacity of the walls. It is clearly divided in two parts. The first one describes the analytical tools which have been applied for predicting the capacity of the unreinforced brickwork walls – Eurocode-6 and ACI-530 formulations, theoretical 2nd order bending deformation calculus in comparison with a simplified section strength criterion and Southwell plot method – and the obtained results. The second part is focused on the TRM-strengthened walls and only two methodologies were considered and their results presented: the Southwell plot method and a section strength criterion.

Chapter 6. Conclusions and further research

This last chapter presents the general conclusions of the thesis which are based on the particular conclusions corresponding with each specific task. Further research topics are defined by taking into account the lacks observed during the current investigation.

Annex 1. Experimental data annex

This annex presents all the experimental information obtained in the current research. This means all the testing procedures, the detailed description of the specimens and test setups, and the structural response of each wall.

Annex 2. Finite Element Analysis data annex

This annex shows the results obtained with the finite element analysis implemented and summarises the input data used for each wall. The vertical and lateral deformations, the vertical stress distribution and the response of the contacts are analysed for each wall.

2

State of the Art

2.1 Introduction

The current state of the art in the structural analysis of unreinforced and strengthened load-bearing masonry walls under in plane eccentric load is presented in this section. A review of the experimental, numerical and analytical approaches, which have been used to study this structural problem, is presented after an introduction to the main characteristics of the masonry.

First of all, this chapter includes a general explanation on the mechanical characteristics of the masonry and how these have influenced on the historical application of this material. This review is focused on the study of the brick masonry response under compressive and flexural loads. Afterwards, load-bearing walls are presented as the most common structural element made of masonry in use nowadays. The loading conditions and the strengthening requirements and possibilities for this type of structures are summarised later on.

The literature research on the analysed structural problem comprises three study areas: reviewing the experimental campaigns which have been carried out, presenting the state-of-the-art on the application of the finite element analysis on this problem and analysing the recommended approaches included in standards and codes.

2.2 Masonry description, evolution, typologies and strengthening systems

This section of the chapter is focused on presenting the basis used to define the current research. Firstly, the masonry is studied from different perspectives: historical use and mechanical properties. Then, the load-bearing masonry walls are introduced and their structural handicaps and requirements are pointed

out. Finally, different strengthening options for masonry structures are described in the last section. Among them, the Textile Reinforced Mortar (TRM) is highlighted as the most promising one.

2.2.1. Historical perspective

Masonry has been one of the most used building materials throughout history. In fact, the first use of masonry might date back to 15000 years [1]. However, the first known city with masonry structures dates from approximately 4000 b.C. and it was located in Anatolia. The masonry technology has evolved from the first dry stone piling to the current industrialised masonry elements. For example, the load-bearing brick masonry walls, which are the most extended application of the masonry, were commonly used with structural purposes until the first half of the 20th century and most of them are still in service.

At the first development stages, walls and piers were commonly built using masonry. This application took advantage of the masonry's high compressive strength because these elements were usually compressed when they bore gravity loads. The wall was the most widespread structural element back then. Roofs were usually made of wood and only short lintels were built with large stone pieces (see the Parthenon in Figure 2.1).

With the technical evolution, the masonry's use became more effective and buildings' shapes were adapted to make the most of the characteristics of this material (low or negligible tensile strength and high compressive strength). The design of the buildings intended to assure that all the masonry elements were compressed under the usual loading conditions. Arches, vaults and domes were progressively developed. This optimisation of the structural design resulted in the construction of the exceptional Gothic cathedrals (see the second picture in Figure 2.1). In addition, the brick masonry gradually replaced the stone masonry because of economic reasons. In the 19th century, the brick masonry was widespread as a common building material.

Parthenon, Greece

Steve Swayne, Wikimedia

Sta. Maria del Mar, Spain

Reinforced masonry

Wikimedia

Figure 2.1 Masonry evolution. From a framed construction in ancient Greece to a gothic cathedral to go back to the framed usual structures nowadays

However, the industrial production of steel and reinforced concrete, which can bear tensile forces, allowed using these materials to cover large spans and the structural design went back to framed

structures. Using beams and columns in the construction of new buildings is a common practice nowadays. In addition, these building typologies are cheaper than the masonry structures. This is one of the reasons which might explain the decreasing use of brick masonry during the last decades of the 20th century.

The current masonry elements are regular walls used as load-bearing walls, which are part of a larger framed structure, or as partitioning elements. These applications might be qualified as a technical regression of the use of masonry because it is likely that tensile stresses appear under some loading conditions: wind, earthquakes, transmission of bending moments from horizontal structures, etc. Because of this, strengthening masonry walls, with the aim of increasing the tensile strength of the masonry and enhancing the resistance of the walls, might be required in several cases.

2.2.2. Mechanical response of the masonry

Masonry might be considered a composite material composed of pieces (generally stones, blocks or bricks) which are bound together with a mortar. These pieces are assembled following a geometric pattern and the mortar is usually casted in-situ. In some cases, essentially ancient masonry, it is also possible to leave the joints dry, with no mortar. Finally, including steel reinforcement bars inside the masonry improves the tensile strength of this composite. The resulting material is called reinforced masonry.

As can be noticed, the concept “masonry” is broad. However, the current research is limited to a single typology of masonry. The brick masonry used in most of the buildings in Barcelona’s area has been chosen to carry out the research.

The mechanical response of the masonry under different loading conditions- has been studied by other authors. In addition, the possible failure modes associated with this material’s collapse have already been described: masonry crushing under compressive stresses, tensile or flexural failure of the joints between the mortar and the pieces, joint sliding associated with the application of shear forces or the simultaneous failure of the joints and the pieces observed in biaxial in-plane loading conditions. The most likely failure modes for compressed load-bearing walls, which are the most extended structural typology, are the masonry crushing and the tensile failure at horizontal mortar joints.

The crushing’s main cause is the difference between the stiffness of the pieces and the stiffness of the joint material. In fact, the lateral strain of the joint material, which is due to the Poisson’s effect, causes tensile stresses on the fragile pieces which suddenly, break. This failure mode is characterised by showing cracks which are oriented parallel to the main compressive load (see Figure 2.2). The compressive strength of the masonry is associated with this failure mode and several parameters might influence this variable. For example, by increasing the compressive strength of the mortar, the compressive strength of the pieces, the tensile strength of the pieces or the mortar stiffness, the strength of the resulting masonry is increased. Reducing the mortar thickness might also increase the compressive strength of the masonry. In

contrast, when reducing the adherence between the mortar and the pieces, the compressive strength of the masonry is reduced.

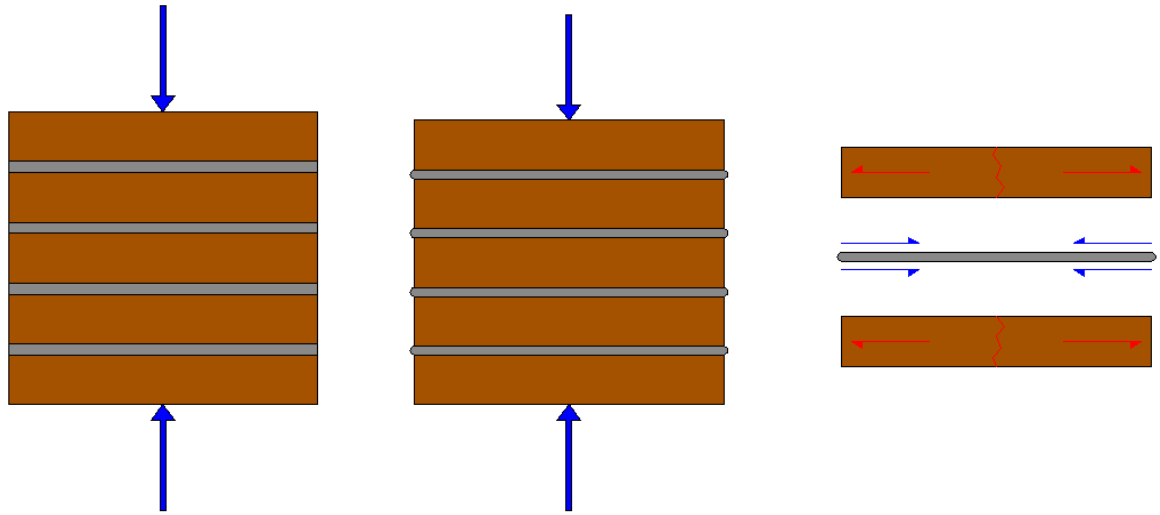

Figure 2.2 Compressive response of the masonry

The tensile failure of the masonry usually affects the joints. Two possible failure patterns are documented: the tensile failure of the joint material and the adherence failure between the mortar of the joint and the piece. This second failure pattern, which is related with the properties of the mortar-piece interface, is the most common for the commonly used mortars and pieces.

Thus, knowing the main properties of the two component materials as well as the mechanical properties of the interface between them is necessary to completely define the mechanical response of the masonry. Several researches have been carried out with the aim of characterising this complex material for different configurations and loading conditions. Among them, it is worth remarking two works which analysed the size effects on the mechanical response of the masonry: the research by Page [2], which studied the influence of the brick's size on the compressive strength of the masonry, and the work by Lourenço et al. [3], who analysed the size effect on the out-of-plane response of the masonry and the tensile behaviour of this material [4]. Moreover, this out-of-plane response was also studied by Sinha et al. [5] and Van der Pluijm [6], who also considered the shear effects in a previous work [7]. This complex characterisation of the masonry under bending and shear forces was also a research subject for Gazzola et al. [8] and Reyes et al. [9]. All these researches remarked the possible influence of the building procedures on the masonry response. In fact, the work by Maurenbrecher [10–12] studied this dependence on the production methodology. In addition, Maurenbrecher also analysed the influence of the load's eccentricity on the compressive strength and the Young's modulus of the masonry. This influence of the boundary conditions on the structural response of the masonry was studied by other researchers, like Roca et al. [13], who focused their investigation on the masonry as a part of different structures. Finally, a general description of the masonry's mechanical characteristics was presented by Tassios [14] and Molins [15], this last one more focused on historical materials, who remarked the significant scattering of the

masonry's properties. Thus, the literature review has shown that the mechanical response of the masonry has been analysed in a comprehensive way by the researches carried out to date.

These experimental researches have been complemented by the proposal of analytical methods and numerical models to represent the mechanical response of the masonry. Among the wide range of analytical models, it is worth highlighting some of them. It is the case of the work by Yokel [16], who proposed a simple failure criterion based on the principles of elasticity. This early analytical formulation evolved with the years resulting in more complex models, like the one presented by de Falco et al. [17,18], who proposed an analytical formulation for the masonry failure criterion which took into account the plastic response of this material. This non-linear compressive response of the masonry has been also modelled with a parabolic strain-stress relationship. It is the case of the analytical formulation used by Mura [19]. Finally, some authors have dealt with the analytic modelling of the reinforced masonry. The research of Chen et al. [20], who analysed the moment/thrust interaction diagrams for reinforced masonry, is a good example. Thus, these representative examples are just a part of the wide range of analytical proposals which can be found in the literature review. The analytical formulations aimed to study full walls, including the ones included in codes and standards are analysed with more detail in section 2.3.2.

According with the literature review, there are two main methodologies for the numerical modelling of the mechanical response of the masonry: the macromodelling and the micromodelling. Both are analysed in subsection 2.3.3, which includes detailed literature references, but a brief initial description is presented here with the aim of completing the general description of the different approaches used to represent the mechanical response of this material. The macromodelling technique is based on representing the masonry as a homogeneous material. This approach is useful at calculating large structures but it is difficult to correctly define the required constitutive equations and failure criteria. The first macromodels date from early 80's. Some relevant examples of macromodels are presented in the works by Samarashinge [21], Dhansekor et al. [22] or Rots [23]. Thirty years later, the definition of the homogenised properties of the masonry is still a research subject. Along this time, several micromodels have been used to obtain homogenised properties of the masonry from the properties of the component materials and taking into account different loading conditions. This is the case of the works carried out by Pande et al. [24], Lourenço [25–27], López et al. [28], Andreaus [29], Zucchini [30], Mistler at al. [31], Cecchi et al. [32,33], Salerno et al. [34] and Sacco et al. [35].

In contrast with the macromodelling, the micromodels consider the masonry components (bricks and mortar joints) separately and, according with the literature review, there are two different levels of micromodelling: the simplified micromodelling and the detailed micromodelling. The first one uses "equivalent" pieces with homogeneous properties, which usually represent the compressive response of the masonry, and contact interface elements with no thickness, which usually control the tensile and shear response. By contrast, the detailed micromodelling represents the pieces, the mortar joints and the

contacts between these two phases separately. Some significant micromodels used to represent the masonry response are the ones proposed by Page [36], Ali et al. [37], Lourenço [38], Ainsworth et al. [39], Orduña et al. [40] and Aref et al. [41]. The review of the literature has shown that micromodels are not suitable for calculating large structures because of its computational cost. However, this modelling technique is more accurate than the macromodelling at predicting the masonry response.

2.2.3. Strengthening options. Textile Reinforced Mortar

The negligible tensile strength of the masonry can be increased, when fabricating this material, by reinforcing it or, after the masonry is built and the structure in service, by applying strengthening techniques. Both reinforcing and strengthening are aimed to provide the tensile strength that the masonry requires in some cases.

The masonry reinforcing techniques that use fibres are as old as masonry itself. In fact, the first adobe walls had vegetal fibres embedded. These fibres provided a small tensile strength, which would enhance the properties of the structure, especially against wind and earthquake. As years went by, the technological evolution of the masonry resulted in the arrival of shape resistant structures (arches, vaults...) and the dry joint construction. These building techniques, which used discontinuous pieces, did not allow using embedded reinforcing fibres. Consequently, the reinforcing fibres were replaced by strengthening iron chains, plates and bars, which were mechanically attached to the masonry structure. The application of these strengthening elements originated significant problems. These were related with the irreversibility of this strengthening methodology, the mechanical incompatibility between these different materials and the durability problems of the iron. In some cases up to the 19th century, these metallic bars were embedded into the masonry joints from the first construction steps. This was an early reinforcing technique which has evolved. Eladio Dieste was one of the most significant practitioners who used reinforced masonry [42]. Nowadays, this methodology has been industrialised and adapted to plain walls made of blocks. The resulting material, which is known as reinforced masonry, is commonly applied in seismic areas and its use is regulated by various codes, for example [43,44]. Some state-of-the-art applications of the reinforced masonry might be the systems Allwall® and Flexbrick®. It has to be remarked that these techniques are reinforcing methodologies which cannot be easily applied to strengthen existing masonry structures.

In the last decades, two main techniques have been widely used for upgrading the existing masonry walls: attaching steel profiles or steel plates to the masonry wall and placing a ferrocement layer on the wall's surface. Ferrocement consists of an electrowleded steel grid embedded into a microconcrete layer. This microconcrete is bonded to the masonry and it transmits the forces from the masonry surface to the strengthening steel grid. Similarly nowadays, there are two main strengthening techniques for masonry walls that show some analogy with the previous technologies. One of the systems consists of bonding a high performance composite material on the masonry surface using chemical adhesives. In this case, the

strengthening material is a Fibre Reinforced Polymer, FRP, instead of steel elements, which were previously used to strengthen masonry structures. The other current strengthening technology is composed of an inorganic matrix and a fibre grid placed inside it. This system, called Textile Reinforced Mortar, TRM, is similar to the ferrocement option.

Before analysing these two popular techniques (FRP and TRM), it is worth mentioning the current alternatives. In particular, Sathipara [45] proposed using plastic bands to improve the tensile strength of the masonry and Maalej et al. presented a structural rendering called Engineered Cementitious Composites (ECC) [46], which showed promising results against blast and impact loads. Finally, Blanksvärd [47] compared the TRM performance with two other systems called Fibre Reinforced Concrete (FRC) and Mineral Based Composites (MBC).

The FRP is a composite material composed of high performance fibres embedded into a matrix made of organic resin, which is usually an epoxy resin. The most common fibres used in the FRP production are glass and carbon fibres. The FRP strengthening system can be applied in four different ways on masonry walls: (a) bonding a precured FRP laminate using an additional adhesive based on epoxy resins; (b) inserting a precured FRP bar into a masonry joint and bonding it with epoxy adhesive (called Near Surface Mounted, NSM technique); (c) inserting precured FRP bars across the masonry to stitch cracks using epoxy adhesive; (d) and curing the FRP on the masonry surface to be strengthened so no additional adhesive is necessary. This last technique is called wet application of the FRP and it is not commonly used.

The TRM, or Textile Reinforced Mortar, is a technological solution consisting of embedding a fibre grid into an inorganic matrix (usually a mortar). The strengthening grid can be made of almost any high performance fibre: glass, carbon, basalt, steel wires or vegetal fibres. The only requirement is assuring a perfect bonding between the fibres and the strengthening mortar used as a matrix. The grid-mortar adherence relies in two properties: the chemical affinity between the grid and the mortar (which also assures the durability), and the grid geometry, whose gaps must allow the mortar penetrating across the grid in order to achieve a good mechanical anchorage. Thus, less mortar will penetrate across the small gaps causing a lower grid-mortar adherence. In contrast, as more fibres are included in the TRM, a larger tensile strength of the TRM will be obtained. The first aim of the mortar is transmitting the loads from the masonry surface to the fibre grid, which is the material that is supposed to bring the tensile strength. In addition, the mortar layer offers protection to the grid against the environmental conditions. This component of the TRM might consist of any inorganic matrix, although it is usually composed of Portland cement or lime mortar. The mortars used to produce TRM are specifically developed for this use and have especial additions, so that each mortar is oriented to be applied with a specific fibre grid, which may be uni or bidirectional.

Both strengthening techniques, TRM and FRP, might fail in three different ways: (a) debonding from the masonry surface because of insufficient adherence; (b) superficial masonry failure, which is associated with a peeling phenomenon. The original cause of this failure pattern is that the masonry surface cannot withstand the tensile stresses transmitted by the TRM. And the last failure pattern (c) shows when the fibres inside the TRM or FRP reach their maximum tensile strength. This last failure mode needs a strong adherence between the strengthening systems and the masonry and between the matrix and the fibres in order to be likely.

Some researches comparing these two strengthening methods (TRM and FRP) have been carried out and are published. Among them, the work of Papanicolaou et al. [48] is particularly interesting for the description of TRM and its comparison with other strengthening systems like FRP (Fibre Reinforced Polymer) or NSM (Near Surface Mounted) FRP laminates. Similarly, Hamed and Rabinovitch's study [49] also provides a good experimental comparison between TRM and FRP.

FRP was firstly oriented to repair and upgrade concrete structures. The satisfactory results obtained on concrete structures motivated its later application to masonry and several specific researches were carried out since the early 90's (see for instance [50–53]). However, some of these researches detected possible problems concerning the application of FRP to masonry elements. These problems are mostly due to the use of organic resins in both the production of the FRP laminates and their bonding with the masonry substrate [50]. Some of these drawbacks are: (a) the negligible vapour permeability of the resins, which might alter the hygrometric equilibrium of masonry with its environment; (b) the extremely large difference of stiffness between masonry and FRP, which can lead to overloading the connection areas; (c) the loss of strength of epoxy resins at temperatures above 150°C-200°C (glass transition temperature); and (d) some practical application problems like the dangerous manipulation of toxic products, the non-applicability on wet surfaces or at low temperatures and the difficult adaptability to special shapes and geometries if using precured laminates. Because of these problems, there has been significant research on alternative reinforcing methods and materials.

Like FRP, TRM was initially developed to be applied on strengthening reinforced concrete structures (see [47,54–56]) but it has recently gained popularity as a way to overcome the problems of FRP in the application to masonry. Hence, an important part of the research about TRM has been oriented to study its use as a suitable strengthening material for masonry. TRM has been applied to masonry arches (see the work of Garmendia et al. [57]) and walls. For example, Augenti [58] analysed the in-plane lateral response of TRM strengthened masonry walls and Papanicolaou et al. [59] studied the effectiveness of this strengthening system against seismic loads. The comprehensive work of Papanicolaou et al. was based on their first studies, [48,60], which presented the TRM as the most suitable solution for strengthening masonry elements subjected to shear or out-of-plane loading conditions. According to Velazquez-Dimas et al. [61], this last loading condition is the most critical one for the structural safety of masonry walls.

However, the TRM strengthening technique has also drawbacks. The two main technical problems are the time-consumption, mostly associated with the long time required for the mortar to cure, and the smaller stiffness of the TRM, which is more deformable than FRP or steel plates. Thus, if the strengthening intervention is aimed to reduce the deformability of the structure, FRP might be more efficient than TRM. The other weaknesses are related with the little research carried out about TRM and its early development stage. Because of this, there is neither an international code nor internationally accepted guidelines. In addition, there is a remarkable lack of TRM's producers which agrees with the fact that there is also a lack of experienced people to apply this strengthening technology. Nevertheless, these last problems, which are related with the technologic development of TRM, are supposed to be overcome when the use of this technique becomes generalised.

2.3 Masonry brickwork walls eccentrically loaded with compressive loads

This section is focused on reviewing the state of the art about unreinforced and strengthened load-bearing brick masonry walls under eccentric compressive loads. First of all, a literature review about the experimental studies related with the current research is presented. Then, the most significant legal codes and analytical formulations are referenced and briefly commented. Finally, the most relevant methods proposed for numerical analyses are listed and briefly discussed as a frame reference for the numerical proposal of this research.

2.3.1. Experimental research on masonry walls

The first significant and extensive experimental researches on masonry walls subjected to eccentric compressive loads were performed in the 1960s. Before these, only a few studies were carried out on the matter. This is the case of the work by Lewicki et al. summarised in [62]. This document includes the material characterisation, the test setup and some calculation methods used by the authors.

The comprehensive work of Kukulsy and Lugez [63] was focused on concrete walls. However, this investigation has to be referenced because its experimental results were used as the basis for the formulation of the current European masonry standard (Eurocode-6 [64]). A few years later, in 1969, the huge experimental work carried out by Gross et al. in the Brick Institute of America, was presented as a recommendation summary [65]. This research comprised the characterisation of the component materials of the brick masonry and the testing of hundreds of brick masonry walls and columns with different eccentricities, slenderness and boundary conditions under vertical compressive load. One of the most remarkable reviewing tasks about the experimental campaigns, which were performed up to the 1960's, was presented in 1964 by Cassinello [66]. However, some of the cases reported in this work lack basic information about the boundary conditions or the properties of the component materials that would be necessary for the comparison with other experiments or for the validation of numerical models.

In the 1970's, the research on eccentrically compressed masonry walls continued. The two most significant experimental works of this decade were presented by Watstein and Allen [67] and Grave and Motteu [68]. The first one was carried out in the Structural Clay Products Institute with the aim of developing high adherence mortars. This particular study analysed the influence of the wall's slenderness ratio and the eccentricity of the applied load on the ultimate capacity of high-bond mortar (HB mortar) and common mortar brick masonry walls. The test setup defined a pinned-pinned configuration with no eccentricity at the lower support. Moreover, as opposite to other research works carried out during the same period, Watstein and Allen took care of measuring the lateral deformation of the walls tested. Years later, in 1991, a similar investigation was presented by Kirstchig and Anstötz [69]. This last study considered common Portland mortar and the same eccentricity at both wall's ends, which were also hinged. Different eccentricities, slenderness and masonry typologies were considered in [69]. Grave and Motteu [68] presented an experimental campaign which was focused on characterising the influence of using different types of pieces (solid bricks and blocks) in the production of structural masonry. Compression tests of masonry walls with different slenderness and eccentricities of the load were performed. This campaign was developed in the universities of Liége and Louvain with collaboration of the Building Industry Research Centre and the Research Centre for the Cement Industry in Belgium. Like for the previous cases, the pinned-pinned configuration was used.

The most relevant experimental researches of the 1980's which were related with eccentrically compressed masonry walls were the ones presented by: Drysdale and Hamid [70] and Hasan and Hendry [71]. The first ones studied the effect of the eccentric application of the compressive load on the structural response of small walls composed of different types of concrete blocks and mortar. Similarly, Hasan and Hendry [71] focused on the investigation of the effect of the slenderness and eccentricity on the load-bearing capacity of masonry walls. They tested walls with different heights and different boundary conditions. In addition, the authors compared the experimental evidence with various standards. However, it has to be noticed that this last research, [71] was developed using small-scale (1:3) walls.

The use of small-scale tests has been justified and applied in several experimental campaigns with the aim of reducing the costs of the investigation tasks. One of the first researches using small-scale brick masonry walls in compression was carried out by Murthy and Hendry [72]. In this same way, the recent experimental campaign by Sandoval [73] studied the slenderness and eccentricity effects on 1:4 scale brick masonry walls with elastic supports at both ends. However, the need for full-scale data to validate the small-scale tests, the analytical formulations and the numeric simulations has led the researchers to perform full-scale experimental campaigns like the ones carried out by Rosell et al. [74] or by García [75]. This first one was intended to develop a methodology for evaluating the properties and calculating the safety factor of in-service slender unreinforced brick masonry walls. In contrast, the second one had the aim of studying the instability problem on ancient multi-leafs masonry walls eccentrically loaded; this latter campaign included the development of a strengthening system using TRM and FRP together.

Thus, the experimental investigation on load-bearing brick masonry walls subjected to vertical eccentric compressive loads is relatively limited if compared with the effort devoted to other materials, such as concrete or steel. This is no in spite of the large amount of masonry walls in service, which largely surpasses, in many cities, that of concrete wall or steel frames structures. This situation causes a gap between knowledge and reality, and specifically causes a lack of sufficiently validated approaches, from a scientific point of view, for the assessment of masonry buildings.

In addition, the environmental requirements and the economic sustainability lead to prefer the retrofitting and upgrading of the existing structures instead of the demolition and substitution by new ones. For this reason, there is the need to study one of the less known failure modes of the load-bearing masonry walls, which is the second order bending, along with the possible strengthening possibilities. Among the strengthening methods presented in section 2.2.3, TRM is the most promising one thanks to its satisfactory compatibility with masonry. Because of this, the current experimental data about the application method and the performance of TRM, when applied on masonry walls, is summarised next.

Regarding the application of TRM on masonry walls, it is observed that most of the researches carried out have been focused on studying the in-plane response by performing static and dynamic tests. This is not a random decision because this strengthening system (TRM) has been mostly applied for retrofitting purposes after seismic damage on masonry structures. In fact, it has been demonstrated that TRM is an extremely effective system at dissipating energy during the application of in-plane dynamic shear loads. This is illustrated in the work presented by Augenti et al. [58], which includes a discussion of the in-plane efficiency of TRM, and the paper by Papanicolaou et al. [59], who also consider the out-of-plane loading condition. In addition, there are some works that specifically deal with the effectiveness of the TRM at strengthening masonry walls against out-of-plane loading conditions. This is the case of the study presented by Harajli et al. [76], who tested TRM strengthened masonry walls against out-of-plane cyclic loads representing wind or seismic situations. The promising results presented in this paper pointed out that the lateral stiffness and flexural strength of the masonry walls is maintained after the cyclic lateral loading. However, there are not relevant investigations about the performance of TRM at strengthening in-plane loaded masonry walls which have lateral deflections because of second order effects induced by the existing eccentricity. One of the few meaningful researches in this area was presented by García [57], who analysed the combined effect of using TRM superficial strengthening and FRP connectors in the load-bearing capacity of three-leaf masonry walls; according to this research, the connectors had a larger influence on the load-bearing capacity of the walls than the TRM, because the connectors kept the three leafs together, maintaining the thickness of the wall and reducing the effective slenderness. Without them, the wall behaved as three thinner independent walls and the effect of strengthening one of these leafs with TRM was less than the effect of keeping the reduced slenderness of the wall with the connectors.

Thus, there is a clear lack of data about the influence of TRM at strengthening single brick masonry walls against in-plane eccentric loads. Contributing to provide information on this application of TRM is

one of the aims to be covered by the current research together with the full-scale characterisation of the structural response of unreinforced masonry walls.

2.3.2. Standards, codes and analytical approach

The first codes for calculating masonry structures were based on experimental evidence and good-practice general knowledge. This is the case of the geometric relationships, which were commonly used as a design criterion for the construction of masonry structures around Europe in the middle ages. The progress on the analytical description of the response of masonry walls, attained thanks to the contribution of different researchers, allowed a gradual improvement of the codes. This bibliographic research about the analytical approaches is limited to the problem of eccentrically loaded masonry walls.

According with professor Magenes [77], the first analytical researches about the compressive response of masonry walls go back to 1937 and were carried out by Nils Royen. His work contributed to the later on development of analytical formulations in the 1940's and 1950's. Among these researches, which led to several reference studies, the investigation on the buckling phenomenon of masonry walls performed by Haller [78] should be remarked. Similarly, the work by Angervo in relation with the buckling failure of non-tensile resistant pillars [79] should be highlighted too. However, these first analytical approaches showed always a limited application range associated with the boundary conditions taken into account. All of them assumed geometric simplifications (such as using a beam to represent a wall), material response simplifications, boundary conditions' simplifications and a limited range of loading conditions.

Simultaneously with the previously mentioned analytical formulations, Southwell (1932) proposed a hybrid method consisting on using experimentally determined data about the structural response of imperfect columns to predict their load-bearing capacity. This procedure considers only the buckling failure mode and initially required an elastic response of the structure (see [80]). This formulation might be applied on walls likely to fail by mechanism formation (as proved in section 5.2.5). A few researches have been done to improve the Southwell Plot method although it is worth mentioning the research of Singer [81] who allowed to extend the application of this method by considering the possibility of a plastic buckling, which occurs before the buckling load because of the reduction of the rigidity of the material.

Following with the review of the most significant analytical formulations developed for compressed masonry walls under eccentric loading conditions, the analytical approach proposed by Gross et al. [65] has to be mentioned. It was developed in the SCPI, the current Brick Institute of America, and resulted from fitting the experimental results of hundreds of full-scale tests. One of the most comprehensive experimental campaigns up to this date was performed in the SCPI, and the proposed formulation was considered one of the most representative and accurate calculation methods of the time.

The next analytical research has to be mentioned because of the number of citations deserved by the method proposed. A large number of researchers, who have studied the compressive response of brick masonry walls, have mentioned the two papers by Yokel [16,82] which stand the as basis for relating the cross sectional strength with the load-bearing capacity of the wall including the effect of the slenderness and eccentricity. A linear stress distribution was considered along with null masonry tensile strength. .

There are several analytical formulations derived from experimental campaigns. It is worth mentioning the analytical approach, oriented to calculate the buckling failure of concrete block masonry, which was derived from experimental results and presented by Hatznikolas et al. [83]. In the same line, the experiments of Kirtschig and Anstötz [69] also resulted in an analytical formulation for calculating the load-bearing capacity of brick masonry walls against buckling phenomenon. Simultaneously, Knutsson [84] studied an analytical approach used by the Danish standards, whose complexity required the use of computers for performing the calculations.

The non-linear response of the masonry was also taken into account in some approaches. For example, the work by Romano et al. [85] was focused on the response of cracked walls, with no tensile strength but considering a complex material response in compression. De Falco's proposals [17,18] on the stability of columns using an elastic-plastic material model stands among the non-linear studies; however, the tensile strength of masonry was not considered in these papers either. More recently, Mura [19] has utilized a parabolic stress-strain relationship to describe the behaviour of the brick masonry under compression loads.

At the beginning of this century, the geometric non-linear response was considered in the calculation of masonry walls. Thus, the proposed methods dealt with the buckling phenomenon. The research carried out by Liu and Dawe [86] outstands for its reliability at predicting the buckling failure load. However, the application of their method requires the aid of a computer. Finally, the importance of the tensile strength in the analytical methods, which were oriented to calculate masonry walls against buckling phenomenon, was justified and considered in researches like the one carried out by Lu et al. [87].

However, considering the non-linear response of the material, the geometric instability of the walls or the tensile strength of the masonry complicates the analytical methods. In addition, it has been observed that the most sophisticated the analytical methods are, the less useful they are for practitioners. Thus, and because of the growing complexity of the analytical formulations, modern computer methods are becoming popular alternatives whereas the standards and codes kept the tendency of using simple formulations.

The first guides and regulations were generally based on geometric rules obtained from centuries of practice. This approach was the most common one until the decade of the 1960's, when the extensive experimental researches allowed the definition of stress limits. However, only uniform or linear stress

distributions were considered in the codes, according with the analytical approaches adopted in the period. Thus, the accuracy at representing the real material response was limited.

The buckling response of masonry walls depends, among other variables, on the cross-sectional area, the material properties, the slenderness (that is, the height out of the thickness ratio) and the effective eccentricity of the load at each end of the element. These factors have been included into the standards in different ways depending on the country and the time.

According with Cassinello [66], the first codes (before the 1960's) might be classified in three categories depending on the type of calculation proposed:

- Estimative: The thickness of the wall was defined taking into account the geometric characteristics of the building. This was aimed to assure a low stress level in the masonry and led to conservative results in general.
- Empiric: This typology was based on adjusting the failure criteria using the results of particular experimental campaigns. The analytical formulations derived from this approach were useful for a limited range of cases because of the scattering of the experimental data and the particularities of the used tests.
- Theoretical: These ones were based on the application of equilibrium equations and assumed a theoretic response of the material (constitutive equation). Some of the theoretical formulations considered the second order bending effects by solving the differential equations corresponding to the case of a beam under clear boundary conditions. The application range of such methods was limited to specific support and loading conditions.

The main characteristics of these first codes, according to Cassinello [66], were:

- The tensile or flexural strength of the masonry was not considered. In fact, the British regulations of the period explicitly forbidden to consider any tensile strength. Nowadays, the importance of these parameters is well-known and it has been demonstrated that these ones are essential variables when calculating walls with large slenderness or eccentricity at the application of the load. Among all the codes before 1965, the Swedish regulations were the only ones which considered the tensile strength for calculating walls under wind conditions.
- The maximum load was calculated, in general, by considering a uniform stress distribution on the cross section. The value of this stress was limited to a portion of the compressive strength. This stress limit was usually calculated by applying tabulated factors which depended on the slenderness, on the eccentricity of the load and/or on the height of the wall. This was the most common approach of the codes of the 1960's, like the German, Canadian, French, British, Hungarian, Indian, Norwegian, Polish, Swedish or Sovietise standards. In addition, geometric limitations of the walls were also included in these codes.

- The theoretical formulation which was included in the regulations, considered simple constitutive equations (linear elasticity, non-tensile materials) and the load application point had to be always inside the central third of the cross-section in order to prevent tensile stresses.

Regarding the current standards, two main codes have to be analysed because of their wide use. These are the North-American ACI-530 code [88] and the European Eurocode-6 [64]. There is one significant difference between them if studying the corresponding analytical approaches for the calculation of brick masonry walls under eccentric axial load; whereas ACI-530 analyses the buckling failure and the cross-section material failure separately (although both criterions have to be fulfilled in a design), EC-6 deals with both failure modes in a single analytical formulation. The particular formulation of these codes, regarding the case of eccentrically compressed walls, is summarised and applied in Chapter 5 (section 5.2.1 for EC-6 and 5.2.2 for ACI-530). Finally, it has to be noticed that these widely-used codes do not consider the tensile strength of the masonry for the calculation of the load-bearing capacity of brick masonry walls although, as mentioned before, the experimental evidence (see [73,87,89]) show the importance of this parameter. Thus, conservative results are expected for the most slender walls or the ones with the more eccentrically applied loading

2.3.3. Numerical simulation of masonry walls

Numerical simulation is the suitable tool for accurately model the structural response of masonry walls. This calculation approach allows considering different boundary conditions, a wide range of materials, various geometries and several loading conditions. The main challenges when modelling a masonry structure with a finite element analysis are: the orthotropic and non-linear behaviour of the material, which is characterised by its brittle tensile failure; the non-linear geometric response of slender elements (buckling or second order bending); and the uncertainty, which is mostly related with the material characterisation. This unknowing is usually due to the large scattering of the results of the few available experimental campaigns.

The rising computational capacity has allowed implementing accurate constitutive laws to describe the non-linear response of all components of the masonry and all components of the strengthening systems, if considered. However, this approach is not useful to analyse full structures due to the high computer effort required, and is normally only used to model small portions of the material. These models are classified as micromodels because each part is independently modelled and an interaction rule between them is defined. The blocks or ceramic pieces are considered independent parts. If the mortar joint is not represented as an independent part, with the corresponding thickness, then the model might be classified as a simplified micromodel. Otherwise, the micromodel is classified as a detailed micromodel. The relationship between parts is controlled by contact elements in both cases.

One of the first micromodels used to simulate masonry was presented by Page [36] who considered a bidimensional (2D) plane stress response and defined contact elements between the bricks. Later on, the

non-linear response of the joints was taken into account in researches like the one presented by Ali and Page [37]. However, the most known model to represent the unreinforced masonry might be the one by Lourenço [38], who defined the interface cap model and considered the plastic strains too. Later, three-dimensional (3D) approaches were proposed, such as the one by Martini [90] who studied the bidirectional out-of-plane response. However, using3D micromodelling approaches require a dramatic increase of computer effort compared to the 2D ones, and they can hardly be considered for applications of a practical character.

The mechanical response of masonry as a composite material has been studied with the aid of micromodels. Among the most significant works in this area, it is worth mentioning the paper by Brencich and Gambarotta [91], who have analysed the influence of the eccentricity, among other parameters, on the compressive strength of the masonry. Similarly, the research carried out by Orduña [92] was focused in analysing the response of the masonry's joints by using micromodels; in this particular case, the pieces were represented as rigid blocs and 3D simulations were performed in order to take into account torsional effects. Recently, the periodic geometric definition of the masonry has been considered for studying its response with lower computational cost than the common micromodels which do not consider this hypothesis. One significant example of this trend is the work by Sacco [35], who analysed the damage evolution in the mortar joint by taking into account the periodic definition of the masonry.

In contrast, a macromodel is a model which does not differentiate between the units and the mortar and considers the masonry as a unique material with equivalent properties. Defining these equivalent properties is complex and one of the most accepted approaches consisted of using micromodels. The properties of the component materials of masonry are inputs for the micromodel and the corresponding results are the equivalent mechanical properties of masonry. This process is called homogenisation and it is one of the most common applications of the micromodelling on masonry.

Several homogenisation studies have been found in the literature review. Among them, it is worth mentioning the early work of Pande et al. [24] who centred their investigation on determining the Young's modulus of masonry. This research has pointed out the significance of this variable when modelling masonry elements. In contrast, the investigation by Andreaus [29] has been focused on defining the failure criterion for each possible failure mode of masonry walls under in-plane bi-axial loading conditions. The resulting criteria might be implemented in a FEA code. López et al. [93] proposed a homogenisation methodology which considered both aims: obtaining the homogenised mechanical properties and defining an homogenised plastic flow formulation to set the failure criteria. Similarly, the state-of-the-art research performed by Milani et al. [94,95] has to be highlighted. This investigation has consisted of using a micromodel to obtain the failure criteria of in-plane loaded masonry. Thus, it is a homogenisation process. These criteria have been used at simulating complex structures (macromodel) later on.

It also has to be mentioned that several researchers have considered the geometric periodicity of brick masonry in the homogenisation procedures. This is the case of the work by Salerno and Felice [34] who analysed a discrete micromodel to develop a continuum macromodel representing the case of a periodic material. In the same way, the research carried out by Cecchi and Sab [32] has to be remarked. They proposed a 3D model with deformable units and took into account the shear deformation.

Other particular applications of the micromodels to obtain a homogenised definition of the masonry are: the case of two-wythes walls (see the work of Cecchi and Milani [33]) and the approach proposed by Dallot et al. [96], who modelled masonry walls as plates to analyse the out-of-plane response.

A different homogenisation approach has been used in other researches like the one by Mistler et al. [31], who have obtained the homogenised in-plane and out-of-plane properties of masonry from the properties of the component materials. However, this particular methodology has not taken into account the interaction properties between the two components.

Before reviewing the most significant macromodels found in the literature, it is worth presenting a hybrid modelling method consisting of combining micro- and macromodels. This is called multiscale model and it is based on calculating the material properties and/or the failure criteria in a meso-scale (micromodel) with the aim of using them in a large scale structure (macromodel) later on. Among others, it is worth describing the works of Zucchini and Lourenço [30], who proposed damage prediction methods for the mortar and the pieces (micro). These data was used for calculating the compressive strength of the masonry, which was going to be used in large simulations (macro). Similarly, Ainsworth and Mihai [39] used a simplified micromodel, which was based on considering the dynamic friction between pieces, to calculate the mechanical response of some parts of a larger structure. Finally, it is worth mentioning the work by Mercatoris et al. [97], who calculated damage parameters in a meso-scale to use them in full structure macromodels.

The trend of using micromodels to obtain mechanical parameters which are going to be used in macromodels, points out the preference of the practitioners for the macromodelling. Thus, the usefulness of macromodels is out of doubt and because of this, several researches have been oriented to improve the accuracy of the macromodels while maintaining their characteristic low computational cost. Along this line, one of the first macromodels was presented by Samarashinge et al. [21], who considered a biaxial response of the masonry (shear and compression case) and set a material failure criterion. Later on, Dhansekor and Page [22] studied the possibility of combing empiric data (masonry's failure criterion) with the theoretical mechanical response of the masonry (elastoplastic in compression) in order to assemble a macromodel. With the computers' evolution, it was possible to set out the definition of fuzzy damage parameters, which have been used to model the softening of the masonry in a more general way than the micromodels do. One of the most significant works in this branch was carried out by Rots [23].

The name of Lourenço deserves to be highlighted because of his comprehensive investigations, which were carried out since the 90's, regarding the numerical simulation of masonry. Three of his most significant publications might be [25,26,98]. In these works an orthotropic macromodel, which considered elastic and plastic strains for the in-plane modelling of masonry walls, was presented, extended to 3D cases and finally, validated. Values for the main parameters of this model have been presented in these same references. Recently, the research of Dawe and Liu [86] has showed that it is possible to analyse the non-linear material response and the non-linear geometric deformations using an one-dimension (beam) approach. Dawe and Liu have studied this case and proposed an analytical formulation which has been implemented in a finite element analysis code. In addition, their work has included the proposal of an interesting approach to an eccentricity-controlled degradation of the stiffness of the masonry. Finally, some particular macromodels should be highlighted because of the specific solutions they include. It is the case of the paper by Chen et al. [99], who have used auxiliary theoretical elements (springs) to define the non-linear response of the joints of the masonry for in-plane loaded bidimensional structures. Likewise, the work of Ramalho et al. [100] is also interesting because of the particular case studied. They deal with the macromodelling of multi-wythes walls with a damage-controlled anisotropic definition of the material.

Finishing with this literature review of the available numerical tools, which are oriented to model masonry structures, it is worth noticing the work of Mohebkhah et al. [101], who used a Discrete Element Model to represent masonry infilled walls. The main difference with all previously presented researches is that the masonry is not considered a continuum material any more. In this particular research the masonry is studied as a group of independent, but connected, pieces for the first time.

After reviewing the state of the art of the numerical tools developed to model unreinforced masonry structures, the up-to-date approaches aimed to study the case of TRM strengthened masonry structures is analysed. First of all, it has to be said that only one paper which analyses this specific but meaningful case has been found. It is the recent work of Milani [102], who has presented a detailed micromodel for simulating the dynamic response of TRM strengthened brick masonry structures.

For this reason, two research fields, which are close to the case of TRM strengthened masonry walls, are considered as a base for the bibliographic review: the numerical simulation of FRP strengthened masonry elements and the simulation of TRM (or Textile Reinforced Concrete, TRC) strengthened concrete structures. The first one is useful because it represents how to model a similar strengthening technique for masonry elements, whereas the second one is also significant because it reviews the numerical modelling of the studied strengthening technique (the TRM) applied to concrete structures.

Regarding the simulation of FRP strengthened masonry elements, Cecchi et al. [103] proposed an analytical homogenisation procedure for in-plane loaded masonry walls strengthened with Carbon FRP (CFRP). This homogenisation process might be a first step to define an equivalent material, which

represented the strengthened masonry, to be used in a Finite Element Analysis (FEA). The next significant investigation was carried out by Valluzzi et al. [104]. This work consisted of a bidimensional detailed micromodel aimed to represent the case of masonry strengthened at both sides with FRP. In contrast, the numerical simulation of walls strengthened with FRP at only one side might be found in the works of Petersen [105] and Milani [106]. The first one was oriented to the study of masonry walls strengthened with Near Surface Mounted (NSM) FRP and in-plane loading conditions, whilst the second one proposed a homogenisation technique for modelling the FRP strengthened masonry walls under out-of-plane loading conditions.

Although theoretical research, aimed to develop numerical tools oriented to model FRP strengthened masonry elements, has been performed on plane elements like little walls, most of the recent works are focused on the simulation of skeletal structures, like arches or vaults, strengthened with FRP. Some of the most significant researches in this field are: the early bidimensional approach presented by Drosopoulos et al. [107], who used asymmetric contacts to represent the effect of placing FRP on masonry; the work by Zheng at al. [108], who performed a numerical analysis of a FRP strengthened arch using a commercial finite element software (ABAQUS) to expand the applicability of their model; and the recent study of the application of CFRP strips on masonry vaults carried out by Mahini et al. [109].

The most relevant researches focused on the numerical analysis of Textile Reinforced Mortar/Concrete (TRM or TRC) have been performed considering a concrete substrate. Among them, one of the most significant works might be the first numerical study of the bonding characteristics of TRC, when applied on concrete structures, which was carried out by Holler et al. [55]. Among the recent studies, it is worth mentioning the investigation of Schladitz et al. [110], who have used a concrete-oriented finite element software (Atena 2D) to model concrete slabs strengthened with TRC. The TRC effect has been simulated using discrete truss elements in this case. Another approach, which has been presented by Larbi et al. [111], consisted of defining the TRC as an equivalent thin layer of reinforced concrete with truss elements inside it. This particular investigation has been carried out using commercial finite element software: ANSYS.

Finally, the three-dimensional micromodel presented by Elsanadedy et al. [112], which is aimed to simulate TRM and FRP strengthened concrete by means of surface-to-surface contacts, is significant because it uses a single methodology for representing both strengthening techniques. This research has been done using general purpose software: LS-DYNA.

2.4 Conclusions

Masonry has been used as a building material since the beginning of the human civilisation. Its use has changed through the ages resulting in the adaptation of the architectural design and the shape of the buildings so that compressive equilibrium conditions could be reached. However, the development of

structurally more efficient concrete and steel structures since the middle of XXth century has set aside the usage and investigation of masonry. Nowadays, the most common structural masonry element is the load bearing wall; it can be seen in a large amount of buildings which are still in use. Thus, studying masonry is necessary because of the importance of this material for our historical heritage and because of its significance in the current building and rehabilitation industry. In particular, load-bearing brickwork walls composed of masonry with "poor" mortar is a relevant and necessary research field.

Regarding the typical failure patterns of load-bearing brickwork walls, it has been noticed that the bending failure is a common process for unreinforced masonry walls eccentrically loaded. This particular failure is induced by the second order deformation and it is associated with the mechanism formation. In this case, the collapse is brittle, and thus, dangerous. However, this failure pattern has not been widely studied.

Comparing experimental campaigns, the effort allocated to concrete or steel is huge compared to masonry. Moreover, the characteristic large dispersion of the experimental researches on masonry suggests that more data are necessary to sufficiently validate reliable calculation tools and standards. In addition, the available publications about the experimental characterisation of masonry walls are old and miss some of the data that might be obtained with an up-to-date experimental campaign using current sensors and data acquisition equipment. In addition, some of the testing set ups utilized years ago make it difficult using their data for validating numerical models due to the uncertainty about the boundary conditions, which are one of the most influents parameters. In conclusion, it might be interesting to perform an experimental campaign with clear boundary conditions and current equipment.

Knowing the mechanical limits of masonry and the current structural requirements for masonry walls, it is evident that strengthening procedures will be needed in the near future to preserve the safety level and upgrade existing structures. Thus, a brief review of the most significant strengthening techniques for masonry walls has been performed. It resulted that the Textile Reinforced Mortar (TRM) is the most promising strengthening method due to its compatibility (physical, chemical and thermal) with masonry. Hence, it is noticed that studying the ability of the TRM at strengthening load-bearing masonry walls against mechanism formation failure is an interesting and meaningful research field. The importance of carrying out a study about this application is even more evident when considering that this strengthening system has been applied with no code or standard regulations.

In the bibliographic research it has been observed that there is a clear tendency to use commercial general purpose finite element software because it is more accessible for practitioners. Thus, the complexity of most of the proposed models developed until the beginning of this century with the aim of accurately simulate the masonry response make it hardly applicable for practical engineering purposes. Instead, the engineering applicability bets for simple and reliable models which can be used through a wide range of finite elements packages. However, this review has pointed out that the any numerical

model aimed to simulate masonry structures should be a micromodel to correctly represent the joints response.

In conclusion, the review of the state of the art leads to highlight the necessity of performing an experimental real-scale campaign to characterise the structural response of load-bearing brickwork walls under eccentric compressive loads. It is also necessary to experimentally study the possibility to strengthen these walls with TRM and to propose a simplified numerical model or analytical approach for the analysis of these structural cases.

3

Experimental Campaign

3.1 Introduction

This chapter presents the experimental campaign carried out with the aim of contributing to the understanding of the structural response of unreinforced and TRM-strengthened brick masonry walls loaded with eccentric compressive forces.

Firstly, the brick masonry characterisation tests, including the characterisation of the component materials, are presented. These tests are necessary to define the brick masonry properties, which are essential to understand the results of the full scale tested walls, presented later on. These characterisation tests are required because masonry is a complex composite material whose mechanical characteristics, in the case of historical masonry, are highly heterogeneous due to the manual production. In addition, the tests on full scale unreinforced masonry walls are significant because there is a large stock of buildings whose main structure consists of brick masonry load-bearing walls but the corresponding research is little in comparison with other materials like steel or concrete.

And it is this large stock of buildings supported by masonry walls which makes rehabilitating them an interesting alternative. This actual trend to prefer rehabilitation and conservation of the existing buildings rather than demolition and new construction, requires a large range of technological solutions. These solutions are oriented to improve all aspects involved by the management of existing masonry structures, from energetic consumption to structural strength. Within the strengthening options, TRM is actually one of the most promising available technics for masonry, as seen in Chapter 2. Tests oriented to characterise the strengthening mortars, tests aimed to assess the structural performance of the TRM when applied on masonry and loaded out-of-plane and tests on full scale TRM-strengthened walls have been carried out to enhance the knowledge about the structural behaviour of TRM-strengthened brick masonry walls under eccentric compression.

To sum up, this chapter covers the justification, design, description, execution and results of the experimental tests performed on mortar specimens, brick samples, brick masonry prisms and masonry walls both unreinforced and strengthened with TRM.

All tests were carried out in the premises of LITEM research group (Universitat Politècnica de Catalunya) between April 2009 and February 2012. Detailed information of the tests is presented in Annex 1.

3.2 Materials selection

One of the objectives of this research is to enhance the knowledge of the structural behaviour of walls manufactured with common brick masonry during the XIXth century and the beginning of the XXth in Spain. This typology of masonry is composed of solid clay bricks and poor Portland mortar or lime mortar. For this reason, a mortar with low compressive strength has been selected to build the real scale walls. The geometry of the solid clay bricks has been chosen to represent the ones used in real structures in Catalonia (northern Spain).

Finally, the strengthening materials to produce the TRM have been chosen in agreement with the advice of experimented TRM workers. Complete TRM systems, which included the fibre grid and the specifically for-the-purpose designed mortar, have been used in the current research.

3.3 Laboratory tests on materials

The aim of the tests described below is characterising the main physical and mechanical properties of the used materials, which are necessary for the calculations presented later on. The brick masonry has been studied as a composite material. However, the two component materials (bricks and mortar) have been also characterised with the aim of providing detailed information to be applied in further researches.

3.3.1. Mortars characterization tests

Five different mortars have been studied. Two of them have been used to manufacture the masonry joints, whereas the other three have been applied as part of the TRM strengthening system. All these mortars have been tested to obtain the flexural tensile strength and the compressive strength.

3.3.1.1 Mortars summary

In this subsection, the used mortars are identified and briefly described. It is important to distinguish them because they have different compositions and characteristics. In addition, the mixing and application procedures are not the same for all them.

a) Propamsa M7,5

It is a Portland cement pre-dosed mortar commercialised in 25kg paper bags. Propamsa M7,5 is a common bricklaying mortar usually prepared by mixing the provided powder with water. Mechanic and manual mixing systems are allowed. It is produced by Ciments Molins Group.

b) Durland M7,5

Durland M7,5 is equivalent to the previous one, with the same nature and application procedures. The only difference is that Durland M7,5 is produced by Durland Cementos S.L.

c) Planitop HDM Maxi

This mortar is specifically designed to be applied as part of a TRM system. According with the manufacturer, this product is a two-component, high-ductility, fibre-reinforced cementitious mortar with a pozzolanic-reaction binder base. The first component is a grey powder (25kg paper bag) whilst the second one is a white latex solution (6.75kg drum). According with the producer (Mapei S.p.A.), this mortar has to be prepared with a low-speed mechanical mixer. It is compliant with European Standard EN 1504-3 R2 requirements.

d) Planitop HDM Restauro

Like the previous one, this mortar is also designed to be applied as part of a TRM system. It is a two-component, high-ductility, fibre-reinforced, hydraulic lime mortar with Eco-Pozzolana. The first component is a white powder (25kg paper bag) and the second one is a white latex solution (5kg drum). According with the producer (Mapei S.p.A.), this mortar has to be prepared with a low-speed mechanical mixer. It is part of the TRM system. It is compliant with European Standard EN 998-1 GP and EN 998-2 G-M15 requirements.

e) XMesh M25

This mortar is developed to be used as part of a TRM system. According with the producer, it is a highly adhesive stabilized mortar consisting on pozzolanic binder, predosed aggregates, sand and additives. It is commercialized in 25kg paper bags and is usually mixed with water using a low-speed mechanical mixer. This mortar is produced by Ruredil S.p.A.

3.3.1.2 Specimens production

All the tested specimens were moulded by pouring the fresh mortar in a standardised triple prismatic mould (160mm x 40mm x 40mm). The mixing procedure was:

- Propamsa M7,5 and Durland M7,5 mortars were manually mixed with water for quantities up to 5kg. The mixing was mechanical for larger quantities.
- Planitop HDM Maxi, Planitop HDM Restauro and XMesh M25 were low-speed mechanically mixed.

- After mixing, the mortars Planitop HDM Maxi and Planitop HDM Restauro had to repose for 2 minutes before remixing them. This variation respect to the producer's recommendations was suggested by a Mapei certified workman.
- Mortar XMesh M25 was mixed with the 90% of the water recommended by the producer. This variation was an advice given by a Ruredil certified workman.

All the specimens were air cured in the current laboratory atmospheric conditions. These samples were taken out of the moulds five days after the casting. The tests were performed, at least, after 28 days of curing.

3.3.1.3 Flexural tensile strength tests

Flexural tensile strength tests were carried out according with the standard EN1015-11:2000 [113]. The procedure proposed by this standard is a force-controlled three-points-bending test on standardised specimens (40mm x 40mm x 160mm). The test set up includes a normalised tool to assure the correct application of the load (see Figure 3.1). The press used to apply the load was an electromechanical press with a maximum load of 50kN.

All specimens were, at least, 28 days old when tested. The same response, characterised by a brittle failure, was obtained for all these tests. Load and displacement were measured at 5Hz during the tests. However, the main result was the maximum applied load, which was used to calculate the flexural tensile strength (f_{xm}) under the hypothesis of a linear stress distribution. The obtained results are summarised in Table 3.1. A more detailed description of the test setup, the testing procedure and the obtained results is included in Annex A1.

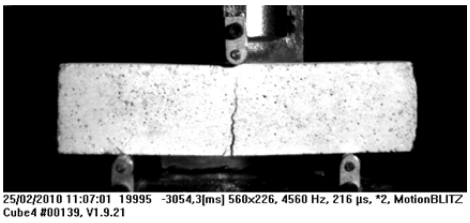

Figure 3.1 Flexural tensile strength test on Durland mortar

3.3.1.4 Compressive strength tests

The guidelines of the standard EN1015-11:2000 [113] were followed to carry out the compression tests. The previous flexural test divided the original standardised prism in two halves. Each halve was tested under uniformly distributed compression up to failure (see Figure 3.2). The force was applied with the same press (Suzpecar 50kN) as the previous tests, except for the specimens made of mortar XMesh M25, which were tested with a hydraulic MTS actuator of 100kN of force range. The tests were load-controlled and both load and displacement were measured. The compressive strength (f_{cm}) was calculated from the

resisted load by assuming a uniform distribution of stresses. The obtained results are summarised in Table 3.1. More detailed information about the test set up, the procedure and the results is shown in Annex A1.

Mortar	f_{xm} ***(MPa)***	f_{cm} ***(MPa)***
Propamsa M7,5	1.24 (0.30)	3.18 (0.33)
Durland M7,5	1.25 (0.89)	3.70 (0.63)
Planitop HDM Maxi	8.06 (0.18)	42.20 (0.27)
Planitop HDM Restauro	6.57 (0.03)	14.53 (0.08)
XMesh M25	9.39 (0.10)	34.47 (0.08)

Table 3.1 Results of the tests on mortars. CV in brackets

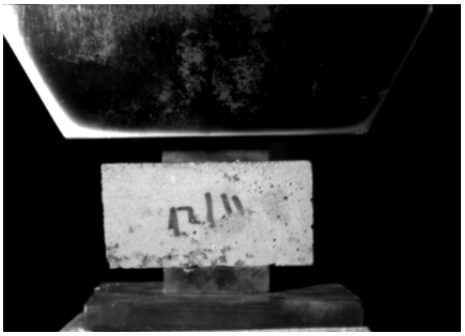

Figure 3.2 Compressive strength test on Propamsa mortar

3.3.2. Bricks characterisation tests

One typology of solid clay bricks was used in the experimental campaign. The nominal dimensions of these bricks were 45mm x 132mm x 280mm. A local producer, *Calvente Hermanos, S.A.*, was chosen to provide this material, which was commercialised under the name of "*Tocho macizo máquina*".

Flexural tensile strength tests, compressive strength tests and water absorption tests were performed to characterise the bricks.

3.3.2.1 Flexural tensile strength tests

Three-points-bending tests were carried out with the aim of indirectly obtaining the tensile strength of bricks. The tensile strength (f_{tb}) was estimated from the flexural tensile strength (f_{xb}), which was obtained with the three-points-bending tests, by applying an expression that relates these two parameters for concrete. This expression is included in the Spanish concrete standard (EHE-08 [114]). This methodology to estimate the tensile strength from the flexural tensile strength has been previously used with accurate results by some authors like Charry [115].

These tests were load-controlled and they were executed with the same press (Suzpecar 50kN) as the previous two described tests. The specimens' preparation consisted of a basic surface cleaning. During the tests, the applied load and the corresponding deformation at mid-span were measured. The average of the results of these tests is shown in Table 3.2. Annex A1 contains more detailed information about these tests.

3.3.2.2 Compressive strength tests

The compressive strength tests that were performed on bricks were based on the regulations of the standard EN 772-1:2002 [116]. The testing procedure consisted of applying a uniformly distributed compressive load on a brick sample. The two major surfaces of the brick were prepared with a thin sulphur mortar regularisation layer in order to assure a uniform contact between the plates of the press and the brick. A few tests were carried out with the aim of studying the effect of using a sulphur mortar instead of the Portland cement mortar recommended by the standard. Results did not show significant differences between these two regularisation systems.

Regarding the testing procedure, it has to be highlighted that the original bricks were mechanically cut to test brick halves instead of complete bricks. This adaptation was required because the used hydraulic press was limited to a maximum compressive force of 1MN. All tests were load-controlled with a constant load increase of 10kN/s.

Figure 3.3 Compressive strength test on a half brick

Once the maximum applied load was obtained, the compressive strength of the brick (f_{cb}) was calculated assuming a uniform stress distribution and taking into account the shape correction factor (δ) suggested by the standard EN 772-1:2002 [116]. The average of the experimental results is presented in Table 3.2. Extended information about these tests can be consulted in Annex A1.

3.3.2.3 Water absorption tests

The water absorption of the bricks is an important characteristic for the masonry execution. If a brick has high water absorption when it is placed to produce a masonry structure, this brick quickly absorbs the water of the mortar in contact preventing the cement components to correctly set and causing a low bonding strength between the mortar and the brick. Thus, the mortar-brick adherence strongly depends on the water absorption of the brick when the masonry is produced. In some standards, the water absorption of the bricks is limited; e.g. at ACI-530 [43] the limit value is 0,0016g/(min·mm^2).

Water absorption tests were carried out according with the standard EN 772-11:299 [117]. The tests consisted of measuring the weight variation of the bricks due to the water absorption. The area of the

brick which is in contact with the water has to be measured and the immersion time has to be controlled in order to calculate the absorption parameter.

Two different tests were performed. The first testing procedure was intended to determine the value of the water absorption for the dry bricks. The second methodology was aimed to obtain the absorption value for bricks which had been previously immersed into water during one minute. Both results are presented in Table 3.2 and extended information about these tests is included in Annex A1. Table 3.2 also contains the coefficient of variation of the strength parameters in brackets.

Tensile strength f_{tb} (MPa)	***Compressive strength f_{cb} (MPa)***	***Water absorption(mg/(mm^2·min))***
2.81 (0.28)	27.93 (0.19)	1.46 dry / 0.65 wet

Table 3.2 Results of the tests on bricks. CV in brackets

3.3.3. Grids characterization

The mechanical characteristics of the fibre grids, which have been used to produce the studied TRM strengthening systems, are required. These grids are an industrialised product so the values included in the corresponding technical data sheets are assumed to be reliable. For this reason, no experimental characterisation tests on the fibre grids were carried out in the current research.

3.3.3.1 Grid summary

Two different grids have been used. A brief description of each one is presented to identify them in later on discussions.

Mapegrid G220

It is a bidirectional alkali-resistant coated glass fibre grid with a mesh size of 25mm x 25mm. It is used in conjunction with Planitop HDM mortars (Maxi and Restauro) distributed by Mapei S.p.A. The ultimate strength of this grid is 45kN/m and its elongation at rupture is 3%.

Xmesh C10

It is a bidirectional carbon fibre grid with a mesh size of 10mm. The carbon fibre content is 168 g/m^2. It is used in conjunction with XMesh M25 mortar and distributed by Ruredil S.p.A. The ultimate strength of this grid is 160kN/m and its elongation at rupture is 2.1%.

3.3.4. Unreinforced Brick masonry characterization tests

Studying the components the masonry is composed of separately is necessary but not enough to characterise the mechanical response of brick masonry as a composite material. Thus, different typologies of brick masonry samples have been built and tested with the aim of experimentally determine the values of the compressive strength, the compressive deformability and the brick-mortar bonding strength.

3.3.4.1 Unreinforced brick masonry samples summary and construction

All the tested brick masonry samples were built into the facilities of the LITEM's laboratory. These were air cured in the current atmospheric conditions for at least 28 days before testing them. The fabrication of these specimens was done according to the following steps:

- Superficial cleaning of the bricks and immersing them under water for one minute.
- Levelling the supports used to build the samples on.
- Mixing the mortar (Propamsa or Durland) with water up to a workable consistence.
- Placing the bricks and the mortar while controlling the levelling of each row.

Two typologies of samples were built: 5 stacked brick prisms for the compressive strength tests and the compressive deformability tests; and 3 stacked brick prisms for the bonding tests.

3.3.4.2 Compressive strength tests

The compressive strength tests, which were carried out on brick masonry prisms, did not follow any standard; instead, the specimens' design was oriented to reach a height out of width ratio over 2. This geometric limitation was aimed to reduce the friction effects between the plates of the press and the specimen. Although higher slenderness would have been preferred, maintaining a relatively small specimen was necessary to test it with the available resources. For this reason, the brick masonry samples were designed to be 5 bricks high.

A Veritest hydraulic press, with a maximum load capacity of 1MN, was used to test the masonry samples in compression. The test procedure was force-controlled and the load was constantly increased at 10kN/s up to the failure of the brick masonry.

Four different series of masonry prisms were tested in compression (See Table 3.3). Three of these series (A, B and C) were associated with a group of real scale walls. These brick masonry samples and the corresponding walls were manufactured with the same materials and at the same time. The prisms of the D series have no real scale wall associated. Similarly, some of the walls have no corresponding masonry prisms to be tested in compression. In this last case, an average of the results of the prisms built with the same materials is considered. Results of the compression tests on brick masonry samples are summarized in Table 3.3.

Series	***Mortar***	***Corresponding walls***	***# of tests***	***f_c (MPa)***
A	Propamsa M7,5	1	3	18.2
B	Durland M7,5	2 to 5	4	12.9
C	Durland M7,5	6 to 9	6	13.7
D	Durland M7,5	None	16	9.1

Table 3.3 Results of compressive strength on masonry prisms. See the wall's reference in section 3.4.1

Propamsa M7,5 mortar was used to build the prisms of the A series, whilst the prisms of series B, C and D were fabricated with Durland M7,5 mortar. For walls W#10 to W#29 (see section 3.4.1 for the wall's

definition) an average value of the compressive strength (taking into account B, C and D series) was considered. This value was 10.8MPa.

Moreover, eight extra prisms were fabricated with two purposes: five of them were produced to analyse the effect of the thickness of the mortar joint on the brick masonry compressive strength; and the other three were aimed to study the influence of wetting the bricks before its collocation on the compressive strength of the resulting brick masonry.

As expected, the thinner the mortar joint was, the greater the compressive strength of the brick masonry resulted. In fact, the compressive strength increased from 11.4MPa to 21.2MPa when the cumulative joint thickness changed from 40% of the total height to 11% of the height. No difference was observed between the compressive strength of the masonry prisms constructed with wetted bricks and those constructed with dry bricks.

Detailed results and extra data about the compressive tests on masonry samples are presented in Annex A1.

Figure 3.4 Compressive strength test of a brick masonry prism from the D series

3.3.4.3 Modulus of deformability tests

The modulus of deformability is one of the most important characterisation parameters because knowing the relation between stresses and strains is essential to achieve accurate results in any calculation or simulation. However, the modulus of deformability (E) of the masonry is one of the parameters that show a bigger scattering if observing the values presented in the bibliography.

The tests used to obtain the modulus of longitudinal deformation of the masonry (E) in the current research did not follow any standard. The test set up (see Figure 3.5) consisted of four potentiometric sensors measuring the distance between a fix support, where the specimen was settled, and a mobile plate, which applied a uniform compressive load. The descending displacement of the four vertexes of the mobile plate was measured with the potentiometers and the load was applied with a hydraulic MTS actuator of 250kN force range. The test was load-controlled and three loading-unloading cycles were

applied. Each loading-unloading cycle reached a larger maximum compressive load than the previous cycle for the same sample. The maximum applied load, which was reached at the third cycle, was around the 50% of the collapse load of the prism by uniform compression.

One Young's modulus value was calculated for each loading cycle, so three values of this parameter were obtained for each sample. These Young's modulus were calculated taking into account the loading data of a range defined from the maximum load of the previous cycle (0 for the first cycle) to the maximum load of the current cycle, which corresponded with the absolute maximum loading force for the third cycle. The global Young's modulus of each sample was calculated as a weighted average of the three moduli. The weights of the average depended on the range of the force which was used to calculate the modulus for each loading cycle.

The prisms used to obtain the modulus of linear deformability were used to test the compressive strength later on. These specimens corresponded with the D series (see Table 3.3). Hence, 15 tests were performed to obtain the modulus of deformability (one of the 16 prisms failed before finishing the modulus of deformability test). For the first six prisms, the loading ramp was defined up to 100kN, 175kN and 250kN for the three loading cycles. The load was increased at 25kN/min. For the other nine tests, the cycles finished at 40kN, 80kN and 120kN respectively with a constant loading speed of 15kN/min.

The average modulus of deformability, taking into account the 15 tests, was 780MPa which represented 72 times the compressive strength (f_c) of the prisms with the same material (B, C and D series in Table 3.3). The value obtained for the ratio E/f_c is extremely low compared with the correlations suggested by current standards [64], but not so low if compared with other authors' experimental results (see [91], [118] [119]) with E/f_c values about 100.

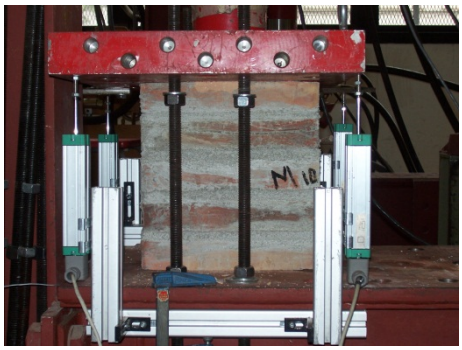

Figure 3.5 Modulus of deformability test set up

3.3.4.4 Mortar-brick bonding strength

The value of the bonding strength under flexion-compression loading conditions was calculated in accordance with ASTM C1072 (bond wrench test). However, the methodology proposed by this standard was not completely followed because the standardised loading tools were adapted to the current

laboratory resources. The test set up consisted of two parts: the first, a static base whose aim was to fix the specimen just below the joint that was going to be tested; and the second part was a tool that perfectly grabbed the upper brick of the specimen and had a mechanical arm where the load was applied to cause a flexion-compression condition on the tested joint. See Figure 3.6.

Figure 3.6 Bond wrench test set up for determining the mortar-brick bonding strength

The specimens were three bricks high. Three samples with Propamsa M7,5 mortar were tested whereas 23 samples with Durland M7,5 mortar were used in the experiment.

The test was displacement-controlled and the load was applied with an electromechanical testing machine Suzpecar (50kN of maximum load), which was the same used for the tests on mortar samples. Most of the tests (see exceptions in Annex A1) were carried out with a constant loading ratio of 2mm/min. For each test, the minimum distance from the compressed edge of the tested joint to the load application point was measured. The weight of the upper brick and the tool that grabbed it were also measured. All this information was used to determine the maximum tensile stress that the joint could resist in flexo-compression conditions. The performed calculus assumed a linear stress distribution. The obtained results are summarised in Table 3.4.

Mortar	***# tests***	***f_t (MPa)***
Propamsa M7,5	3	0.23
Durland M7,5	23	0.36

Table 3.4 Bond wrench test results

3.3.5. Strengthened brick masonry characterisation tests

The flexural-tensile behaviour of the TRM-strengthened brick masonry prisms is studied in this section. Although the strengthening mortar has a greater compressive stiffness than the studied brick masonry and this might influence the compressive response when the TRM was compressed, the current experimental study of the behaviour of the TRM strengthened masonry was limited to the case in which the TRM is tensioned. Thus, the presented analysis is aimed to characterise and understand the real scale walls which had the TRM system applied on the tensile side as seen, later on, in subsection 3.4.3.

Fourteen prisms consisting of ten stacked bricks were constructed, cured, and finally strengthened on one of their widest sides. Three different TRM solutions were tested under three point bending conditions.

This test set up was considered in order to analyse the behaviour of the TRM strengthened brick masonry under bending loads and to study the debonding possibility of TRM in this configuration.

The description of the specimens, its preparation, the test procedure and the obtained results are presented below.

3.3.5.1 Strengthened brick masonry samples summary and preparation procedure

Three different types of TRM were applied on brick masonry prisms to test these samples under three-points-bending configuration. The prisms were constructed with the same bricks as the real scale walls or the previously mentioned brick masonry samples. Durland M7,5 mortar was used in the joints of all these prisms which reached 10 rows high.

The construction of the prisms followed the steps previously mentioned in section 3.3.4.1. This building procedure involved the initial cleaning of the bricks, the levelling of the supports, the mortar mixing and piling the components and verifying their levelling at each row.

The strengthening application was carried out, at least, 28 days after the prisms construction. The following combinations of grids and mortar were tested. See Table 3.5.

A brief summary of the TRM application procedure is presented below. However, consulting Annex 1 is recommended for a more detailed explanation specifically oriented to each TRM system. On the whole, the necessary steps to apply a TRM system are:

- Surface cleaning
- Wetting the masonry
- Uniform application of a first layer of the strengthening mortar
- Placing the grid on the fresh mortar and pressing it until the grid is inserted into the mortar
- Uniform application of the second layer of the strengthening mortar

Sample series	***Strengthening mortar***	***Grid***	***Number of samples***
SP_Rest	Planitop HDM Restauro	Mapegrid G220	3
SP_Maxi	Planitop HD Restauro	Mapegrid G220	3
SP_Xmesh	XMesh M25	XMesh C10	6
P_Ctrol	None	None	2

Table 3.5 Strengthened brick masonry samples and corresponding TRM combinations

The pictures in Figure 3.7 represent the strengthening procedure. Once the TRM was applied the strengthened brick masonry prisms were air cured at environmental conditions for at least 28 days before testing them.

Figure 3.7 TRM application procedure on the brick masonry prisms

3.3.5.2 Test for the determination of the ultimate bending strength of TRM strengthened brick masonry

The tests were carried out with an electromechanical testing machine Suzpecar with a loading range of 50kN. The experiments were set up into the frame of this press and the two supports were set with a specific tool as seen in Figure 3.8.

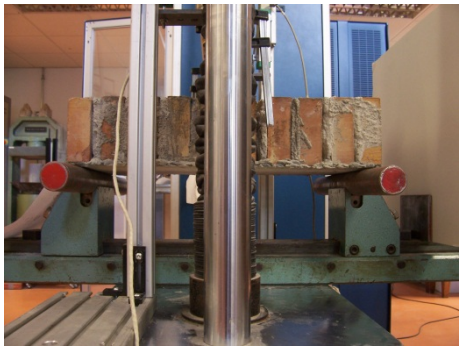

Figure 3.8 Supports for the TPB Tests of strengthened brick masonry prisms

The strengthened prisms were placed in horizontal position, as a beam, with the TRM strengthening upside down. The load was applied at mid-span and it was displacement-controlled with a constant ratio of 1mm/min. The applied force and the mid-span deflection were acquired at 5Hz. The deformation at mid-span was externally measured to avoid the effects of the deformation of the loading and the supporting systems. Two potentiometers were used to measure this deformation. The test was stopped when the applied load descended below 1kN after reaching its maximum value. The real thickness of the strengthening mortar layer at mid-span was measured after the collapse of the specimen.

The average values of the results of the tests are summarised in Table 3.6. Only the samples which collapsed because of the tensile failure of the fibre grids were considered in the average calculation. This included all the specimens except two of the samples strengthened with XMesh M25 mortar and XMesh C10 fibre grid. For these two cases, the TRM strengthened prisms failed by masonry shear near one of the supports. After this, the TRM locally debonded as part of the collapse mechanism.

The failure of the samples strengthened with glass fibre grids (SP_Rest and SP_Maxi series in Table 3.6was always associated with the complete failure of the fibre grid in tension. It is, the grid was separated in two parts and all the longitudinal fibres were broken. In contrast, the four samples strengthened with carbon fibre grids (XMesh system) which collapsed because of the TRM tensile failure showed a different response. In these cases, the fibre grids were not separated in two parts and only a few fibres failed in tension (see

Sample series	***Average ultimate moment Mu (N·m)***	***ER***
SP_Rest	1457	0.93
SP_Maxi	1610	1.01
SP_Xmesh	1602	0.26
P_Ctrol	<25	---

Table 3.6 Load bearing capacity of strengthened brick masonry prisms

According with the results in Table 3.6, the TRM composed of Planitop HDM Maxi or Planitop HDM Restauro mortars and Mapegrid G220 fibre grid correctly reached the distributor's specifications regarding the tensile strength of the fibre grid. In contrast, the XMesh system does not show such a good agreement between the tensile strength of the fibre grid declared by the producer and the experimentally obtained value. In fact, the tests showed that the effectiveness of the XMesh fibre grid was around 26%. It might be related with the sliding of the fibres inside the mortar layer observed in the experimental campaign.

Figure 3.9). It seems to point out that the adherence between the strengthening mortar and the carbon fibre grid was not complete. Thus, the load was not correctly transmitted to the fibres. In fact, it was observed that the carbon fibres slid inside the strengthening mortar layer. This might be a reasonable

justification to explain the low strength values experimentally obtained for the XMesh system, and the corresponding low value of *ER* (see Table 3.6).

An effectiveness ratio, *ER*, was defined according to (Eq. 3.1). This ratio was proposed with the aim of taking into account the effectiveness of the installed fibre grids. The application of *ER* is limited to the cases in which the fibre grid is used as a part of a TRM strengthening system applied on bended masonry structures. Thus, the value of the tensile strength of the fibre grid, which is going to be considered in later on calculations within the current research, might be adjusted using this ratio. This ratio, *ER*, was calculated for each tested series and the results are summarised in Table 3.6.

$$ER = \frac{\text{Maximum applied tensile force } [F_{max}]}{\text{Manufacturer's tensile strength}} \qquad \text{(Eq. 3.1)}$$

Sample series	***Average ultimate moment M_u (N·m)***	***ER***
SP_Rest	1457	0.93
SP_Maxi	1610	1.01
SP_Xmesh	1602	0.26
P_Ctrol	<25	---

Table 3.6 Load bearing capacity of strengthened brick masonry prisms

According with the results in Table 3.6, the TRM composed of Planitop HDM Maxi or Planitop HDM Restauro mortars and Mapegrid G220 fibre grid correctly reached the distributor's specifications regarding the tensile strength of the fibre grid. In contrast, the XMesh system does not show such a good agreement between the tensile strength of the fibre grid declared by the producer and the experimentally obtained value. In fact, the tests showed that the effectiveness of the XMesh fibre grid was around 26%. It might be related with the sliding of the fibres inside the mortar layer observed in the experimental campaign.

Figure 3.9 Completely open failure crack. TPB tests on sample from the series SP_XMesh

Finally, observing Table 3.6, it is noticed that the ultimate bending moment of the TRM strengthened cases is always greater than the ultimate bending moment of the unreinforced samples (P_Control). This significant increase is even more evident if taking into account that the unreinforced brick masonry samples immediately failed under self-weigh load when placed horizontally.

More detailed information about the testing procedures and the results can be found in Annex A1.

3.4 Laboratory tests on walls

The tests described and commented in this subsection are the main source of new information on the performance of load bearing masonry walls in the present study. The aims of the experiments carried out were: (a) analysing the structural response of single-wythed brick masonry walls under in plane eccentric load; (b) studying the bending-buckling combined failure mode; and (c) investigating the effect of the TRM strengthening system on the structural response of this brick masonry walls.

The tests presented in part 3.3 were necessary to characterise the materials used in the tests on the real scale walls summarised here. As previously mentioned in Chapter 2, there is little available information regarding full scale tests on unreinforced masonry walls loaded with eccentric compressive forces which are oriented to study the buckling possibility and the second order bending effects. For this reason, the current experimental campaign includes 20 tests on full scale walls which are aimed to analyse these mentioned failure causes.

The TRM has shown many advantages at strengthening masonry structures (see Chapter 2). Taking into account that this is one of the strengthening systems that have created greater future expectations, studying its capacity to strengthen structural masonry walls has been considered interesting. For this reason, nine specimens were built and strengthened in order to analyse the effectiveness of the TRM at dealing with the out-of-plane axially induced bending failure.

The following four subsections explain how the walls were built, cured, strengthened, and moved to the testing position. The obtained results from the carried out tests are summarised in sections 3.4.6 and 3.4.7.

3.4.1. Design and Construction of the walls

The geometric design of the walls was done together with the design of the test setup and the definition of the transporting procedure. Taking into account all these phases of the experimental campaign, it was decided to build the walls on a specifically designed steel tool, called heading element (see Figure 3.10), which became the linking element between the walls and the transport or testing systems.

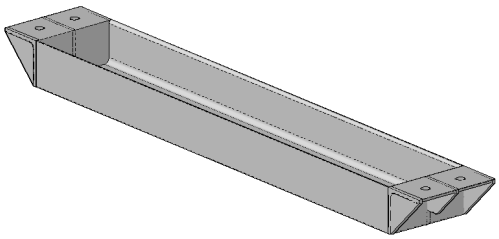

Figure 3.10 Heading element

Walls were designed and build representing four different geometries, whose theoretical main dimensions are summarised in Table 3.7. The height, wide, thickness, slenderness and number of specimens for each series are shown in Table 3.7. It has to be remarked that the slenderness presented in this table is calculated with the total height of the wall without considering the boundary conditions. Nine walls had the most slender geometry (H and F series) and were not strengthened. However, the wall of the F series was tested with fixed-pinned boundary conditions so the effective slenderness to consider in the calculations is lower than the one showed in Table 3.7. Sixteen walls were defined with the M-series geometry. Nine of these walls were TRM strengthened. The three walls with the S-series geometry were built with the aim of analysing the compression failure and these are the less slender. Finally, one wall was built with two wythes, T-series, in order to study how this configuration might affect the structural response.

Geometry type	***Height, H (mm)***	***Wide, b (mm)***	***Thickness, t (mm)***	***Slenderness, λ***	***# specimens***
H	2700	900	132	20.5	8
F	2700	900	132	20.5	1
M	1650	900	132	12.5	16
S	1000	900	132	7.6	3
T	1800	900	270	6.7	1

Table 3.7 Theoretical dimensions of the constructed walls

H-series walls were intended to represent real brick masonry walls. Their height, 2.7m, is close to the common inter-storey distance (3m). In fact, the effective height of these walls, which corresponds with the distance between hinges, is around 3m in the testing configuration. M-series walls were defined with enough slenderness to develop a second order bending failure, but they were also thought to keep a reduced height which eased the movement and installation procedures. S-series walls were built representing cases which were likely to fail because of masonry crushing in compression. Finally, the wall of the F-series was designed to analyse a different boundary condition case and the T-series wall was though to represent a different structure typology, with two wythes.

The real dimensions of the walls were measured before testing them and the corresponding slenderness' values were calculated taking into account the boundary conditions later on.

Three different teams of builders fabricated the 29 walls but they followed the same guidelines, which were:

- Mechanical cutting of the bricks with a circular saw.
- Wetting the bricks by immersing them into water for at least 1 minute.
- Mechanical mixing of the mortar using a concrete mixer, except for wall W#1 (see Table 3.8) whose mortar was manually mixed.
- Levelling the heading element.
- Setting a first mortar layer inside the heading element. It was over 2cm thickness and was needed to uniformly distribute the applied loads at the bottom of the wall.
- Building the walls while controlling their alignment and verticality at each row. Vertical and horizontals joints were fulfilled with mortar. The first masonry row was build inside the heading element.

Walls W#1 to W#9 (see Table 3.8) were constructed and cured indoors, at the laboratory facilities of the LITEM research group. The rest of the walls were built and cured in outdoors conditions (see Figure 3.11). Thus, an additional transport system was necessary to move the walls to the testing site.

Table 3.8 presents the correlation between the walls' names (W#1 to W#29), their corresponding building team, the mortar used and the geometry type. The construction date is also shown. More detailed information is presented in Annex A1.

Wall	***Geometry***	***Building team***	***Mortar***	***Building date***
W#1	H	LITEM	Propamsa	March '09
W#2/W#3/W#5	H	Const Med 94	Durland	July '09
W#4	F	Const Med 94	Durland	July '09
W#6-W#9	H	Local bricklayer	Durland	October '09
W#10-W#16	M	Const Med 94	Durland	December '09
W#17	T	Const Med 94	Durland	December '09
W#18-W#20	S	Const Med 94	Durland	December '10
W#21-W#29	M	Const Med 94	Durland	December '10

Table 3.8 General data of the wall's construction

Figure 3.11 Walls W#18 to W#29

3.4.2. Curing and transporting the walls

All walls were at least 28 days old when handled, tested or TRM strengthened. Walls W#1 to W#9 were air cured into the LITEM's laboratory, with indoors environmental conditions. Walls W#10 to W#29 were air cured at ETSEIAT's school outdoors facilities. None of the walls was wetted nor covered during the curing process.

As previously mentioned, it was necessary to move the walls W#10 to W#29 from the outdoors area into the laboratory. The main premise, which was considered for the movement of any wall, was that the weight of the wall had to be supported by the bottom heading element. Thus, the walls were always lifted by pulling from the ends of the lower heading element. A transporting tool (in grey in Figure 3.12) was used to enter the walls.

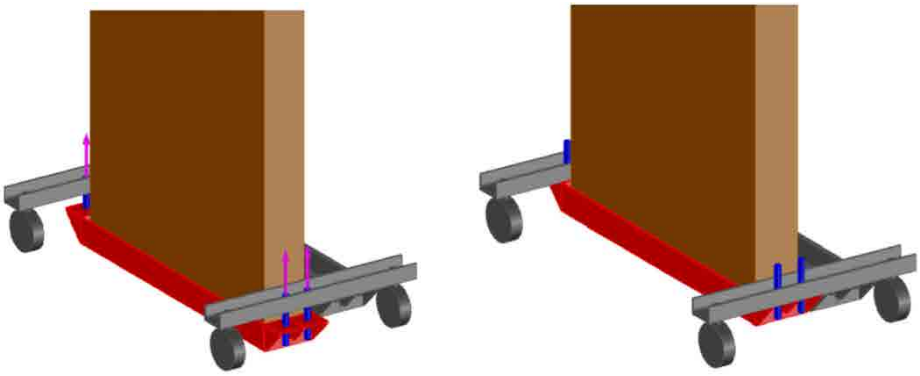

Figure 3.12 Elevation tool to enter walls W10 to W29 into the lab

The handling operations inside the laboratory facilities were done with the aid of an overhead travelling crane. In order to safely lift the walls with this crane, the upper heading element was mounted and 4 steel bars were installed between the heading elements (see Figure 3.13). The aim of the bars was transmitting the force to hang the wall from the bottom heading element so the weight of the wall was always supported by this lower part. The top heading element was put in order to absorb the horizontal forces due to the inclination of the elevation chains and to avoid the overturning of the wall (see Figure 3.13).More details about the handling procedures are exposed in Annex A1.

Figure 3.13 Elevation setup inside the laboratory facilities

3.4.3. Strengthening procedure

The TRM strengthening procedure was analogue to the one presented in section 3.3.5.1. However, some modifications were necessary to adapt the method to the real scale walls. These adaptations were:

- The TRM was not applied near the top of the wall because the top heading element had to be placed after the TRM was applied. The top heading element was used to connect the wall with the testing system. The top 10cm of the wall were net strengthened.
- For walls W#25 and W#26, two fibre grids were placed into the same layer of mortar so there was no mortar between them.
- Connectors were placed for walls W#28 and W#29. Installing the connectors consisted of: a) cutting some pieces of fibre grid and preparing them to be used as connectors, b) drill holes through the wall's thickness with the aim of passing the connectors from one side to the other, c) embedding the connector into the first mortar layer together with the fibre grid in the tensile side, d) filling the holes with strengthening mortar and e) bonding the connector on the compressive side using the same technique then to install the TRM

Specific details on the strengthening procedure and graphic information are included in Annex 1.

3.4.4. Test setup

The test setup consisted of two main parts: the upper loading system and the lower supporting system. The first one consisted of a hydraulic jack attached to a reaction beam which is part of the testing frame of the laboratory. This jack applied the load throughout a distribution steel beam which was connected to the upper hinge of the system. The top of the wall was connected to this upper hinge. The distribution

beam had its horizontal movement impeded in the out-of-plane direction. Thus, the upper boundary condition of the wall was always pinned.

The lower supporting system varied depending on the geometry of the wall. A hinge was directly laid on the floor for walls of the H and F series. This hinge was free for H-series walls and its rotation was fixed for the F series case (W#4). The lower hinge was laid on a structural steel beam for M, T and S series. This lower beam was placed at different heights with the aid of metallic auxiliary elements to adapt to the distance requirements according with the height of each wall. A sketch of the test setup for S, M and H series is shown in Figure 3.14. Figure 3.15 shows the details of the connection of the walls to the testing system.

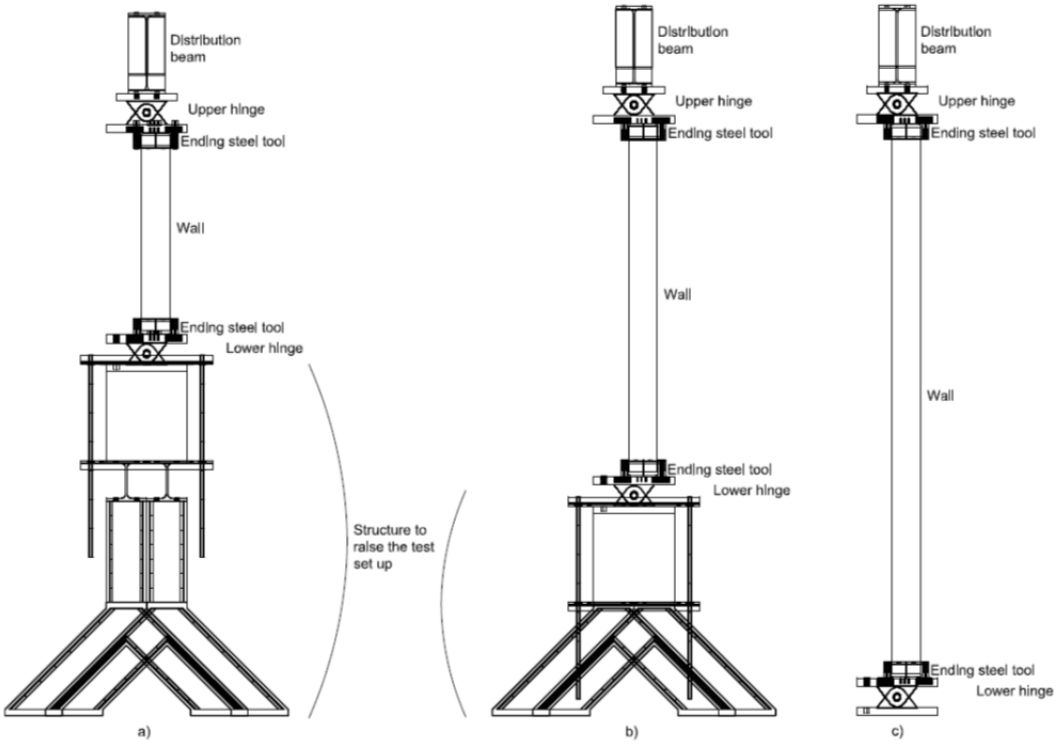

Figure 3.14 Test setup a) for walls from series S, b) for walls from series M and T and c) for walls from series H

It is worth mentioning that the first five walls, W#1-5, had different systems to avoid the lateral displacements of the distribution beam than the one used of the rest of the tests. The system used in W#1 consisted in a couple of steel plates, one at each side of the distribution beam, which constrained this movement, whereas steel lattices were used to avoid the lateral movement of the distribution beam for tests on the walls W#2-5. The effectiveness of these first methods was less than for the final solution and very little displacements were measured. However, the lateral movement was not significant in any case. Finally, it is also important pointing out that the jack had a little hinge installed for tests W#1 to W#3. This hinge was placed between the piston and the distribution beam. Further details of the test setup are presented in Annex 1.

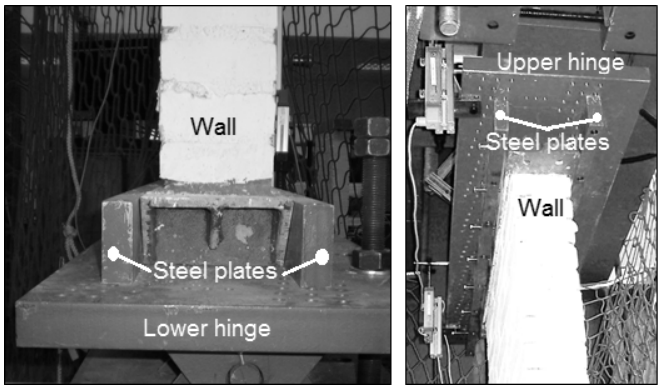

Figure 3.15. Detail of the connection between the wall and the test system at the lower end (left) and the upper end (right)

3.4.5. Walls positioning, sensors installation and testing procedure

In this section, it is briefly explained how the walls were placed in position and which type of sensors were used and where these measuring tools were placed. Finally, the testing procedure is presented. Further details on these topics are included in Annex 1.

Different procedures were used to place the walls in the testing position depending on the geometry. The tallest walls (H and F series) were lifted with an overhead travelling crane and they were put on the lower hinge, which had its rotation fixed. Before this, several free steel rods were placed below this lower hinge, which was positioned in front of the final testing position. Then, the wall was fixed to the lower hinge and this group (wall + lower hinge) was manually pushed. The wall slipped on the rolling rods to the testing position. Finally, the rods were removed and the lower hinge rest on the floor in the desired position.

Regarding the walls of the M, S and T series, the procedure consisted of lifting the wall with a forklift, approaching it to the place where the lower hinge was definitely placed and leaving the wall on this hinge. It has to be mentioned that the rotation of the hinge was constrained during the positioning tasks. After this, the wall was fixed to the lower hinge and the forklift removed.

For all the tests, the last positioning step consisted of descending the upper loading system (upper hinge + distribution beam) and connecting it to the wall in the same way the wall had been connected to the lower hinge before.

Once the wall was placed in the testing position, the next action was measuring its real geometry. This phase included measuring the out-of-plane initial deformation with a laser distance sensor installed on a vertically aligned guide. One measure of this lateral deformation was recorded at each two or three masonry rows (depending on the geometry). Measurements were done at both vertical edges of the face of the wall which was expected to be compressed during the test. The real distance between the rotation axes of the hinges in vertical (H_{eff}) and horizontal (d) directions were taken. Finally, the main dimensions of the wall were also measured.

After measuring the wall, the sensors were placed in position: 4 potentiometers measured the descending and rotation movements of the distribution beam and 4 more measured the rotation of the hinges (2 potentiometers per hinge). A pressure transducer measured the oil pressure which entered inside the hydraulic jack with the aim of indirectly obtain the applied load. Laser distance sensors were used to measure the lateral displacement of the wall and the distribution beam. In some cases, strain gages were installed on the surface of the TRM to control the response of this strengthening system. Data from all these sensors were simultaneously acquired at 50Hz by an HBM MGCPlus data acquisitor. Finally, two video cameras recorded the test: one with a general perspective and the other (the high-speed camera) recording a lateral side of the wall to better capture the failure mode.

After installing the sensors, the test area was covered with a safety net to prevent the projection of big elements around the laboratory at the wall's collapse. The testing procedure was, then, initiated. It consisted of freeing the lower hinge (except for wall W#4), starting the data acquisition, connecting the hydraulic pump and manually controlling the applied pressure to transfer an increasing compressive axial load to the wall up to the failure. The test finished with the collapse of the wall.

3.4.6. Description and results of the tests on Unreinforced Walls

After performing the tests on the 20 unreinforced masonry walls (URMW), the obtained results are presented in Table 3.9. The testing conditions are also included in this chart together with the geometry type (as outlined in Table 3.7) and slenderness. The mid-height eccentricity ratio (e/t), calculated as the ratio of the real mid-height eccentricity (e) to the thickness (t) of the wall, is also listed. A dimensionless measure of the hinge vertical alignment (d/t), describing the overall initial rotation of the wall, is also calculated and shown in Table 3.9. If d/t is positive, the upper hinge was displaced in the out-of-plane direction (the right side in the configuration of Figure 3.14) with respect to the lower hinge. The contribution of the initial alignment (d) to the eccentricity at mid-height was systematically estimated as $d/2$. With respect to the experimental results, the load-bearing capacity of the wall, P_{max}, and the ratio, ϕ_{max} (Eq. 3.2) of this maximum load out of the maximum theoretical uniformly distributed load, P_u (Eq. 3.3), are included.

$$\Phi_{max}=P_{max}/P_u \qquad \text{(Eq. 3.2)}$$

$$P_u = b \cdot t \cdot f_c \qquad \text{(Eq. 3.3)}$$

The mid-height lateral (out-of-plane) deformation at the maximum load, h_{max}, and the descending displacement of the upper hinge at the maximum load, v_{max}, both measured from the effective height (H_{ef}), are shown in the last columns of Table 3.9. H_{ef} is the real vertical distance between the axes of the hinges, except for wall W#4. In this case H_{ef} is 0.7 times the distance between hinges.

Wall	*Geometry*	*λ*	*e/t (%)*	*d/t (%)*	P_{max} *(kN)*	Φ_{max} *(%)*	$h_{max}/H_{ef}\cdot10^{-3}$	$v_{max}/H_{ef}\cdot10^{-3}$
W#1	H	22.3	4.2	0.0	169.3	7.8	4.5	2.5
W#2	H	22.2	14.9	0.0	65.7	4.3	5.9	1.4
W#3	H	22.1	8.5	7.6	133.8	8.7	9.2	2.4
W#4	F	15.0	3.9	4.9	578.6	37.8	12.7	10.8
W#5	H	22.1	10.6	5.3	239.8	15.6	5.1	2.2
W#6	H	21.7	16.1	-9.5	30.0	1.8	4.9	0.5
W#7	H	21.8	5.4	-4.5	134.7	8.3	6.7	1.9
W#8	H	22.3	0.3	6.1	129.4	8.0	5.6	1.5
W#9	H	21.9	9.8	-6.4	109.8	6.7	4.5	1.3
W#10	M	14.1	8.1	8.0	423.9	33.0	8.2	6.0
W#11	M	14.3	18.1	7.6	371.2	28.9	9.2	5.5
W#12	M	13.9	5.0	3.8	471.1	36.7	8.9	6.0
W#13	M	14.1	25.6	1.5	83.8	6.5	9.4	2.2
W#14	M	14.1	16.0	0.0	518.5	40.4	9.0	5.4
W#15	M	14.0	24.3	2.3	236.7	18.4	10.1	3.2
W#16	M	14.1	12.5	-2.3	408.2	31.8	8.5	4.5
W#17	T	6.8	66.9	9.1	491.1	38.3	8.8	4.8
W#18	S	9.1	15.8	2.3	803.4	62.6	2.9	5.4
W#19	S	9.2	22.9	0.0	686.1	53.5	4.5	8.7
W#20	S	9.3	25.0	2.3	152.6	11.9	7.6	4.3

Table 3.9 Experimental results of the test on URMW

Walls were compressed until failure. Three different collapse mechanisms were observed. The most common failure mode was the formation of a single horizontal crack at approximately mid-height with a sudden out-of-plane displacement and collapse of the entire wall. The brick-mortar tensile failure caused the opening of a natural joint leading to the corresponding collapse of the wall. This mechanism was observed for all unreinforced masonry walls (Figure 3.16) except W#4, W#14 and W#17.

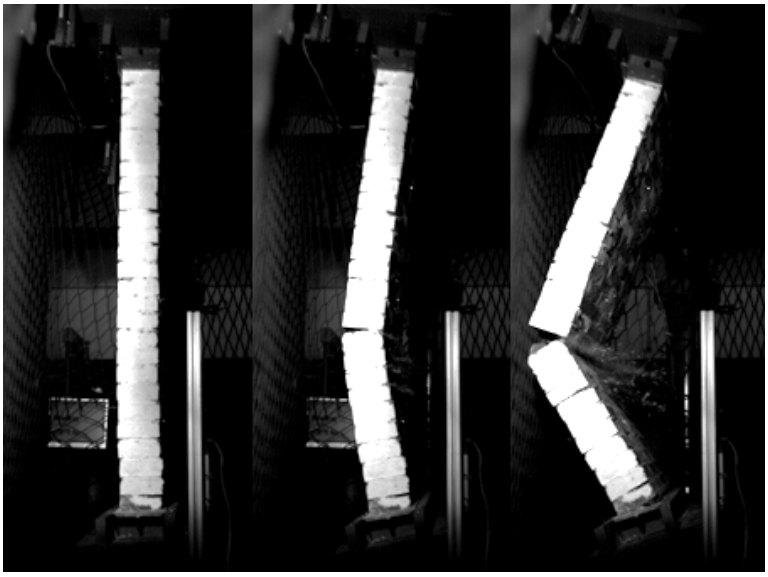

Figure 3.16 Failure mode of wall W#10. Opening of a joint and mechanism formation

Walls W#14 and W#17 (T series) failed in a mixed mode of joint opening at the tension side and masonry crushing at the compression side (Figure 3.17). Wall W#4 failed by out-of-plane shear near the

upper edge of the wall. Thus, the collapse was caused by geometric instability in 17 of the 20 tests and it was more evident in the case of the most slender walls or the most eccentrically loaded ones.

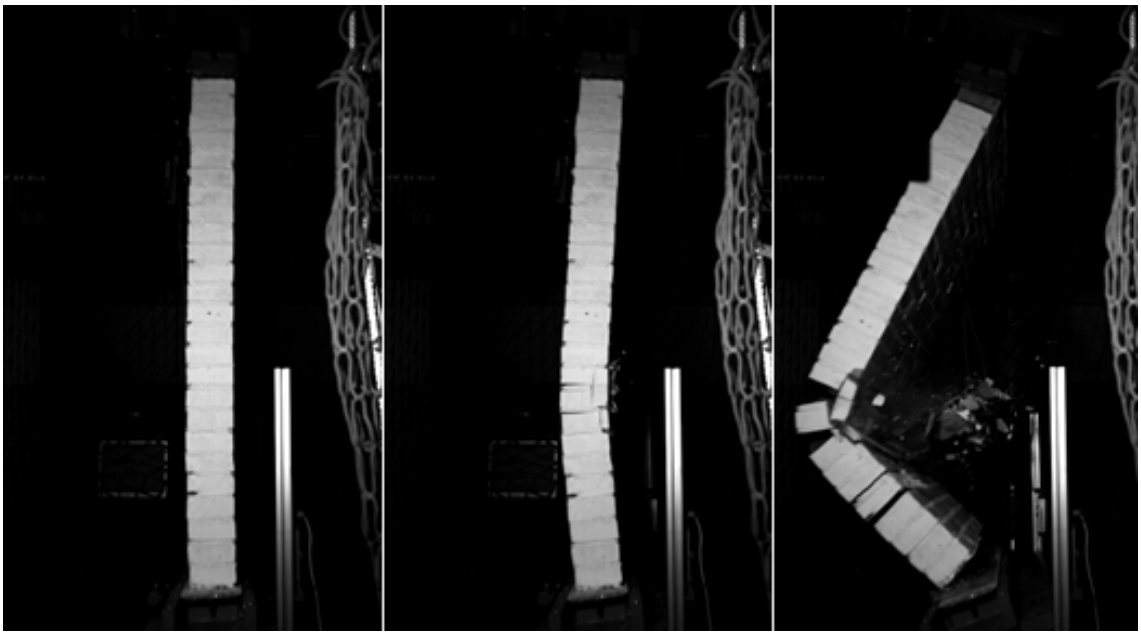

Figure 3.17 Failure mode of wall W#14. Crushing of the compressed side mixed with the tensile opening of two joints to form a mechanism

In the following analysis, the results of wall W#5 were not taken into account because they show an anomalous response that is inconsistent with the rest of the H-series walls. As expected, the results show that the load-bearing capacity decreases significantly with the increase of the load eccentricity and the slenderness (see Figure 3.18 and Figure 3.19). For an actual eccentricity of approximately 16% of the wall thickness, changing the slenderness from 9.1 to 14.1 or 21.7 causes a loss of the load-bearing capacity of 35.5% or 96.3%, respectively. Similarly, the load-bearing capacity of the walls in the H series (with a theoretical slenderness of approximately 21) decreases by approximately 75% if the eccentricity is increased from 0.3% to 16.1% of the wall thickness.

The load-bearing capacity decreases by approximately 80% if the eccentricity is increased from 5% to 25.6% of the wall thickness for M-series walls. Furthermore, a non-linear force out-of-plane displacement response is observed (see Figure 3.19), especially from out-of-plane displacements over 6% of the wall's thickness (t).

The results in Figure 3.20 exhibit a linear relationship between the vertical displacement of the walls and their maximum load-bearing capacity. As the results in Figure 3.21 show, the descending displacement of the wall's top section at the failure instant depends on the initial eccentricity at mid height (which, if the alignment of the hinges is not taken into account, is equal to e/t-d/2t). Practically, the

experiments show that, for a fixed slenderness, the vertical displacement required to cause the collapse of the wall decreases with an increase in eccentricity. Slenderness also affects this relationship.

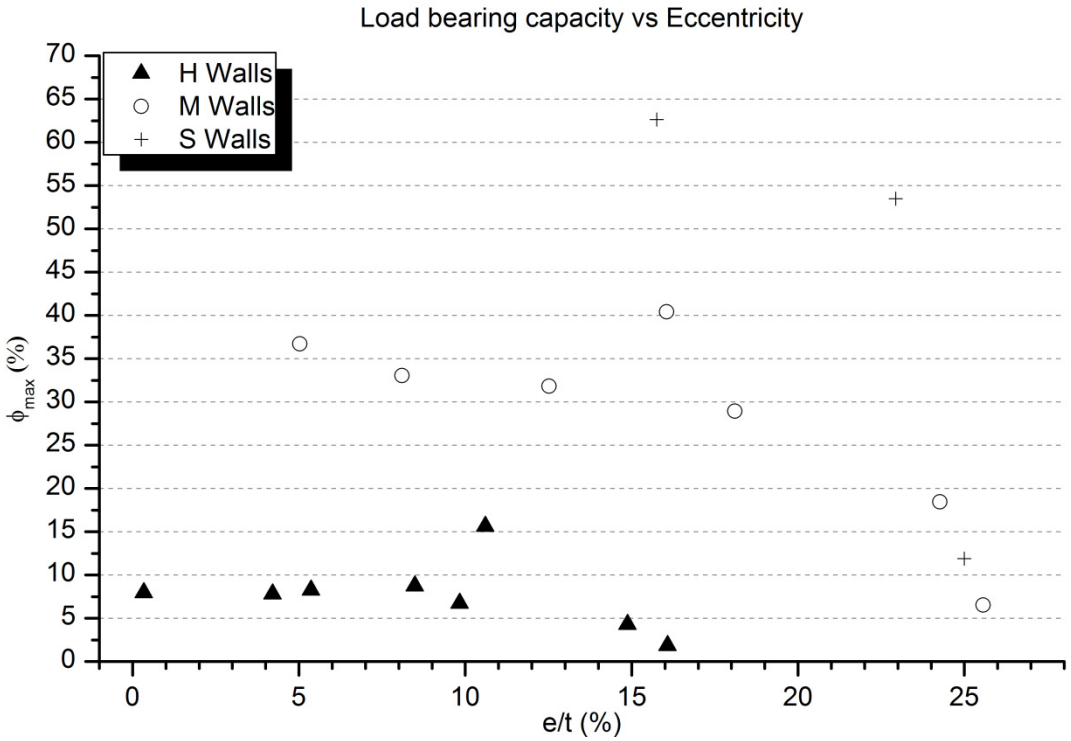

Figure 3.18 Experimental relationship between eccentricity and load-bearing capacity for three different theoretical values of slenderness corresponding to wall geometries H, M and S.

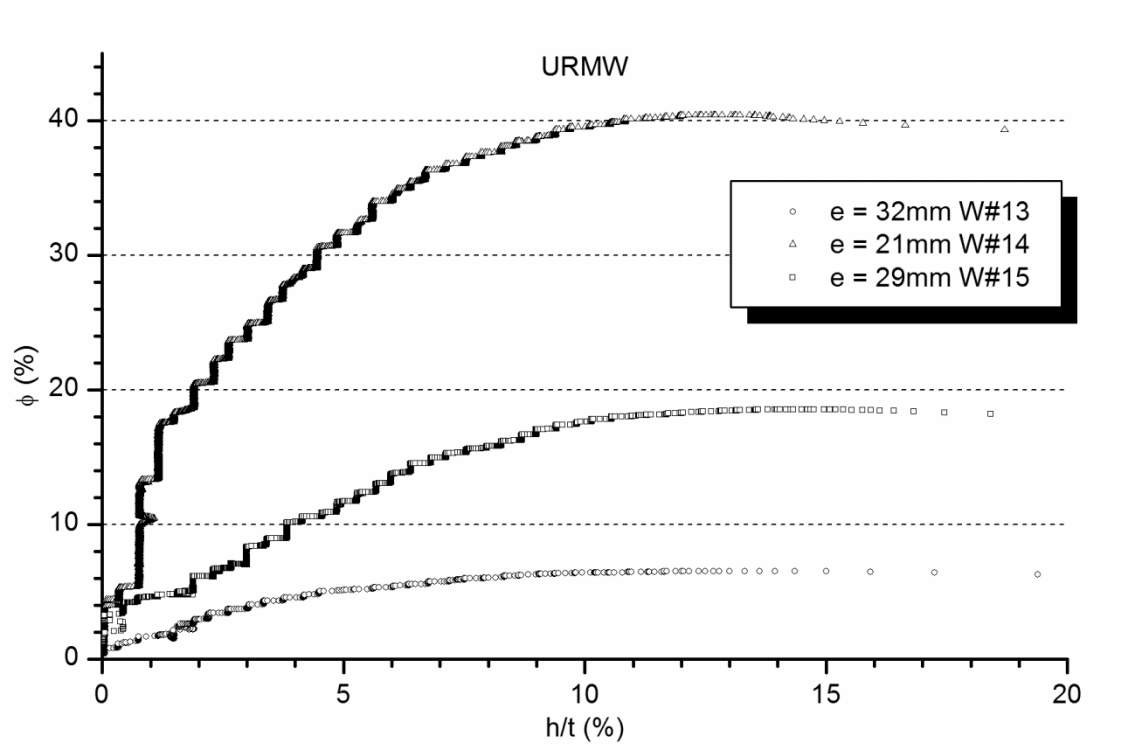

Figure 3.19 Dimensionless force (ϕ) vs. dimensionless out-of-plane displacement (h/t) for three close comparable eccentricities in M series.

The results differ between walls from series H, M and S, as shown in Figure 3.21. For example, an increase of the normalised initial eccentricity (without the hinge-misalignment effects) from 4.2% to 20.8% causes a reduction in the vertical displacement needed to reach failure from 2.5% of the effective height to 0.5% in H-series walls (i.e., a reduction of 80%). A similar behaviour is observed for the M-series walls. As shown in Figure 3.21, an increase in the normalised initial eccentricity from 3.1% to 24.8% causes a 63% reduction in the vertical descending movement needed to cause the failure of an M-series wall, which is less than for H series. As for the results in Figure 3.20, these results are consistent with the fact that most of the walls, as mentioned, failed because of geometric instability.

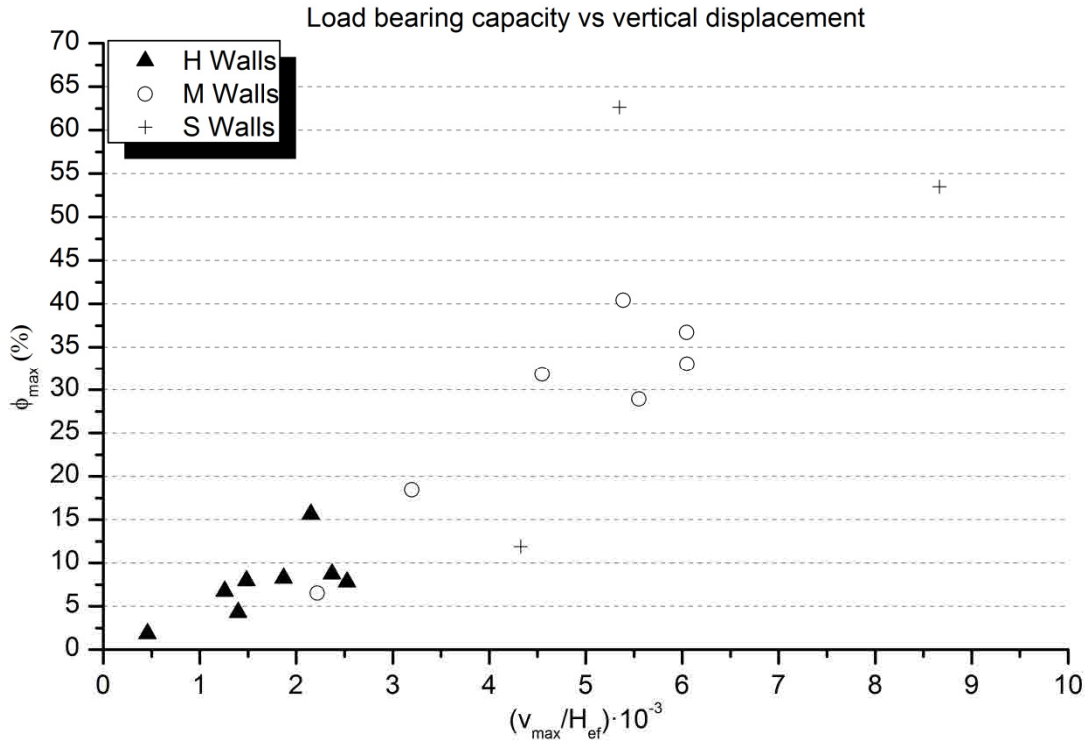

Figure 3.20 Experimental relationship between downward displacement at maximum load and load-bearing capacity for three different theoretical values of slenderness corresponding to wall geometries H, M and S.

The experimental results show that the initial shape (eccentricity) affects both the load-bearing capacity and the vertical deformation at the instant of failure. This effect increases with the slenderness of the wall.

The graph in Figure 3.22 is provided as an example. In this graph, it is clear that the in-plane behaviour included an initial settling stage, followed by a proportional force-descending movement relation which finished with a softening process after the collapse load. The behaviour was approximately the same for all unreinforced walls.

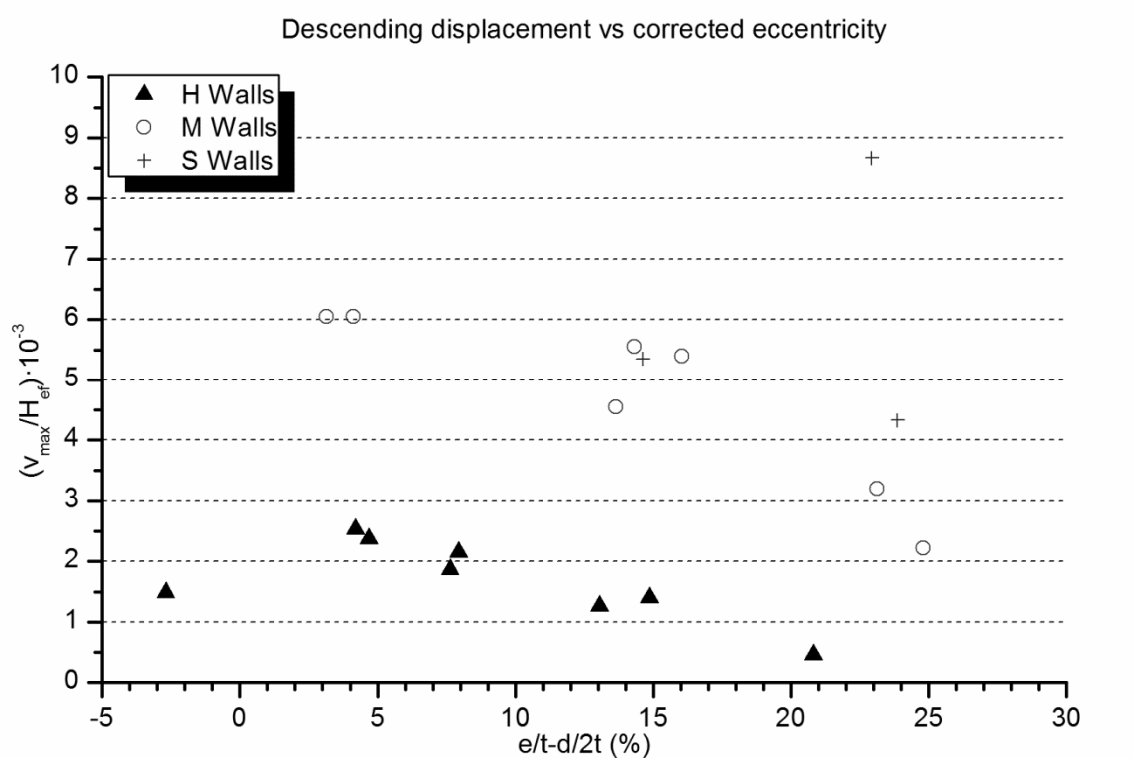

Figure 3.21 Experimental relationship between actual eccentricity (not taking into account hinge alignment) and the descending vertical displacement at maximum load for three different theoretical values of slenderness corresponding to wall geometries H, M and S.

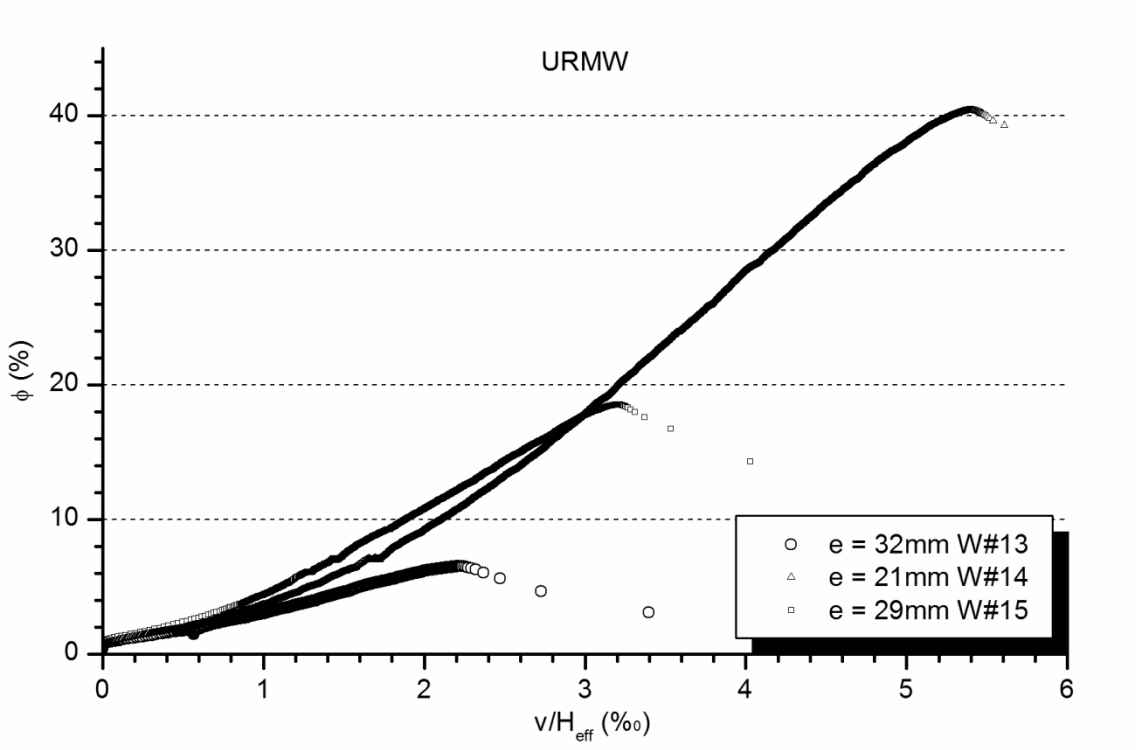

Figure 3.22 Dimensionless force (ϕ) vs. dimensionless in-plane displacement (v/H_{eff}) for Unreinforced Masonry Walls (URMW)

The obtained results provide useful information. The corresponding scattering could be attributed to the lack of homogeneity in the properties of the component materials (see Table 3.1 and Table 3.2), the manual procedure used to build the walls and/or the variation in the curing processes. The tests performed on the material components resulted in coefficients of variation slightly higher than those found in literature. The vertical position of the walls during the construction and the manual brick layering may also explain some of the scattering compared with other test studies (e.g.,[73]). In addition, imperfections in the walls' geometry were measured and may partially explain the scatter in the results. These imperfections are acceptable according to the current manufacturing standards recommendations. The air curing conditions may also explain part of the scattering. Some of the walls were built and cured in summer outdoor conditions, whereas others were produced in winter conditions, both indoors and outdoors.

The scattering in the results is comparable to the scattering typically observed in similar studies [67,69]. Although this scattering is significant, these tests are more close to represent actual masonry structures than strict laboratory-controlled tests. The data obtained in this study are representative of real structures and the relationships with eccentricity and slenderness exhibit the same trends reported in previous research. Nonetheless, the scattering should be taken into account when analysing and comparing these results.

Using two mechanical hinges in the experimental design has proved to be advantageous for the purpose of validating the numerical tools (presented in Chapter 4) because the boundary conditions are more precisely known and can be more accurately modelled.

3.4.7. Description and results of the tests on TRM Strengthened Walls

Two different failure modes were observed during the tests on TRM strengthened walls. Two of the walls (W#21 and W#23) failed due to the second order bending effects and the geometric instability or buckling. In these cases, a horizontal crack was generated at the mid-height on the tension side (see Figure 3.23) turning the structure into a mechanism. The rest of the TRM strengthened walls (W#22 and W#24-W#29) failed by shear-compression mixed mode near the upper or the lower ends (see Figure 3.24).

In order to compare the experimental results of different walls, the dimensionless variables previously defined in section 3.4.6 have been used. They are the load bearing capacity ratio, ϕ, the dimensionless mid-height lateral deformation out of the thickness, h/t, and the descending displacement of the upper hinge out of the effective height, v/H_{eff}.

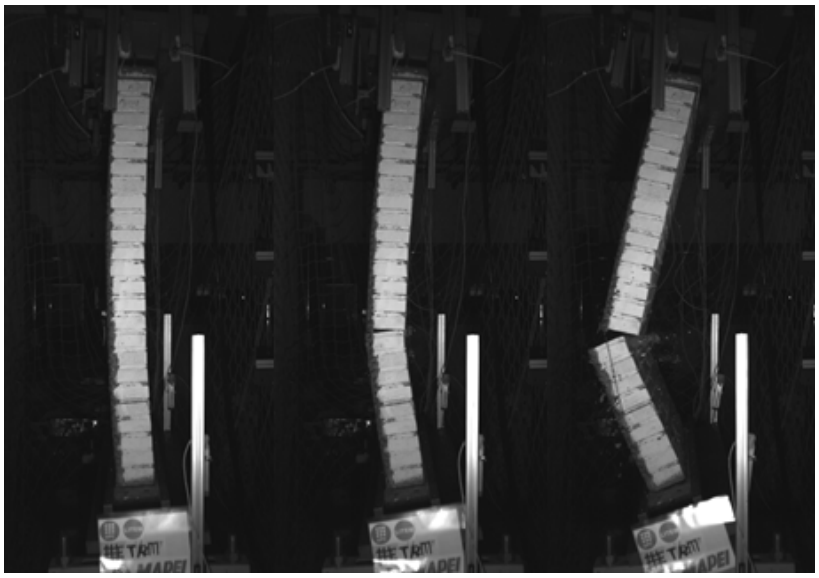

Figure 3.23 TRM strengthened wall W#21. Buckling failure mode

The comparison of the experimental results is shown in the graphs corresponding with Figure 3.25 to Figure 3.31. In these graphs, the real mid-height eccentricity, *e*, was calculated using the measurement of the real shape of each wall. The load-bearing capacity increase, which is associated with the application of the TRM, is summarised in Table 3.10. This increase is calculated by comparing the capacity of each strengthened wall with the average of the load-bearing capacity of the unreinforced walls which had close real eccentricity values (W#13 and W#15) to that considered in the tests on TRM strengthened walls.. In Table 3.10, the TRM system codification includes the mesh type (G: glass fibre or C: carbon fibre), the mortar type (P: Planitop HDM Maxi, C: Planitop HDM Restauro or X: XMesh M25), the number of fibre grids (1 or 2) and the number of connectors (0, 6 or 9).

Figure 3.24 TRM strengthened wall W#22. Upper edge compression failure mode

Wall	*TRM system*	*Fibre layers*	*Connectors*	N_{max} *(kN)*	*Load-bearing capacity increase (%)*
W#21	G_P_1_0	1	0	299.7	87
W#22	G_P_1_0	1	0	328.6	105
W#26	G_P_2_0	2	0	390.3	143
W#23	G_C_1_0	1	0	270.9	69
W#24	G_C_1_0	1	0	285.6	78
W#25	G_C_2_0	2	0	414.0	158
W#27	C_X_1_0	1	0	345.7	116
W#28	C_X_1_6	1	6	313.5	96
W#29	C_X_1_9	1	9	330.2	106

Table 3.10. Load-bearing capacity increase by the application of TRM strengthening system

In Figure 3.25 and Figure 3.26, the effect of placing two fibre grids is noticeable as an increase of the load-bearing capacity and the wall's out-of plane stiffness. For the cases strengthened with one fibre grid (W#21-24) the lateral deformation was proportional to the applied load up to a lateral deformation around the 10% of the wall's thickness (*t*). This linear response was observed up to a lateral deformation of 3% of the wall's thickness for the walls strengthened with two fibre grids. The Figure 3.27 presents the influence of using connectors on the lateral displacement. It is remarkable that placing connectors increases the out-of-plane stiffness but seems not to affect the load-bearing capacity.

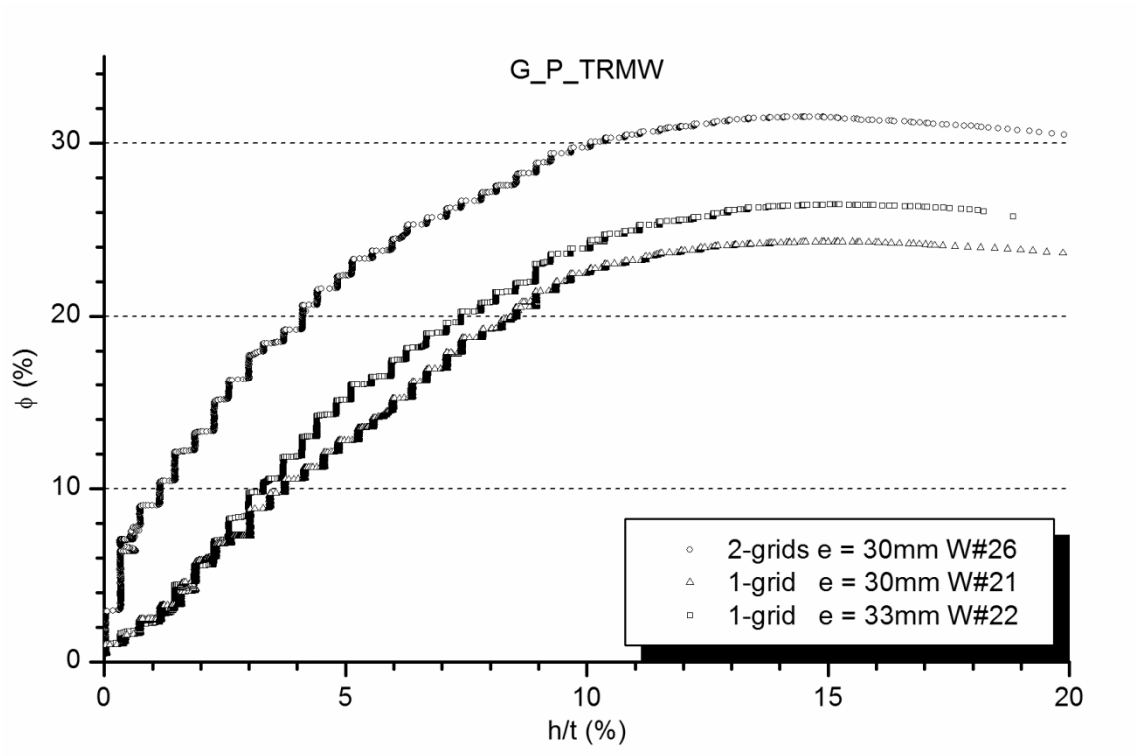

Figure 3.25 Dimensionless force (ϕ) vs. dimensionless out-of-plane displacement (*h/t*) for glass fibre grid and Portland based mortar (G_P_TRMW strengthening combination)

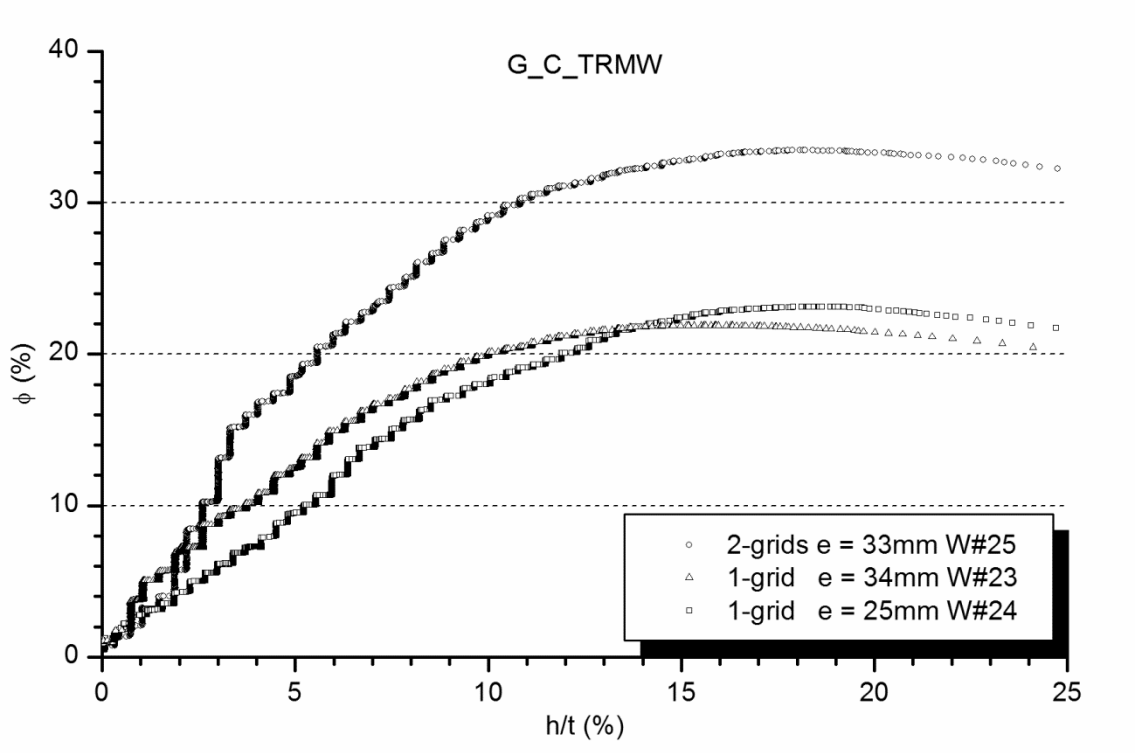

Figure 3.26 Dimensionless force (ϕ) vs. dimensionless out-of-plane displacement (h/t) for glass fibre grid and lime based mortar (G_C_TRMW strengthening combination)

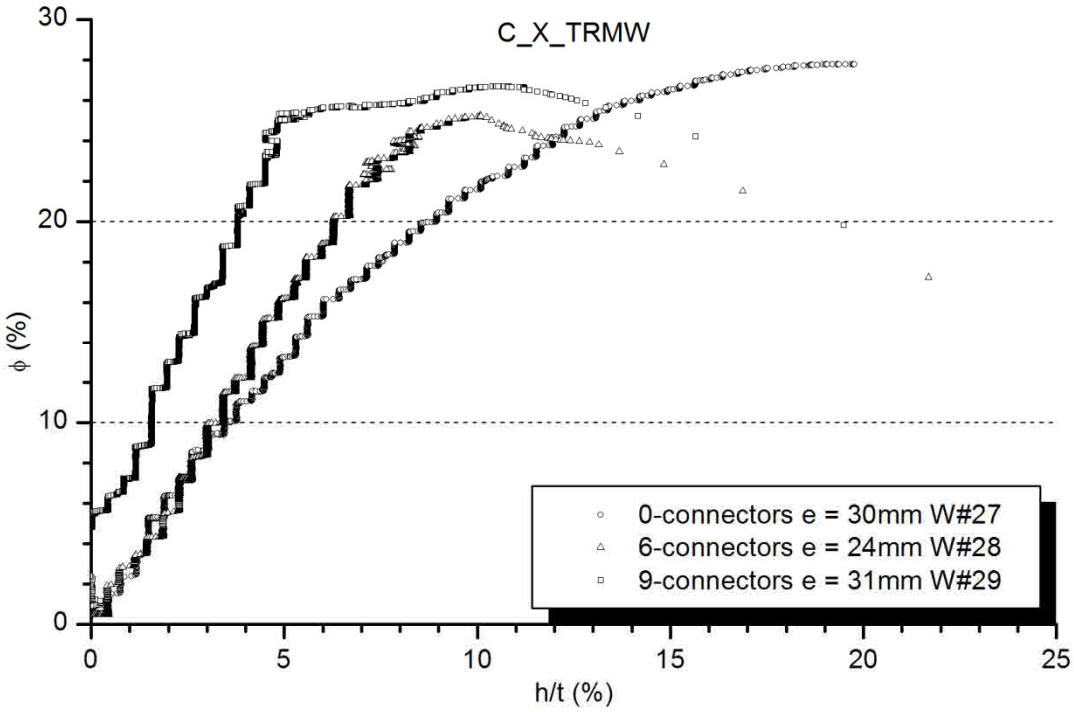

Figure 3.27 Dimensionless force (ϕ) vs. dimensionless out-of-plane displacement (h/t) for carbon fibre grid and Portland based mortar (C_P_TRMW strengthening combination)

The number of fibre grids seems not to influence the in-plane response of the walls strengthened with glass fibre and Portland based mortar (see Figure 3.28). However, those walls strengthened with lime-base mortar and glass fibre grids (see Figure 3.29) shows relationship between the number of installed grids and the in-plane stiffness. Those with one grid (W#23-24) presented greater in-plain deformations than that with two fibre glass grids (W#25). Similarly, it seems that placing connectors is related with a stiffer in-plane response (see Figure 3.30).

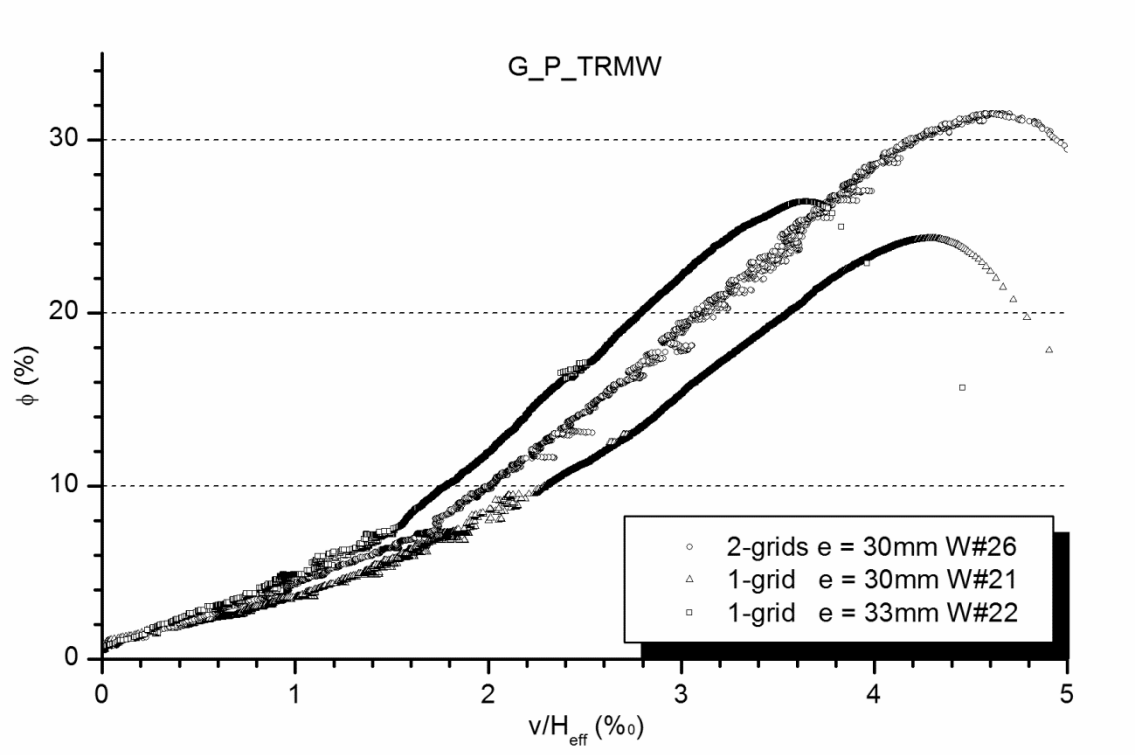

Figure 3.28 Dimensionless force (ϕ) vs. dimensionless in-plane displacement (v/H_{eff}) for glass fibre grid and Portland based mortar (G_P_TRMW strengthening combination)

The wall's response near the collapse load strongly depends on the strengthening system. This can be observed in Figure 3.31, where the curves corresponding with a strengthening system (G_P_TRMW, G_C_TRMW and C_X_TRW) are gathered together and they show a gap with the curves of the other TRM systems for the largest strains. The strain, which was measured at the wall's central position on the strengthened side near the collapse load, shows similar values for the two cases with the same strengthening (W#21 vs. W#22 and W#23 vs. W#24) independently from the observed failure mode. However, the failure mode might be directly related with the structural response observed at the beginning of the loading process. Figure 3.31 shows that the walls which failed by compression at their ends (W#22 and W#24) present smaller strains in the strengthening system than comparable walls which collapsed by reaching the TRM tensile strength (W#21 and W#23) for the same in-plane displacement.

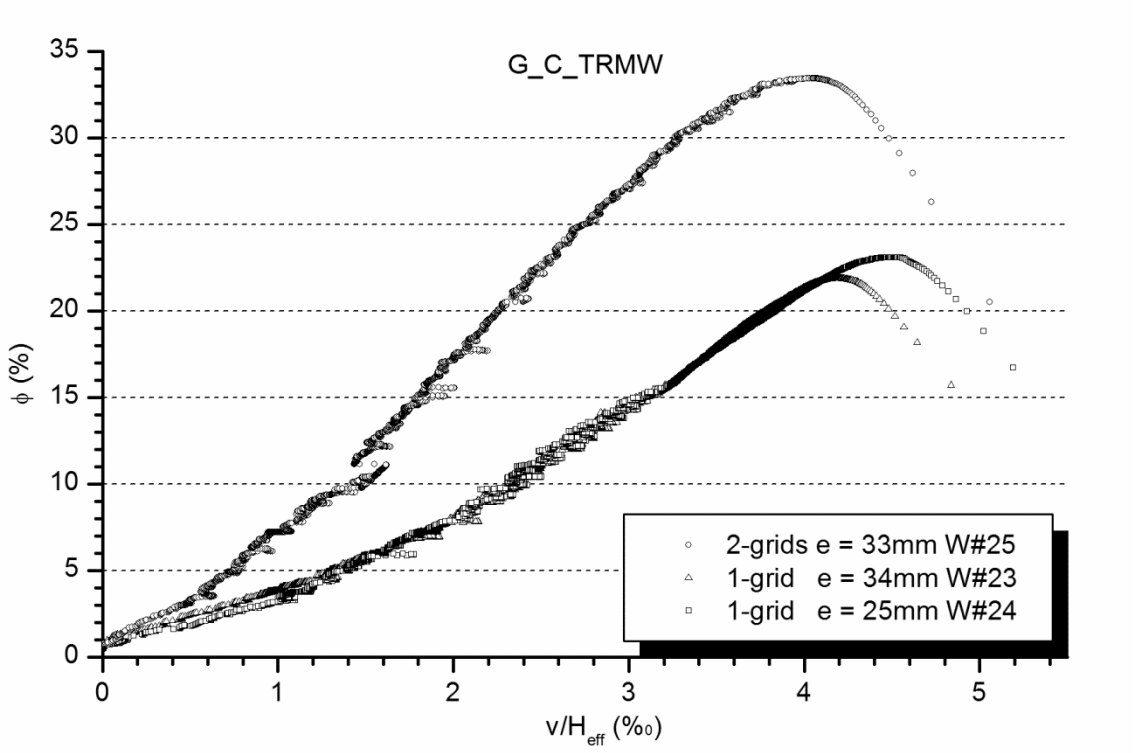

Figure 3.29 Dimensionless force (ϕ) vs. dimensionless in-plane displacement (v/H_{eff}) for glass fibre grid and lime based mortar (G_C_TRMW strengthening combination)

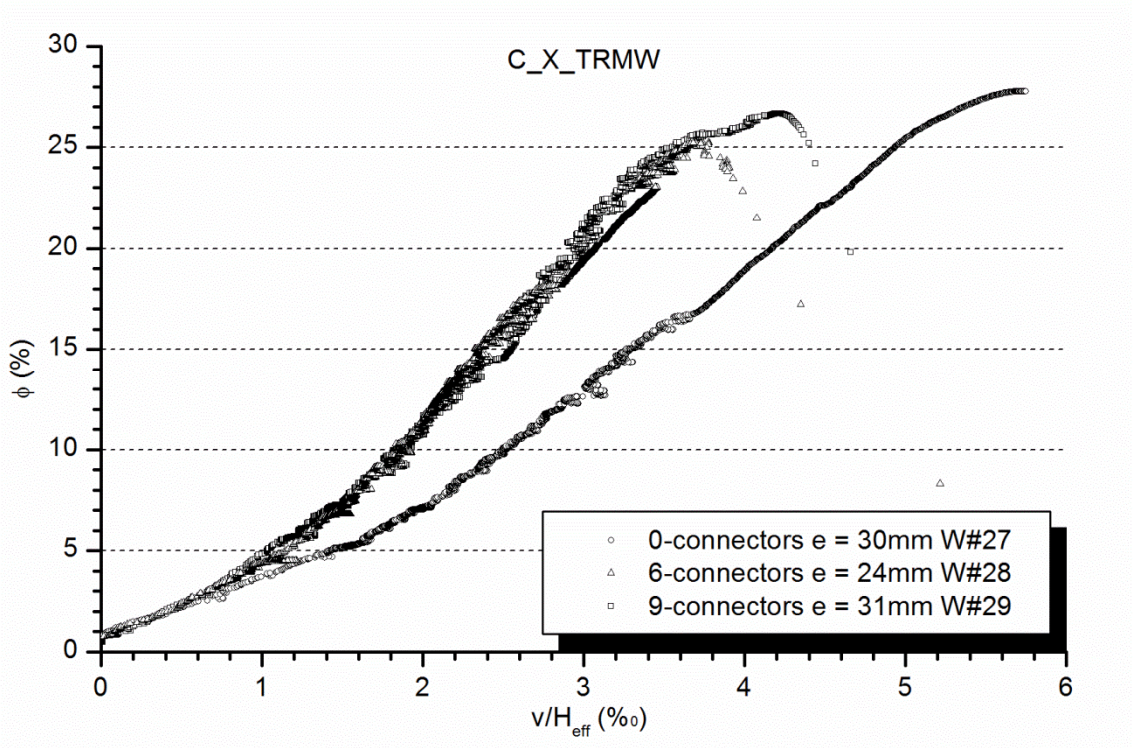

Figure 3.30 Dimensionless force (ϕ) vs. dimensionless in-plane displacement (v/H_{eff}) for carbon fibre grid and Portland based mortar (C_P_TRMW strengthening combination)

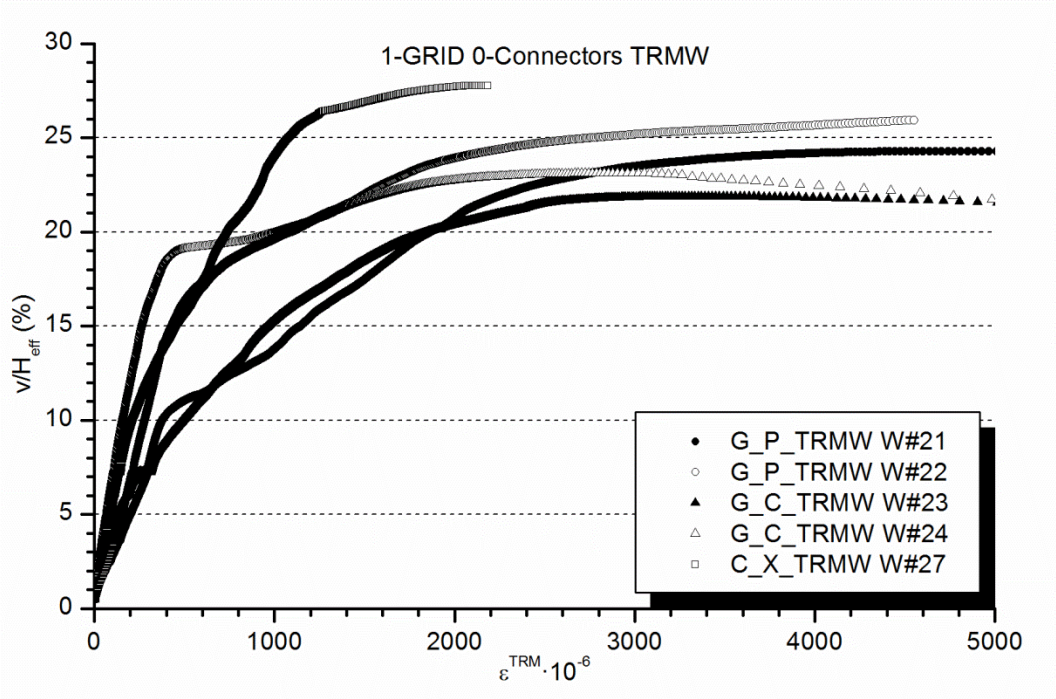

Figure 3.31 Dimensionless in-plane displacement (v/H_{eff}) vs. experimental strain (ε^{TRM}) at wall's central point

3.4.7.1 Comparison with URMW

Walls W#13 and W#15 are the two non-strengthened unreinforced masonry walls, URMW, which have the same theoretical eccentricity (30mm) as the series of the TRM strengthened walls (W#21-W#29). Thus, the load-bearing capacities of the TRM strengthened walls are only compared with the average result of W#13 and W#15 (P_{max}=160.3kN) because these walls have comparable boundary conditions (same eccentricity at wall's ends). This comparison is aimed to evaluate the load-bearing capacity increase associated with the application of different TRM strengthening systems. The eccentrically applied axial load which was resisted by each TRM strengthened wall has been summarised in Table 3.10. The average increase of the load-bearing capacity is over 100% when using TRM.

Some practical implications arise from these experimental results. To begin with and regarding the analysis of the type of fibre grid, it can be concluded that applying a glass fibre grid is close to an optimised strengthening solution for the used testing configuration. It is noted by comparing the results of walls W#21-24 and W#27. This conclusion is based on the fact that both failure modes (reaching the ultimate tensile strength of the TRM system, Figure 3.23, and failing by shear-compression near the wall's ends, Figure 3.24) were observed when testing walls W#21 to W#24. Thus, the glass fibre grid showed enough performance to mobilise the maximum shear-compressive strength of the masonry in this particular test setup and no more fibres seem necessary. Moreover, by comparing the manufacturer's properties of the fibre grids, it is noticed that the tensile strength of the carbon fibre grid is far higher than the tensile strength of the glass fibre grid. This indicates that the masonry would always fail far before

reaching the carbon fibre TRM tensile strength, as experimentally observed. In conclusion, one glass fibre grid (comparable with those used in the current research) might set the limit of the amount of fibres needed to strengthen the designed walls with TRM.

In relation with the number of applied fibre grids, by comparing walls W#21-26 it is noted that placing two fibre grids inside a single mortar layer does not notably increment the maximum load-bearing capacity of the walls because the failure mode becomes associated with the shear and compressive strengths of the brick masonry. However, it has been observed that placing two fibre grids causes a stiffer in-plane response of the wall when eccentric axial loads were applied (see Figure 3.28 and Figure 3.29).

By analysing the effect of the plastering mortar, it has been observed that improving the mechanical properties of the used mortar might lead to stiffer in-plane behaviour of the wall. This is noticeable by comparing Figure 3.28, Figure 3.29 and Figure 3.30.

In the same way, placing connectors seems to increase the in-plane stiffness of the wall (see Figure 3.30). However, as no adherence problems between the strengthening mortar and the masonry were noticed in the experimental campaign, the use of connectors seems unnecessary for strengthening structural masonry walls against buckling phenomena. Moreover, using connectors might be, even, unsuitable if regarding to the practical problems found at casting mortar inside the connectors or at bending these connectors to embed them into the mortar layer. It is also remarkable that the connector's holes seem to guide the creation of weaker failure surfaces when the walls fail by compression at their ends.

By comparing the strain of all analysed TRM systems on the whole (see Figure 3.31), it is noticed that the cases are divided into groups depending on the later on observed failure mode if taking into account the data at the beginning of the tests (low loading levels). In contrast, the same cases are divided into different groups depending on the applied TRM system if observing the data near the collapse load. Thus, the information acquired during the first loading steps might be useful at predicting the failure mode but it cannot be used to distinguish between different strengthening systems. In conclusion, taking into account that the failure mode could be related with the mid-height TRM's strain growing at the beginning of the tests, an early failure mode detection procedure based on the structural response at low loading levels might be implemented.

Regarding the performance increase when strengthening the walls with TRM, it is noticed that the initial linear response lasts more for the strengthened walls than for the unreinforced masonry walls (see Figure 3.19, Figure 3.25, Figure 3.26 and Figure 3.27). In addition, the TRM also contributes to a stiffer response of the out-of-plane deformation. Hence, the TRM strengthening technique seems to be a good option to linearize the out-of-plane behaviour and to stiffen the wall's response in this direction. Improving the TRM's mortar, increasing the number of fibre grid layers or placing connectors might also contribute to the increase of the in-plane stiffness. Moreover, and even more important, using TRM

brings a more uniform response in comparison with URMW cases (in the sense of reducing the scattering of the results). This fact might make it possible to optimise the design of TRM-strengthened masonry structures and to increases the confidence on the mechanical response of these elements.

Regarding the increase of the load-bearing capacity of URMW when applying TRM strengthening systems (Table 3.10), it is remarkable that an average increase of 100% is obtained. This satisfactory result is even more significant taking into account that the failure mode changed from buckling/second order bending failure to masonry shear-compressive collapse. It seems to prove that TRM is highly effective at strengthening masonry walls in front of instability effects. However, a careful approach to the design or assessment of TRM strengthened masonry walls is required because several failure modes are possible and have to be taken into account by the practitioners.

3.5 Conclusions

The present experimental campaign has allowed fulfilling one of the main aims of the present investigation, consisting of contributing with new experimental evidence on the structural response of unreinforced and TRM strengthened walls under eccentric compressive loading.

The tests on mortars (143 compressive tests and 269 flexural tests) have proved the high performance of the strengthening mortars developed to be applied as part of the TRM. In particular, their high flexural strength, which might be associated with the presence of microfibers in the mortar composition, has to be mentioned.

Regarding the tests on bricks, it can be concluded that using a concrete formulation for calculating the tensile strength of the bricks from their flexural strength has provided accurate data if observing the results of the simulations summarised in Chapter 4. This agrees with previous investigations carried out by other researchers. In addition, using sulphur mortar to uniform the contact surfaces of the bricks used in compressive strength tests has proved to be an effective alternative to the proposed cement mortar overlaying.

Analysing the masonry characterisation tests, some conclusions arise. By comparing the experimental results with literature values, it can be concluded that the non-conventional testing configuration used to obtain the compressive strength and the Young's modulus of the masonry provided accurate results. In addition, the proposed methodology for obtaining the Young's modulus, which is presented for the first time herein, has reached good results. The ratio of the Young's modulus out of the compressive strength of the masonry is extremely low if compared with the correlations suggested by the standards but it fits other authors' references. Thus, it is concluded that the masonry composed of solid clay bricks and low-strength mortar is more flexible than the one calculated accordingly with the current standards. In addition, it has been observed that the brick-mortar adherence highly depends on the used mortar.

Finally, the results on the characterisation tests show a significant scattering for the materials' properties, specially the Young's modulus of masonry. This fact demonstrates the complexity of this material and justifies the need to carry out the proposed experimental campaign. It is believed that the results show the real scattering of this particular masonry because market materials and real building conditions have been considered. In part, the scattering of the results might be due to the relevant scattering associated with the low strength mortar used for brick layering.

Focusing on the full-scale tests, it is concluded that the designed experimental campaign on unreinforced masonry walls achieved the aimed goals as the geometric instability was the direct failure cause in 17 of the 20 tests. In addition, the use of the pinned-pinned configuration for testing real scale walls has shown to be an efficient and clear way to set well-known boundary conditions. Clearly know boundary conditions are necessary for an adequate validation of the numerical models presented later on.

The experimental evidence show that the descending displacement of the wall's top section at the failure instant depends on the initial eccentricity at mid height. Thus, the vertical displacement required to cause the collapse of the wall decreases with an increase of the eccentricity. From the results, it is concluded that this relationship is more evident for the most slender unreinforced masonry walls. Moreover, the study of the influence of the walls' slenderness and the load eccentricity has shown that the load-bearing capacity of the strengthened walls is less dependent on these parameters than the unreinforced ones.

From a qualitative point of view, it can be concluded that different failure modes are possible: the joint opening and mechanism formation for the unreinforced walls, the TRM tensile failure, the masonry crushing in compression and the shear-compressive masonry failure near the wall's ends for the TRM-strengthened walls. Each failure mode is more or less likely depending on the wall geometry, the eccentricity of the load and the strengthening pattern according with the results presented.

Finally, some conclusions have been obtained in relation with the TRM effectiveness. These are:

- Using the TRM strengthening system tends to make the wall's behaviour more uniform and to reduce the out-of-plane non-linear response.
- The strengthened brick masonry characterisation tests proved that the tensile capacity of the fibre grid is not always mobilised. The proposed effectiveness ratio, *ER*, is a useful tool to characterise the performance of each mortar and fibre grid combination.
- The combination of carbon fibre grids with pozzolanic mortar does not fully mobilise all the capacity of the carbon fibres because of adherence problems between the mortar and the fibre grid. In contrast, the TRM configurations with glass fibre grids correctly worked as expected.
- The initial linear response of the walls lasts more for the strengthened walls than for the unreinforced masonry walls.

- Using two fibre grids embedded into one mortar layer provides just a slightly higher load-bearing capacity and a noticeable increase of lateral stiffness. However, the in-plane stiffness is reduced when placing two fibre grids embedded into one layer of the most deformable strengthening mortar.
- Applying one glass fibre grid, like the one used in the current research, is an optimised strengthening solution for the testing configuration because it showed enough performance to mobilise the maximum shear-compressive strength of the particular studied masonry.
- Using connectors makes no difference in the load-bearing capacity because the debonding failure mode has not been observed in the studied cases. However, placing connectors increases the lateral and in-plane stiffness of the TRM strengthened wall.
- Improving the mechanical properties of the strengthening mortar leads to a stiffer in-plane behaviour of the wall.

In addition, the experimental evidence point out that the wall's response near the collapse strongly depends on the strengthening system whereas the failure mode might depend on the wall's response at low loading stages.

Based on the obtained results, it is concluded that the TRM is an effective strengthening method against the geometric instability and the failure modes associated with second order bending phenomena. It is remarkable that the TRM strengthening method provides an average increase of the load-bearing capacity over 100%. This increase reached 158% for the most effective case. Thus, for the first time, the TRM has proved its effectiveness at strengthening brick masonry walls against second order effects and buckling phenomenon.

Finally, it has to be remarked that all the obtained data are useful for the comparison with the numerical and analytical tools presented in the following chapters.

4

Finite Element Analysis

4.1 Introduction

In the last decades Finite Element Analysis (FEA) has proved its performance at solving structural problems. However, using FEA to model masonry structures is not a general practice yet and most of these applications are limited to in-plane compressive cases which do not consider second order effects. The first reason which might explain this fact is the complexity of the structural problem: masonry is an anisotropic, non-linear and heterogeneous material whose properties are characterised by a large uncertainty due to its manual in-situ fabrication; load-bearing masonry walls are commonly affected by geometric non-linearity (buckling). In addition, there is little experimental information if comparing with other materials the masonry competes to. Thus, there is a lack of an efficient model capable of simulating real-scale structures like buildings, bridges, etc. at a relatively low computational cost.

Moreover, using textile composites with cementitious matrix (TRM) is a relatively new strengthening technique. This method has been tested on masonry with successful results (see [47,48,56,57]). However, there is not an internationally accepted model to deal with the simulation of TRM-strengthened masonry structures.

Developing a simplified FEA model, which should be capable of accurately predicting the load-bearing capacity of strengthened and non-strengthened masonry walls, is one of the aims of the present research. There are many models which have already represented masonry with detail, see [34,38,90]. However, in the current research it is not intended to reproduce the masonry behaviour in a very detailed way, but to describe the structural response of masonry walls in a simple and sufficiently accurate manner. The developed model should be easily implementable under the most common commercial finite element packages.

The implemented model is described at the beginning of this chapter (section 4.2). Then, it is validated by comparison with the experimental tests presented in Chapter 3 (subsections 4.3.1 to 4.3.3). Finally, the model is used to theoretical cases with the aim of enhancing the experimentally-acquired knowledge.

Results are summarised and commented in this chapter. Extended information of all simulations is presented in Annex 2.

4.2 Model definition

The implemented model assumes the hypothesis of plane strain. It is a bi-dimensional (2D) simplification of the three-dimensional (3D) real case. Using a 2D simplification reduces the computational cost of the analysis and eases the definition of the materials and contacts. The plane strain hypothesis requires a uniform definition of the problem along the perpendicular direction to the simulated section. For the particular case of compressed masonry walls, this means that the load is uniformly applied along the wall's width. In addition, the strains in the perpendicular direction to the analysed plane are supposed to be negligible. This hypothesis is closer to the real situation for the wider walls. Thus, the model herein presented might be not suitable for calculating masonry piers.

Simplified micromodelling has been used. This approach performs better than most of the homogenised models, in which the masonry is assumed to be a unique continuous material. The simplified micromodelling does not need so much information as detailed micromodelling, which represents bricks, mortar and interfaces separately. Hence, the proposed method is something intermediate. It models each brick together with the surrounding mortar as a homogenised material. Interfaces are set to define the contacts between the objects that represent each masonry row (see the definition of simplified micromodelling in Chapter 2). This approach saves half the contacts and the material definitions and thus, eases the convergence of the numerical simulation.

Finally, the model was defined to calculate the structure considering large deformations to accurately represent the buckling phenomena.

The model has been implemented using ANSYS® v.12.1. All required parameters are provided in this section and the corresponding annex (Annex 2) in order to allow reproducing the simulations using other finite element analysis packages. Materials, contacts and geometric definitions have been set as general as possible to assure that the model can be reproduced. The definition of the contacts, which is required to achieve accurate results, is the most complex part of the proposed model.

4.2.1. Geometry modelling

The 2D geometry consisted of as many piled rectangular parts as masonry rows were in the wall. In addition, for those walls with TRM strengthening, supplementary rectangular bodies placed next to the ones which represented the masonry rows were used. Two extra bodies, one triangle in each end of the

wall, were defined to represent the hinges, correctly place the load application point and set the rotation axes. The simplification of the hinges and the wall modelling is represented in Figure 4.1. This simplification was oriented to correctly simulate the real boundary conditions in a simple way. Obviously, the hinges were not accurately modelled so the analysis of these parts of the testing machine was not possible with the proposed model. The testing machine was not taken into account in the finite element analysis except for the steel hinges which determined the boundary conditions of the real tests. Thus, the definition of these supports has been considered in the geometry to compare the numerical analysis with the experimental results and accurately validate the model.

Finally, fictitious interfaces were placed in an inclined line crossing and dividing the masonry bodies near the extremes of the TRM-strengthened walls. The two divided parts of each row were in contact one to each other. The aim of these fictitious contacts is allowing the compressive/out-of-plane shear collapse mode experimentally observed in some of the TRM strengthened walls.

Thus, real and theoretical geometries for unreinforced and TRM strengthened walls were studied. In the next subsections the particularities of each case are detailed.

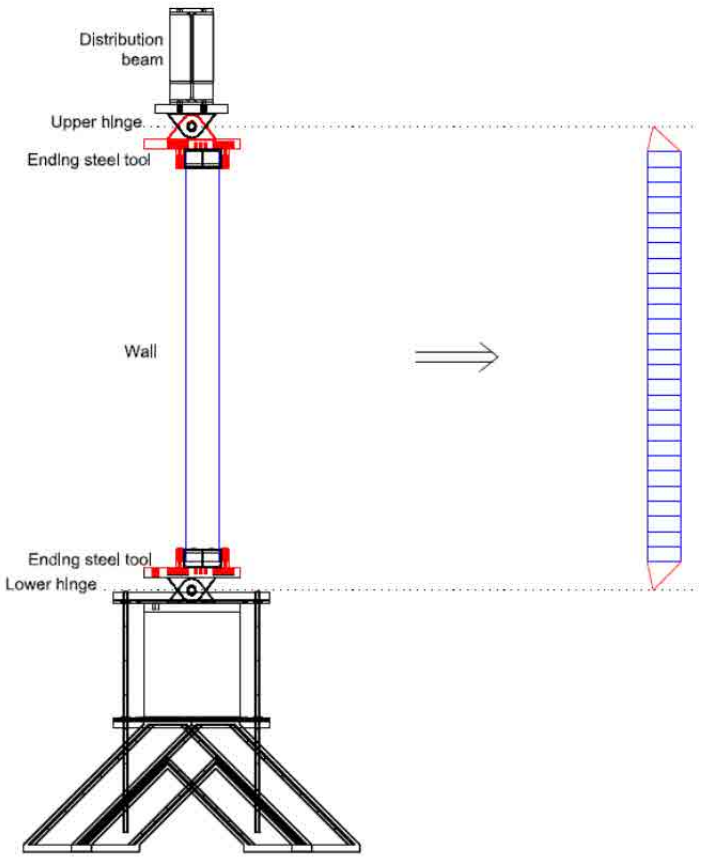

Figure 4.1 Geometric simplification used in the finite element analysis

4.2.1.1 Experimental URMW case

The model's geometry was defined taking into account the experimental measurements of the wall once it was placed in the testing position and before being loaded. The geometry was created using a computer assisted drawing program (in this case AutoCAD® 2011) according to the following steps:

a) First of all, the two points used to define the boundary conditions were drawn. These were the top and bottom vertexes of the triangles which modelled the hinges (red triangles in Figure 4.1). The height of the wall and the lateral alignment of the hinges were the used data.

b) The triangles representing the hinges were completely drawn taking into account the eccentricity at each extreme of the wall.

c) The outline of the wall was drawn considering the real measured initial shape. It has to be remarked that any torsional deviation was neglected because the data used for drawing purposes was the average of the measurements at both edges of the same face of the wall. A constant wall thickness was defined.

d) Once the outline of the wall was defined, this area was split in as many bodies as masonry rows had the wall.

Walls W#1 to W#20 were modelled using a geometry defined according to the method explained in this subsection. A typical geometry of a URMW case is shown in Figure 4.2 left. The colours in this figure are only aimed to distinguish the different bodies.

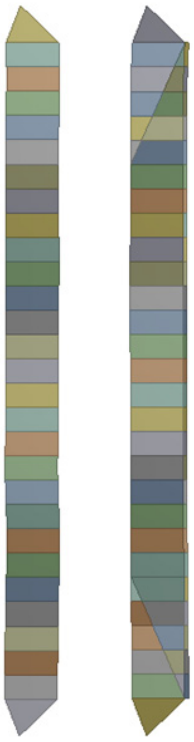

Figure 4.2 Geometry of a URMW (left) and a TRMW (right)

Wall W#4 was an exception: the lower hinge was not modelled in the analysis because it was fixed during the test. In this case, the lower edge of the wall had the displacements constrained simulating the fixed support which corresponded with the testing real boundary conditions.

4.2.1.2 Experimental TRMW case

The general procedure was the same than for URMW but the TRM layer was also drawn. These are the main differences:

- A line, which was set to be equidistant to the tensile edge of the outline of the wall, was drawn in order to represent the TRM layer. This line defined a gap which coincided with the experimentally measured thickness of the TRM at mid-height of the wall.
- The masonry outline and the TRM outline were split in as many parts as masonry rows.
- Finally, the five masonry rows which were closer to the ends of the wall were divided. This division was aimed to allow the compressive/shear failure observed in most of the strengthened walls. Each row was split in two parts by an inclined straight line. The orientation of this dividing line corresponded to the average inclination of the cracking line observed in the experimental collapses of the TRM-strengthened walls.

For comparison purposes, wall W#21 was modelled with and without the inclined division of the masonry parts near the ends.

Walls W#21 to W#29 were geometrically defined with the particularities presented in this subsection. A typical geometry of a TRMW case is shown in Figure 4.2 right.

4.2.1.3 Theoretical URMW cases

Four theoretical URMWs were modelled with the aim of analysing the effect of considering an inclined failure plane near the ends of the wall. It was expected that using this inclined contact did not affect the unreinforced cases which actually failed by mechanism formation.

The general dimensions of the analysed walls corresponded to those of H and M series. One wall with the inclined contact and one without it were defined for each wall's size (H and M series). In contrast with experimental walls, perfectly straight edges defined the outline of these theoretical cases. The hinges were vertically aligned. Hence, the eccentricity was constant along the wall's height.

Walls H0 (H shape with neither strengthening nor inclined contacts), H0S (H shape with no strengthening but predefined inclined failure plane), M0 (H shape with neither strengthening nor inclined contacts) and M0S (H shape with no strengthening but predefined inclined failure plane) were geometrically defined according to the method described in this subsection. The Table 4.1 summarises the characteristics of these walls.

4.2.1.4 Theoretical TRMW cases

Ten TRM-strengthened theoretical walls were analysed with a double aim: (a) determining the influence of predefining a failure plane in the analysis of TRMW; and (b) analysing the effect of modifying the configuration of the TRM (placing more fibre inside a single layer of mortar or installing the TRM system on both sides of the wall). The former aim was achieved by studying four walls, two corresponding with H general dimensions (called HS11 and HS11S) and 2 with M shape (MS11 and MS11S). The second goal required analysing six walls, three for the H shape and three for the M shape. The studied cases were HS12S, HS14S, HS21S, MS12S, MS14S and MS21S.

The Table 4.1 summarises the geometric characteristics of all simulated cases. The codification used to label the theoretical models followed the next criteria:

- First letter: H or M series according to the theoretical shape
- Second symbol: 0 if it was an unreinforced masonry wall and S if the wall was theoretically strengthened with TRM
- Third symbol (optional): Number of sides of the wall which are considered to be strengthened with TRM, 1 or 2
- Fourth symbol (optional): Number of fibre grids installed, 1, 2 or 4.
- Last symbol: an S indicates that an inclined failure plane was predefined and no symbol indicates that the inclined division and the corresponding contacts were not considered.

Case	***Geo m. type***	***Predefined failure plane***	***# strengthened sides***	***# fibre grids***	***TRM thickness***	***Eccentricity at hinges (mm)***	***Hinges alignment (mm)***
W#1	H	No	---	---	---	20	-16.0
W#2	H	No	---	---	---	20	15.0
W#3	H	No	---	---	---	10	10.0
W#4	F	No	---	---	---	---/0	6.5
W#5	H	No	---	---	---	5	7.0
W#6	H	No	---	---	---	25	-12.5
W#7	H	No	---	---	---	10	-6.0
W#8	H	No	---	---	---	10	8.0
W#9	H	No	---	---	---	5	-8.5
W#10	M	No	---	---	---	10	10.5
W#11	M	No	---	---	---	20	10.0
W#12	M	No	---	---	---	10	5.0
W#13	M	No	---	---	---	30	2.0
W#14	M	No	---	---	---	20	0.0
W#15	M	No	---	---	---	30	3.0
W#16	M	No	---	---	---	20	-3.0
W#17	T	No	---	---	---	80	12.0
W#18	S	No	---	---	---	20	3.0
W#19	S	No	---	---	---	30	0.0
W#20	S	No	---	---	---	30	3.0
W#21	M	No/Yes	1	1	13.0	30	0.0
W#22	M	Yes	1	1	8.0	30	0.0

Case	*Geo m. type*	*Predefined failure plane*	*# strengthened sides*	*# fibre grids*	*TRM thickness*	*Eccentricity at hinges (mm)*	*Hinges alignment (mm)*
W#23	M	Yes	1	1	9.5	30	5.5
W#24	M	Yes	1	1	9.0	30	0.5
W#25	M	Yes	1	2	7.5	30	0.5
W#26	M	Yes	1	2	8.0	30	6.0
W#27	M	Yes	1	1	8.0	30	9.0
W#28	M	Yes	1	1	9.0	30	0.5
W#29	M	Yes	1	1	11.0	30	8.5
H0	H	No	---	---	---	20	0.0
H0S	H	Yes	---	---	---	20	0.0
M0	M	No	---	---	---	20	0.0
M0S	M	Yes	---	---	---	20	0.0
HS11	H	No	1	1	10.0	20	0.0
HS11S	H	Yes	1	1	10.0	20	0.0
HS12S	H	Yes	1	2	10.0	20	0.0
HS14S	H	Yes	1	4	20.0	20	0.0
HS21S	H	Yes	2	1	10.0	20	0.0
MS11	M	No	1	1	10.0	20	0.0
MS11S	M	Yes	1	1	10.0	20	0.0
MS12S	M	Yes	1	2	10.0	20	0.0
MS14S	M	Yes	1	4	20.0	20	0.0
MS21S	M	Yes	2	1	10.0	20	0.0

Table 4.1 Geometry definition of the simulated cases

4.2.2. Material definition

Masonry is a complex material which can be defined as a composite. In particular, brickwork is a composite material composed of bricks and mortar. It usually shows an orthotropic response because of the pattern of the joints. Moreover, the tensional response of brickwork is difficult to be represented. Some of the reasons are: its fragile failure; the little amount of experimental data to model the tensile response of different brickwork typologies; the stiffness reduction associated with the joint opening; and the different possible failure modes which would include the brick tensile fracture, the mortar tensile fracture or the brick-mortar bonding failure. The last one is the most common one. Several models have been proposed for modelling the masonry response (see Chapter 2). However, using a sophisticated model of the material behaviour would be in contradiction with one of the main criteria assumed for the construction of the present model, which, as mentioned, is intended to efficiently represent the buckling failure of masonry walls using a commercial FEA software. All used contacts have no thickness.

TRM is also a composite material whose compressive behaviour is mostly influenced by the cementitious matrix. In contrast, the tensile response depends on both the mortar and the fibre grid. For low loads, before the cracking of the mortar, the tensile response of TRM is mostly influenced by the mortar. After cracking the mortar, the fibre grid properties and its adherence with the mortar characterise the tensile behaviour.

The adopted approach to model the materials consisted of defining a homogenised compressive response for each composite material (masonry and TRM) whilst the tensional behaviour was controlled by the definition of contact elements which have neither thickness nor elastic properties.

Regarding the compressive behaviour, brickwork and TRM were both defined as isotropic linear elastic materials with perfect plastic response. Thus, the typical stress-strain diagram has the shape shown in Figure 4.3. The tensile response was controlled by the contact elements (see section 4.2.3) which opened following their own bilinear law.

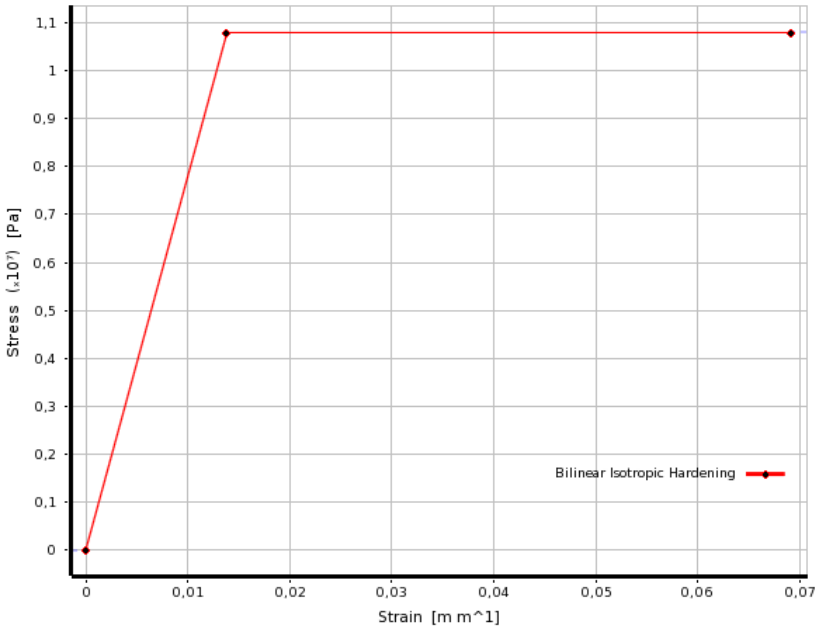

Figure 4.3 Typical stress-strain response used to model brickwork and TRM in compression. The shown values correspond to those used for the brickwork of the theoretical cases and walls W#10-20.

The current steel definition included in the FEA software was used to model the material of the parts corresponding with the hinges (end triangles in Figure 4.2). For all cases, brickwork's density was 1732kg/m^3, brickwork's Young's modulus was 780MPa and brickwork's Poisson's coefficient was 0.35. The two first values were experimentally obtained (see Annex 1) and the Poisson's coefficient was based on values found in the bibliography. Bosiljkov et al. [120] proposed values of Poisson's ratio up to 0.4 for masonry with low content of cement. Moreover, Bosiljkov et al. proposed a relationship between the modulus of elasticity and the Poisson's ratio. It was noticed that the highest Poisson's values correspond with the lowest values of Young's modulus. For this reason, a relatively high value of the Poisson's coefficient (υ=0.35) was used in the current research. Nevertheless, the influence of the Poisson's coefficient on the results is limited. This fact was noticed by using two different values of Poisson's coefficient (0.10 and 0.45) to model H0 case for comparison purposes. The results pointed out that an increase of 450% of the Poisson's ratio was associated with a limited increase of 23% of the ultimate

load. Thus, the ultimate capacity depends on the Poisson's modulus but this dependence is less significative than the influence of other parameters (load eccentricity, slenderness of the wall or Young's modulus). Finally, the compressive strength was 18.2MPa, 12.9MPa, 13.7MPa and 10.8MPa for walls W#1, W#2 to W#5, W#6 to W#9 and W#10 to W#29 respectively. For theoretical walls a compressive strength of 10.8MPa was used.

The compressive behaviour of the TRM was characterised with the compressive variables of the strengthening mortar (Young's modulus and compressive strength). This approach considers that the fibre does not influence on the compressive response of the TRM. As for the brickwork, and knowing that the influence of this variable on the results is limited, the Poisson's coefficient for the TRM was set to 0.35 The density, compressive strength (f_{cm}) and Young's modulus (E) used for modelling each strengthening mortar are summarised in Table 4.2. The values of the first two variables were experimentally obtained and E was provided by the mortar manufacturer.

Strengthening Mortar	***Density (kg/m^3)***	***f_{cm} (MPa)***	***E (MPa)***
Planitop HDM Maxi	1850	42.20	11000
Planitop HDM Restauro	1900	14.53	8000
XMesh M25	1900	34.47	15000

Table 4.2 Mechanical properties for modelling the compressive behaviour of the TRM

4.2.3. Contacts definition

Contacts are defined in order to model the tensile response of brickwork and TRM. All these contacts are initially bonded but some of them have the possibility of debonding or sliding. The tensile and/or shear response of the contact elements, which are supposed to debond and/or slide, is characterised by a cohesive zone model (CZM) that was originally proposed by Alfano et al. [121]. The CZM sets an elastic behaviour up to the brittle failure of the contact. When the tensile or tangential strength is reached, the contact opens or slides while the normal tensile stress or the tangential stress decrease linearly.

The parameters of the CZM required to model the debonding phenomenon are the tensile strength (f_{xt}) and the fracture energy of the first fracture mode (G_f^I). It was considered that the tensile strength might be obtained with a flexural test when this value is used to characterise a horizontal contact of the studied problem (between masonry rows and to define the tensile failure of the applied TRM strengthening system when it depends on the mortar). It is because the walls are mainly bended and the flexural tensile strength could be more representative than the direct tensile strength. The results presented later on support this hypothesis. The maximum shear stress (τ_{max}) and the fracture energy of the second fracture mode (G_f^{II}) are required to model the sliding failure case.

The used contacts might be classified into real contacts and fictitious contacts. The first ones correspond with real masonry joints and interfaces between the TRM and the masonry. In contrast, the second ones are only considered in order to make it possible the observed failure modes. As long as the

materials have been defined in a simplified way, taking into account the real failure modes by defining fictitious contacts is an easy approach which fits in the purpose of the developed FEA. All contacts are defined in the next subsections and summarised in * This value corresponds to the direct tensile strength, not to the flexural tensile strength.

Table 4.3.

4.2.3.1 Real contacts

There are real discontinuity surfaces between masonry rows and between TRM and masonry. These interfaces should be modelled with contacts. The experimental observation proves that the debonding possibility between masonry rows is likely. In contrast, no debonding process was observed between masonry and TRM during the experiments. In addition, the sliding phenomenon was not experimentally noticed for these contacts and thus, it is not required to enable the sliding capabilities of the contact elements.

Thus, the contacts between masonry and TRM are defined as “bonded”. This definition forces the contact nodes of TRM and masonry to be always coincident. The same behaviour is defined in the contact between the first and the last masonry rows with the triangular parts which represent the hinges. The stiffness of this type of contact is automatically set equal to the stiffness of the more flexible material in contact.

The contacts between parts which represent masonry rows are initially defined as “bonded” but the possibility of debonding is considered with the definition of a CZM. The sliding failure is not possible for these contacts. The values used to define the debonding process (f_{xt} and G_f^I) are summarised in * This value corresponds to the direct tensile strength, not to the flexural tensile strength.

Table 4.3. The flexural tensile strength, f_{xt}, was experimentally determined for each brickwork type, depending on the used mortar. The flexural tensile strength is used instead of the direct tensile strength because it is considered to be more representative of the phenomena. In fact, the studied walls are eccentrically compressed and the tensile side response mainly depends on the flexural strength of the masonry. The fracture energy, G_f^I, is estimated using (Eq. 4.1). This expression has been adjusted using the experimental results presented in [7].

$$(N/m) \quad G_f^I = 36.65 \cdot f_{xt} \ \ (MPa) \qquad \text{(Eq. 4.1)}$$

4.2.3.2 Fictitious contacts

Two extra types of contacts, which do not correspond with real joints, are considered in some of the proposed models. These contacts set fictitious joints with the aim of representing real failure modes without adding complexity to the material constitutive equations. Table 4.3 summarises the values of the properties used to define the fictitious contacts.

The first type of fictitious contact is used between pairs of TRM parts. These contacts are defined to allow the debonding but not the sliding. Thus, they make it possible the TRM tensile failure (as observed in walls W#21 and W#23).

Contact	***Wall***	***Contact Failure***	f_{xt} ***(MPa)***	G_f^I ***(N/m)***	τ_{max} ***(MPa)***	G_f^{II} ***(N/m)***
Real. Masonry joint	W#1	Debonding	0.23	8.4	---	---
	W#2 to W#29 and Theoretical walls	Debonding	0.36	13		
Real. Masonry-TRM	W#21 to W#29 and Theoretical TRMW	None	---	---	---	---
Real. Masonry-support	All	None	---	---	---	---
Fictitious. Masonry-Masonry (inclined)	W#21 to W#29 and Theoretical TRMW except H0, M0, HS11 and MS11	Debonding and Sliding	2.8*	100	0.56	20
Fictitious. TRM-TRM	W#21 W#22 HS11 HS11S HS21S MS11 MS11S MS21S	Debonding	8.1	295	---	---
	W#23 W#24	Debonding	6.6	240		
	W#25	Debonding	12.0	440		
	W#26	Debonding	11.3	412		
	W#27	Debonding	20.0	733		
	W#28	Debonding	17.8	652		
	W#29	Debonding	14.5	533		
	HS12S HS14S MS12S MS14S	Debonding	9.0	330		

* This value corresponds to the direct tensile strength, not to the flexural tensile strength.

Table 4.3 Properties of the contacts used in the FEA

The second type of fictitious contact is used in the two inclined lines that divide the five masonry rows near the ends of the wall. These contacts make it possible the compression-shear failure observed in most of the TRMW experimental tests by enabling the debonding and the sliding phenomena.

The maximum tensile strength between TRM elements is calculated as the maximum between: (a) the flexural tensile strength of the strengthening mortar and (b) the tensile load-bearing capacity of the fibre grid uniformly distributed on the area of the TRM section. Thus, occasionally, the flexural tensile strength of the mortar might be higher than the tensile strength associated with the fibre grid embedded. In these particular cases, the fibre grid cannot bear the tensile force released by the mortar when the mortar cracks. Hence, the mortar is stronger than the embedded fibre grid in tension, or what is the same, the addition of the grid did not actually influence on the results. .As previously, the corresponding fracture energy was calculated using the expression in (Eq. 4.1).

The maximum tensile strength between masonry parts of the same row separated by the inclined discontinuity is the tensile strength of the ceramic pieces (see Chapter 3). It has to be remarked that the bricks are not loaded with a bending load but the applied load is similar to a direct tensile force. Thus, the direct tensile strength is the one to be used in these contacts. The corresponding fracture energy is also calculated using (Eq. 4.1). The maximum shear strength (τ_{max}) is analytically calculated from the experimental data as showed below (Eq. 4.2). Using this shear strength, the corresponding fracture energy is calculated using (Eq. 4.1) again.

The load components, normal (*N*) an tangential (*T*) to the failure plane, are calculated from the maximum applied force (*F*) and the observed failure mode (inclination of the crack in walls W#22 and W#24 to W#29) as shown in Figure 4.4. Then, the tangential component (*T*) is supposed to be uniformly distributed on the area ($b \cdot m$) of the observed discontinuity plane, thus allowing to obtain the maximum shear strength (Eq. 4.2). In equation 4-2, *b* is the width of the wall and *m* the length of the failure plane. The values used in the simulations are the average values for τ_{max} and G_f^{II}.

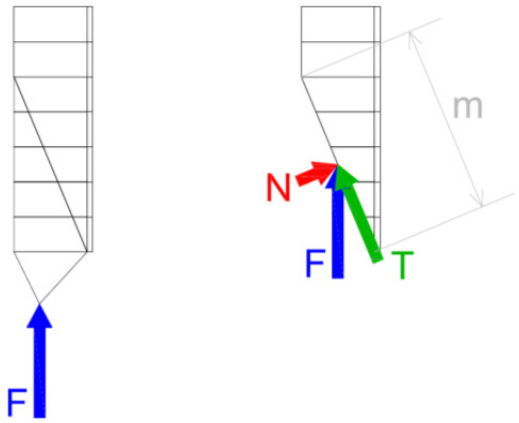

Figure 4.4 Normal and tangential force components on the failure plane

$$\tau_{max} = \frac{T}{b \cdot m} \qquad \text{(Eq. 4.2)}$$

4.2.4. Meshing

The mesh is automatically generated by the FEA software according with these criteria:

- The wall (masonry) and TRM use a uniform structured mesh of quadrilateral elements. Some triangular elements are required if the fictitious diagonal discontinuity is taken into account.
- The parts (triangles) which represent the steel hinges use an unstructured uniform mesh mostly composed by quadrilateral elements.
- The average size of the TRM's mesh is 3mm. The size of the masonry's mesh and hinges' mesh is 5mm for walls of M, T and S series. This size is 20mm for walls of the H and F series.

The used bidimensional (2D) elements are called PLANE183 inside ANSYS software. These ones are 6-nodes triangular elements or 8-nodes quadrilateral elements with quadratic integration of the displacements. The stiffness matrix has 3 and 2x2 integration nodes for triangular and quadrilateral elements respectively. Each node has two degrees of freedom (displacement in x or y).

The elements used to define the contacts are CONTA172 and TARGE169. The first one is assigned to the contact body and the second one to the target body. CONTA172 overlays the 2D solid element defining a boundary. This element adopts the same shape as the solid element it is connected with. TARGE169 is defined as a set of segment elements placed at the edge of a solid element. The contact occurs when the contact element surface penetrates into one segment of the target element. Both element types have three nodes. Assigning CONTA172 or TARGE169 to one side or other of the contact is done automatically.

With the aim of fixing the mesh size presented before, a sensibility analysis has been done. This analysis is complemented with the requirement of carrying out the calculation in a reasonable time. This means spending less than 45 minutes in a Intel(R) Core(TM)2 Duo CPU E8400 @3.00GHz with 3.00GB of RAM memory working with Windows7 32 bits.

Two cases have been analysed to select the suitable mesh size: changing the mesh size of the masonry from 5mm to 3.5mm and the TRM mesh size from 3mm to 2mm causes a change of the maximum load from 344.1kN to 344.0kN for wall W#29. In the same way, a comparison has been done for wall W#7. In this case, changing the masonry mesh size from 20mm to 10mm does not cause a perceptible change on the load bearing capacity (from 116.5kN to 117.1kN). Hence, the main result does not show sensible dependency with the mesh size.

4.2.5. Loading process and Boundary Conditions

The boundary conditions consisted of fixing the lower vertex of the triangular part which represented the lower hinge and fixing the horizontal displacement of the top vertex of the upper triangular part which represented the upper hinge. These constrain allowed the structure to rotate around the fixed nodes and they impeded any possible lateral displacement at the wall's ends.

The load was indirectly applied as a vertical descending displacement of the top vertex of the triangular part which represented the upper hinge. This movement was set at constant speed. The force reaction at this top vertex was taken as the measurement of the applied load to compare with the experimental values. This displacement-controlled simulated loading process made it possible to calculate some steps after reaching the maximum load. When the wall lost its continuity the FEA could not converge in a solution and the calculation was stopped. The applied displacement was defined as a ramp. The calculation was divided into several steps and each displacement increase was applied on the deformed configuration of the wall due to the previous loading steps. The descending speed depended on the

analysed case. This displacement ratio had to be quick enough to reach the collapse of the wall in a maximum amount of 100 steps. However, this speed had also to be slow enough to capture the wall's response (approximately 50 steps up to the collapse). A low descending velocity at the first steps, when the gravity load was applied, could cause the appearance of tension forces because the gravity deformation could be greater than the imposed descending movement. For this reason, the loading ratio was carefully adjusted.

4.2.6. Generic data post processing

The FEA calculation was stopped when the geometric continuity between parts was lost. Values of the reaction force on the top vertex (where the displacement was imposed), the vertical imposed displacement, and the lateral displacement of the wall at mid-height were obtained for each calculation step.

Contour plots, which show the distribution of vertical, horizontal and total (von Mises) stresses for the maximum applied load, were obtained for qualitatively analysis. The distribution of the total deformations, the normal and tangential stresses at the contacts and the gap in these interfaces were also analysed in some cases. All these contour plots can be consulted in Annex 2.

The post-process of the data has included the calculation of dimensionless variables for comparison purposes: ϕ (Eq. 4.3) is defined as the load-bearing capacity of the wall, which is calculated as a ratio of the maximum experimental load, N_{max}, over N_u (Eq. 4.4).

$$\phi = N_{max}/N_u \quad \text{(Eq. 4.3)}$$

$$N_u = b \cdot t \cdot f_{ck} \quad \text{(Eq. 4.4)}$$

N_u is the compressive strength of the cross section if assuming a uniform stress distribution on the width, b, and thickness, t, of the wall. The compressive strength of the masonry is used in the calculation of N_u (Eq. 4.4).

Other calculated dimensionless variables are the mid-height lateral deformation at the maximum load, h_{max}, over the wall's thickness, t; and the vertical displacement of the top hinge at the maximum load, v_{max}, over the effective height, H_{ef}. The effective height, H_{ef}, is defined as the distance between axes of hinges (extreme bottom and top nodes).

The wall's slenderness (λ) defined as the ratio of the wall's thickness (t) over the effective height (H_{ef}) is also used for comparison purposes. Finally, the eccentricity (e) is analysed with a dimensionless ratio of e over the wall's thickness (t).

4.3 FEA Results

Once the described numerical model was implemented, the next step was validating it. The experimental results presented in Chapter 3 and other experimental results from bibliography ([67,69]) were used to validate the accuracy of the proposed numerical model at predicting the maximum load of unreinforced masonry walls (URMW).

A simplified sensitivity analysis, which was aimed to analyse the influence of the compressive strength and the Young's modulus on the load-bearing capacity of the URMW, was performed. This analysis consisted of calculating the load-bearing capacity of the walls for the minimum and maximum values of these variables.

The application of the numerical model on TRM strengthened walls (TRMW) was validated by comparison with the experimental campaign of the present research.

Finally, the model was used to carry out some simulations aimed to extend the studied cases to other TRM configurations.

4.3.1. Results of URMW. Validation with bibliographic results

Two bibliographic references [67,69] have been chosen as independent sources of data to validate the Finite Element Analysis proposed herein. The real-scale size and the hinged boundary conditions of these two experimental campaigns made them suitable for the validation of the FEA because there was neither uncertainty about the influence of the size nor uncertainty about the boundary conditions to be modelled. In addition, these two references provided almost all the geometric and material data required to use the developed FEA.

The tests performed by Watstein & Allen [67], are characterised by placing a concentric hinge at the bottom of the wall and an eccentric hinge at the top of the wall. The cases studied in the present research were referred by the authors with the letters HB in [67] and are the only ones with the value of the masonry flexural strength, f_{xt}. All required material's properties were provided in [67] except for the first mode fracture energy of the brick-mortar bonding, G_f^I, which was estimated using (Eq. 4.1). Four slenderness and three eccentricities combinations were considered in the research of [67]. This is a total of twelve cases.

The tests performed by Kirtschig and Anstötz [69] have both hinges placed with the same eccentricity at each extreme of the wall. The cases consisting of calcium silicate solid units are the ones from [69] which have been considered in the present research. Four slendernes were tested by Kirtschig and Anstötz for each one of the four eccentricities. Thus, sixteen comparison cases have been considered. The flexural strength of the masonry was not provided in [69] so the value of f_{xt} was estimated to satisfy the ratio of the compressive strength, f_{ck}, out of the flexural tensile strength, f_{xt} obtained in the current experimental

campaign: f_{ck}/f_{xt} = 40, which is approximately the average ratio for the material of the present research. The first mode fracture energy of the brick-mortar bonding, G_f^I, which was estimated using (Eq. 4.1). A summary of the masonry's properties to use in the FEA is shown in Table 4.4 for the cases from [67] and [69].

Experimental reference		*E (MPa)*	*f_{ck} (MPa)*	*υ*	*f_{xt} (MPa)*	*G_f^I (N/m)*
Watstein & Allen [67]		25400	44.81	0.30	2.98	110
Kirtschig & Anstötz [69]		8540	12.2		0.3	7
W#1	H-series	780	18.2	0.35	0.23	8
W#2, W#3 and W#5	H-series		12.9		0.36	13
W#6-W#9	H-series		13.7			
W#10-W#16, W#18-W#20	M- & S-series		10.8			

Table 4.4 Properties of the masonry to be used as most representative input values of the experimental tests on unreinforced masonry walls

Once these 28 cases (12 from [67] and 16 from [69]) from bibliography were simulated, the numerical results were compared with the experimental ones. This comparison is graphically plotted in Figure 4.5 and Figure 4.6.

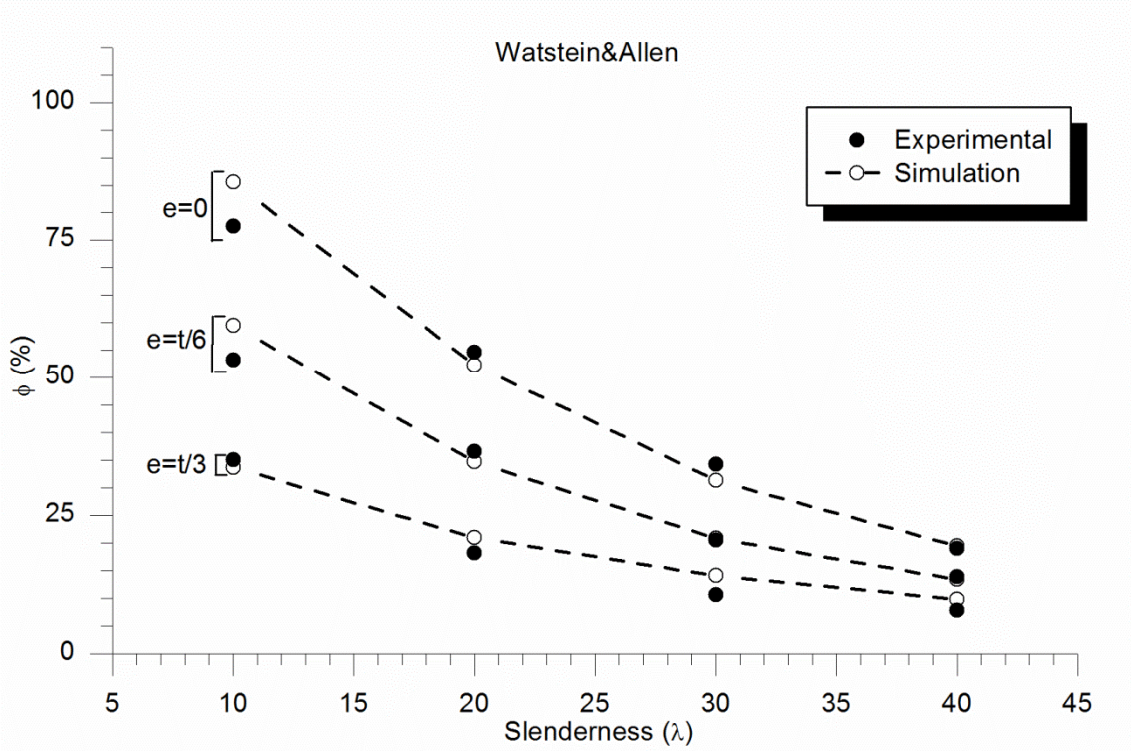

Figure 4.5 Results from the validation of the FEA by comparison with the experimental data from [67]

Figure 4.5 shows that the proposed FEA accurately predicts the ultimate load of the walls tested by Watstein and Allen [67]. The average relative error was 10.5% and the model appears to be balanced (see Figure 4.5) in the sense that it predicts the load-bearing capacity without either a conservative or an unsafe bias. Taking into account that the experimental average relative error was 7.3% (calculated from the results in [67]), obtaining a numerical prediction with a 10.5% of error is a very satisfactory result which supports the validation of the proposed FEA. However, the numerical results with the least error were in the cases with the lowest eccentricities. For e=0, the error was 6.4%; for e=t/3, the error was 19.5 %. The slenderness did not seem to affect the accuracy of the model and good results were obtained regardless of the value of the slenderness.

Looking at the plots in Figure 4.6 it is observed that the proposed FEA correctly predicts the load-bearing capacity of the walls tested by Kirtschig and Anstötz [69]. These tests were the most similar to the ones performed in the present campaign, so a good accuracy at calculating their response sets a solid base for the validation of the FEA and for its application on the herein presented tests later on. The average relative error of the numerical prediction is 28.4%. This error is slightly bigger than the scattering in the experimental results from [69], which is 5.8%, but it is still comparable to the current scatter of the masonry mechanical properties as seen in Chapter 2. However, the agreement is better in the cases with lowest eccentricities and/or slenderness (4.2% for e=0 and λ=5.6). This trend contrasts with the tendency observed for the results reported in [67]. Finally, the numerical model seems to overestimate, in general, the load-bearing capacity of the walls tested by Kirtschig and Anstötz [69] (see Figure 4.6).

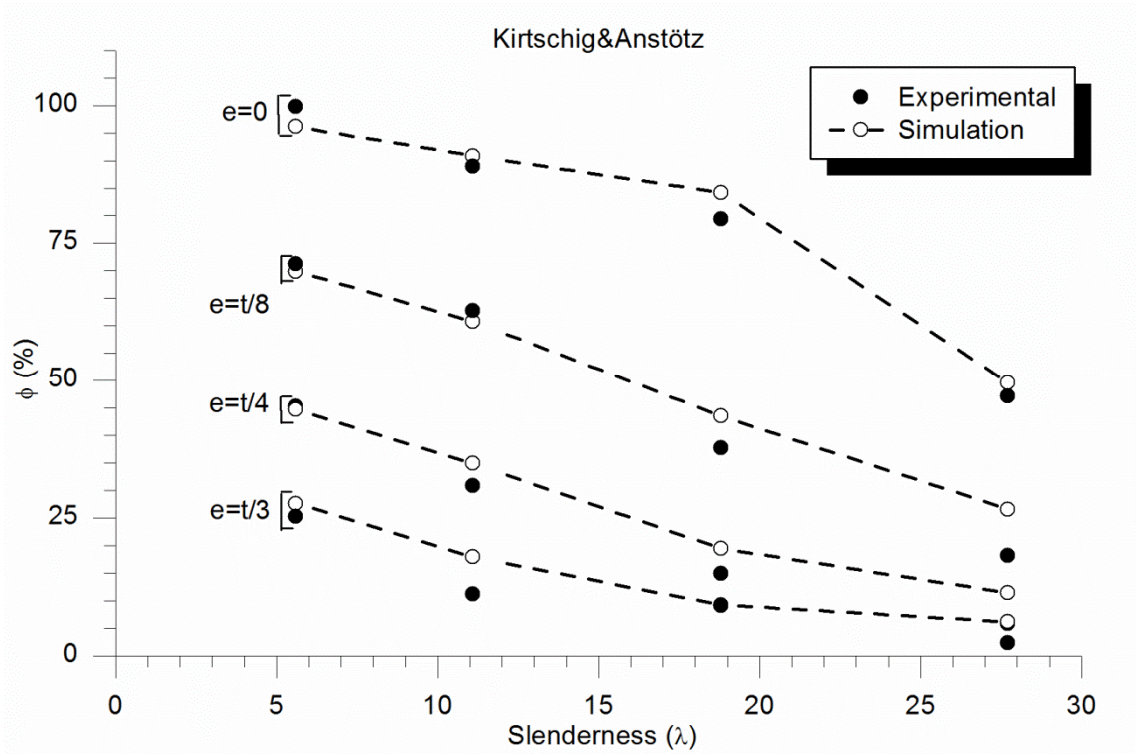

Figure 4.6 Results from the validation of the FEA by comparison with the experimental data from [69]

In conclusion, the presented FEA correctly predicts the ultimate load of the tests carried out by other researchers. The average relative error of the developed model is 18.9% by comparison with the experimental results. This error is within the usual scatter range of the masonry properties as seen in Chapter 2.

4.3.2. Results of URMW. Comparison with the experimental campaign

Once validated, the present FEA has been applied to predict the ultimate load of the unreinforced walls tested in the herein described experimental campaign (see Chapter 3). The details of each particular simulation are fully described in the Annex 2 where the results obtained for each simulation are briefly presented too.

The comparison between the experimental tests carried out and the performed numerical calculations is presented in this subsection. The main aim of the analysis is to determine the application range in which the developed FEA performs better for URMW. Studying which variables affect more on the numerical results and proving the accuracy of the model are also goals of the investigation.

The experimental tests were divided in three groups to analyse the obtained results. Each group corresponded with an experimental series (H, M and S). Only the series with more than one wall were considered for the analysis. Thus, series F and T were discarded. This criterion excluded walls W#4 and W#17. The series were defined according with the initial geometric characteristics of the walls. Thus, H-series, M-series and S-series were separately analysed. In addition, wall W#5 was also excluded from the study because its results were inconsistent with the rest of the H-series. For more details about the experimental tests see Chapter 3 and Annex 1.

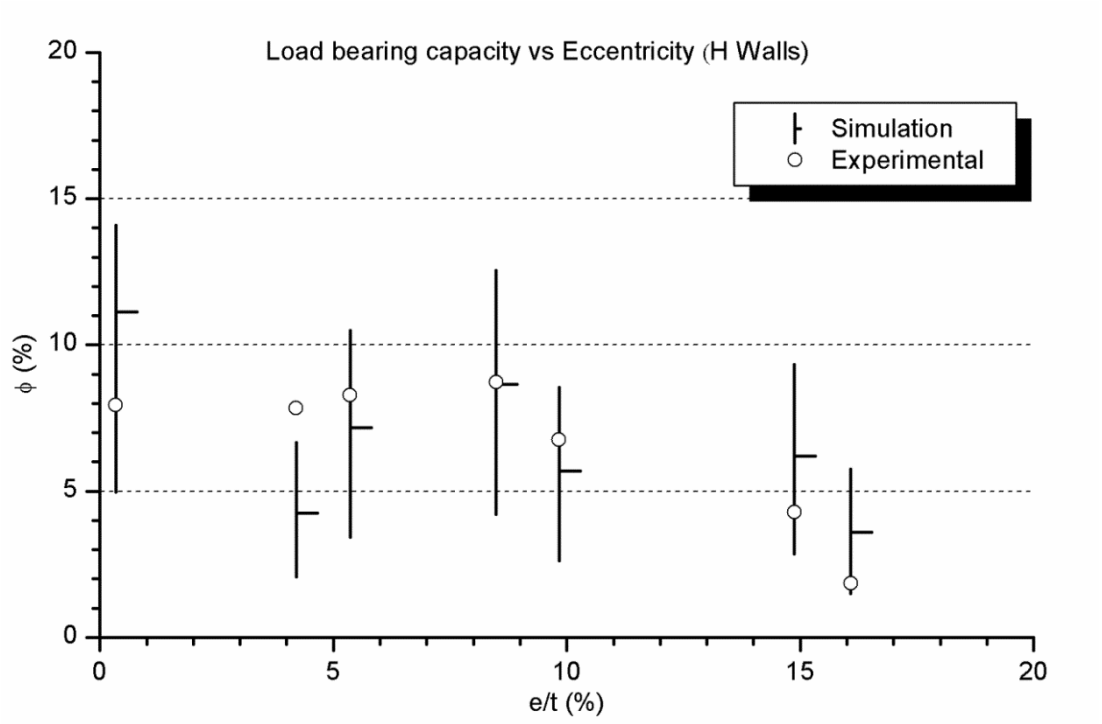

Figure 4.7 Comparison of the numerical and experimental results for the H-series walls

The comparisons between the experimentally obtained results and the results produced by the simulations are graphically represented in Figure 4.7, Figure 4.8 and Figure 4.9. These plots consist of two overlapped graphs. The first one is a scattered plot (white round symbols) representing the experimental load-bearing capacity of each analysed wall. The x-axis shows a dimensionless variable corresponding to the real eccentricity at mid-height for each wall. The second overlapped figure is a high-low-close type plot which represents the numerically obtained result (horizontal segment symbol) and the range of possible solutions depending on the value of the Young's modulus, E, and the masonry's compressive strength, f_{ck}. The maximum and minimum values of these variables were chosen according with the experimental evidence presented in Annex 1. The masonry's compressive strength ranged from 7MPa to 15MPa and the Young's modulus ranged from 400MPa to 1100MPa. The values used to obtain the most representative numerical solution (the one represented by the horizontal segment symbol) are the average of the representative experimental characterisation tests corresponding to each case and are shown in Annex 2.

Looking at the results from the H-series (Figure 4.7) it is noticed that the experimental load-bearing capacity fits inside de calculated range for all the walls except for wall W#1 which was built by a non-professional brick layering team. The x-axis in Figure 4.7 shows the dimensionless variable representing the real eccentricity at mid-height for each wall (eccentricity, e, over wall's thickness, t) and the y-axis shows a dimensionless measure of the load-bearing capacity (maximum applied load P_{max} over the section's compressive strength under uniform compression, P_u). The numerical analysis' results used for

analytical comparisons are the ones obtained with the most representative set of variables for each specific test (see Table 4.4 or Annex 2 for these sets of values). These particular results are represented in Figure 4.7 with a horizontal segment symbol. The average relative error of the model for the H-series is 38.4%. Although these results are not as good as those obtained for the experimental results of previous studies (section 4.3.1), the accuracy is acceptable because it is within the range of the common scatter obtained in the experimental tests for the characterisation of the materials (see Chapter 3). In addition, it is well-known that tests on masonry walls that rely on the flexural strength of the material normally show highly scattered results, e.g.,[8]. In fact, the scatter in the experimental results in this study is larger than the average relative error of the numerical model, so the model correctly predicts the behaviour of the more slender walls (the H-series walls). Observing Figure 4.7 it is also remarkable that the results show no general over- or underestimation for the H-series.

Finally, the significant influence of the Young's modulus, E, and the masonry compressive strength, f_{ck}, is shown in Figure 4.7 and later on, in Figures 4.8-9. The vertical lines of these graphs correspond with the range of the possible solutions depending on the value of these variables. The numerical results for different values of Young's modulus (E) and compressive strength (f_{ck}) make it possible to analyse the influence of these parameters on the load-bearing capacity. It has been observed that the largest influence of the Young's modulus (E) over the axial load-bearing strength of the walls occurs when the load is eccentrically applied and second-order bending appears. As the Young's modulus increases, the deformation of the wall from second-order effects decreases because of the increased stiffness of the wall. A larger axial load is thus needed to develop second-order bending failure. The load-bearing capacity of the walls can also be improved by increasing the masonry compressive strength (f_{ck}). However, the effect of the compressive strength is more apparent when the predominant failure mode is material crushing, as in the case of walls with low load eccentricity (e) and a low slenderness ratio ($\lambda=H_{ef}/t$). Finally, by comparing the cases with different flexural strength of the masonry (f_{xt}) it has been noticed that a larger flexural brick-mortar bonding strength (f_{xt}) contributes on the load-bearing capacity by providing more strength against second-order bending failure.

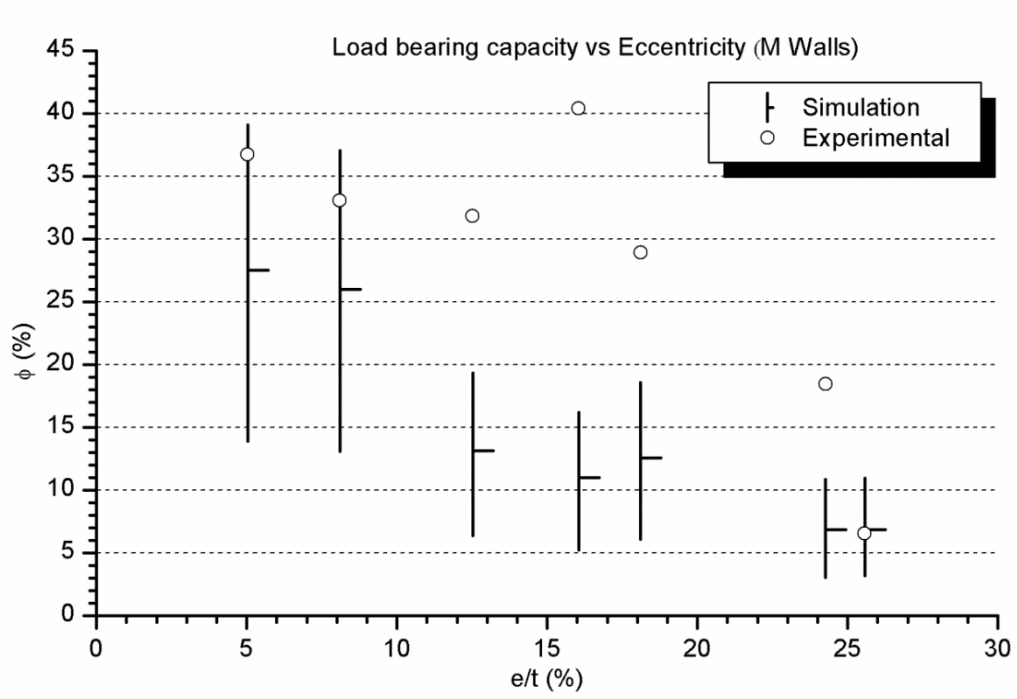

Figure 4.8 Comparison of the numerical and experimental results for the M-series walls

Looking at Figure 4.8 it is noticed that the numerical results follow the same trend than the experimental results although the FEA underestimates the load-bearing capacity of the M-series walls in almost all cases. The model slightly overestimates the wall's strength for the case with the largest eccentricity at mid-height only.

In Figure 4.8 a significant relationship between the eccentricity of each wall and the range of the numerical solutions for this particular eccentricity is observed. The different solutions for each case correspond with the different values of the masonry compressive strength (f_{ck}) and Young's modulus (E). Thus, for the cases in which the compressive behaviour is more relevant (low eccentricity values), the influence of f_{ck} and E is higher and the possible solutions range is wider as can be seen in Figure 4.8. In addition, the error decreases as the eccentricity increases. For example, the error for the most eccentric test of the M-series is just 5.1% and the average relative error of the proposed FEA when applied to represent the walls of this series is 43.2%, which is more than for the H-series. These two results, together, indicate that the numerical model is more applicable to slender and eccentrically loaded walls.

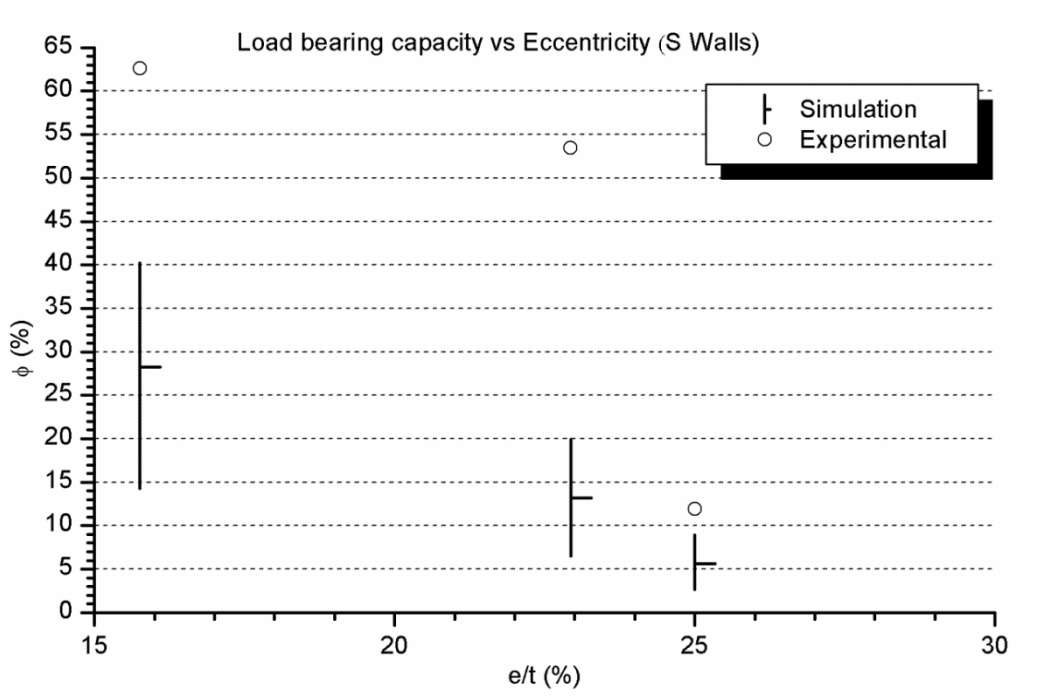

Figure 4.9 Comparison of the numerical and experimental results for the S-series walls

The proposed model is also accurate within the limits of the experimental scatter for the S-series. In this case, see Figure 4.9, the average relative error grows up to 61% although the relative error is 52.8% for the most eccentric wall of the series. Again, it is noticeable that the range of the possible solutions calculated with the model is wider for the walls with lower values of eccentricity. Thus, it has to be remarked that the proposed FEA provide better results when analysing the most eccentrically loaded walls.

Comparing Figure 4.7, Figure 4.8 and Figure 4.9 it is also observed that the eccentricity effects and the slenderness effects added. Thus, the most slender walls (H-series) are correctly represented by the model for lower values of eccentricity than the less slender walls (S-series) which require higher load eccentricity to be simulated by the FEA with the same accuracy than H-series walls. Nevertheless, for the S-series the average relative error still fits into the scattering range of the characterisation tests for the constituent materials of the walls (see Chapter 3).

As mentioned before, by observing the possible range of numerical solutions for all cases it can be noticed that independently from the wall's series (it means independently from the slenderness), this range always represent around 100% of the predicted load with the average values selected for the analysis. Thus, the influence of the Young's modulus and the compressive strength of the masonry are significant. Hence, correctly determine the value of these variables is essential to accurately predict the load-bearing capacity of unreinforced masonry walls using the proposed model.

In general, acceptable agreement is obtained between the experimental results of the UnReinforced Masonry Walls (URMW) and the numerical predictions of the proposed FEA. However, the punctual observed disagreements suggest that using accurate values of E and f_{ck} is a must. Hence, the experimental determination of these variables is essential for a correct modelling of real structures.

4.3.3. Results for TRMW. Validation with the experimental campaign

Analysing the accuracy of the proposed FEA at modelling the Textile Reinforced Mortar strengthened masonry Walls (TRMW) is the next natural step once proved that the numerical solution provides acceptable results for URMW. Like in the previous section, three values of the load-bearing capacity were calculated for each wall although only the one corresponding with the most representative set of variables was used for comparison purposes. The other two results were obtained for the extreme possible values of the compressive strength of the masonry, f_{ck}, and the Young's modulus, E. These ranged from 7MPa to 15MPa and from 400MPa to 1100MPa respectively. Using this ranged solution is an indirect way to represent the influence of the scattering of the most uncertain input variables on the FEA results.

Two main differences are included in the model representing the TRMW in comparison with the simulations of the URMW. The first one is naturally introduced because of the existence of the strengthening system which is modelled including a new material. The second one is a pair of contacts needed to represent an experimentally observed failure mode consisting of the mixed compressive-shear local collapse of the masonry near the wall's endings.

The aim of the simulation's results presented in this section is to analyse the accuracy of the model when representing TRMW and to compare the FEA precision between the strengthened (walls W#21 to W#29) and non-strengthened walls (M-series).

The used input parameters and the particular results for each case are detailed in Annex 2. It has to be remarked that for all considered cases the model predicts a mixed failure cause which includes the tensile breaking of the TRM and the compressive-shear collapse of the inclined contact near the wall's ends. In some cases (W#26 to W#29) the compressive collapse of the masonry at the compression side is also resulting together with the other two failure modes. Thus, the model correctly predicts the possible failure modes although it is not really capable of identifying which one would happen first, being the real collapse cause, in the analysed cases. For the tested configurations, the maximum load corresponding to each failure process is close to the others.

Observing the Figure 4.10 it is noticed that most of the experimental results fit into the solution range although there is a remarkable underestimation tendency in the FEA results. Seven of the nine calculated load-bearing capacities are under the corresponding experimental values. The cases for which the model predicts a higher load than the experimental one are walls W#28 and W#29 both strengthened with carbon fibre grids.

The average relative error of the numerical model is 19.5%, which is far lower than for the analogue unreinforced walls (M-series with an error of 43.2%). Thus, the proposed FEA accurately predicts the ultimate load of the TRMW and its precision is even better than for the unreinforced comparable walls.

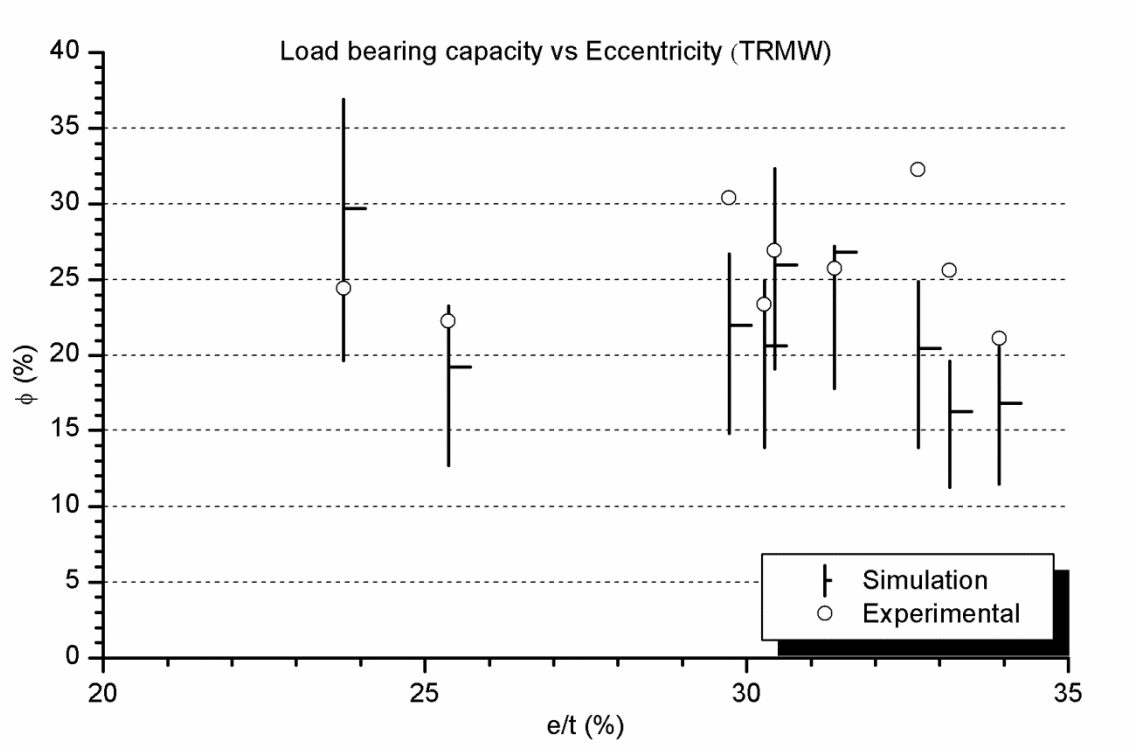

Figure 4.10 Comparison of the numerical and experimental results for the TRMW walls

Like in previous cases, the relationship between the eccentricity and the range of the possible solutions of the model is also observed in Figure 4.10. Thus, the sensitivity of the model to the Young's modulus and compressive strength of the masonry is maintained when considering a strengthening layer.

A part form the general analysis, a particular result was observed in the FEA results. It has been noticed that when the thickness of the mortar of the TRM increase, the elements representing the strengthening system bear more part of the applied load making the TRM tensile failure more likely (cases of walls W#21 and W#23). Thus, according with the model, an overthickness of the mortar layer in TRM might cause a particular failure mode when possible: the tensile failure of the strengthening system.

4.3.4. Results for theoretical analysis of TRMW

Theoretical analyses have been performed in order the study the influence of the TRM on the structural response of brickwork walls for different TRM configurations. The same model used to simulate the experimental TRM walls has been used to extend the range of studied cases. This theoretical approach is interesting because the uncertainties related with the material or the real geometry are avoided. Thus, the comparison between theoretical cases is direct and free of the influence of other parameters.

Fourteen theoretical cases have been considered. The results of the corresponding simulations are presented in this subsection. These cases have been designed with the following aims:

- Analysing the effects of the inclined contacts used for the simulation of TRM strengthened walls.
- Analysing the effects of strengthening a theoretical wall without any uncertainties, neither on the material definition nor on the geometry.
- Analysing different strengthening configurations (number of TRM layers and strengthened sides).
- Studying the previous three items for two different slenderness.

It has to be reminded that the codification of the theoretical walls has been presented in the section 4.2.1.4. The same codification is used for the analysis of the results.

Firstly, a qualitatively comparison of the wall's response is presented. This analysis is based on the graphic representation of the load, lateral deformation and vertical displacement of the simulated walls. In addition, the failure modes are also described and studied. Finally, the quantitative results are presented and analysed to compare the different strengthening patterns considered.

Regarding the failure modes, it has to be said that the walls with no strengthening (H0, H0S, M0 and M0S) failed by opening a horizontal joint. This failure pattern is observed because the tensile stress associated with the bending process is larger than the corresponding strength of the masonry. In contrast, the TRM strengthened walls collapsed due to different causes depending on the slenderness of the wall and the TRM configuration considered. The observed failure causes are discussed below.

- Tensile failure of the TRM. It was the most likely collapse reason for the walls with high slenderness and/or less quantity of fibre embedded inside the TRM layer. According with the results obtained, this was the case of the walls HS11, HS11S, HS12S and MS11.
- The shear-compressive failure of the brickwork near the ends of the wall. This failure pattern was possible for the walls with low slenderness or more quantity of fibre embedded into the TRM. This was the case of the simulations corresponding with walls HS14S, MS11S and MS12S. However, the tensile failure of the TRM and the shear-compressive failure of the brickwork were associated with very close loads. Thus, distinguishing which one was the first was difficult.
- The compressive failure of the brickwork. This failure mode was likely for the less slender walls which had more fibres in the TRM layer. It was the case of the wall MS14S. However, as happened with previous failure mode, the compressive failure was associated with a load which is close to the one corresponding to the two previous failure modes in the considered cases. Thus, distinguishing which failure pattern was the first was complex.

Finally, the studied walls with TRM applied in both sides had similar collapse loads for the three failure modes presented. Thus, it was difficult to distinguish which failure mode was the first. The tensile failure

of the TRM, the crushing of the compressed TRM and the compressive-shear collapse of the brickwork near the ends of the wall were associated to similar loads but this last one appears firstly.

Three of the four described failure modes have been experimentally observed in the previous tests: the tensile failure of the TRM, the shear-compressive failure of the brickwork near the ends of the wall and the compressive failure of the masonry. Thus, the numeric model seems to correctly predict the possible failure modes. Moreover, the performed simulations are useful to qualitatively relation each collapse cause with the properties of the wall and the strengthening pattern.

Finally, it seems that the proposed FEA is able to predict failure modes which have not been noticed in the experimental field. It is the case of the TRM crushing which was theoretically possible for the walls strengthened at both sides. This particular strengthening configuration was not experimentally tested. Thus, the FEA points out that other possible failure patterns, apart from the observed ones, are possible depending on the strengthening configuration.

The main material properties used to model the theoretical walls are presented before analysing the corresponding results with more detail. The full description can be found in Annex 2. The mechanical properties of the brickwork are the same as for the experimental strengthened walls (section 4.3.3) and the properties of the TRM are those associated with the TRM composed of lime-based mortar and glass fibre grids. The analysis presented below considers the possibility of embedding two fibre grids inside the thickness of a current layer of TRM (10mm). Thus, the maximum tensile force that the mortar can resist is the same for cases HS11, HS11S, HS12S, MS11, MS11S and MS12S, but the tensile force the grid can resist is double for the cases HS12S and MS12S. Only for the cases with 4 fibre grids (HS14S and MS14S) the TRM thickness has been increased to 20mm.

The inclined contact, which makes the compressive-shear failure possible by opening a crack near one of the wall's ends, is studied by comparing the numerical results of walls H0, HS11, M0 and MS11S with those of walls H0S, HS11S, M0S and MS11S respectively. These comparisons are graphically represented in Figure 4.11, where the black symbols correspond to the models which do not consider these inclined contact and the red symbols show the response of the models which included these contacts. The lateral displacement at mid-height (left graphs in Figure 4.11) and the vertical displacement at the top of the wall (right graphs in Figure 4.11) are shown and considered for comparison purposes. It is worth noticing that the response of both models (with and without the inclined contacts) is the same during the loading process. Only little differences might be observed for the most slender analysed walls (HS11 and HS11S) after the collapse load is reached. However, the data corresponding to the post maximum load should be analysed carefully because it is obtained under the hypothesis of a continuum medium although the wall's structure is composed of discrete parts after the collapse point and the continuity of the material is not clear.

In conclusion, considering the inclined contacts which allow the compressive-shear failure does not affect the response of the walls which are supposed to collapse with other failure patterns.

Regarding the analysis of different strengthening possibilities (see Figure 4.12), it is observed that the cases which consider strengthening both sides of the wall (HS21S and MS21S) are the ones associated with the highest load-bearing capacities and lower deformations for a given load state. These particular results, which are equivalent for both slenderness cases (H and M geometries), may be associated with two possible effects: firstly, the thickness of the wall is increased the double amount if compared with placing just one strengthening layer on the tensile side (HS11S and MS11S cases) and secondly, the eccentricity of the load is reduced when the strengthening is placed on the compression side.

In the graphs corresponding with the cases HS21S and MS21S (see Figure 4.12), the masonry's crushing becomes evident in the calculated response. It is noticed because the corresponding loading plots show a slope change before the maximum load. This fact may be explained because the thickness of the wall is increased and the eccentricity is relatively lower due to the TRM layer in the compression side. In this situation, the wall bends less and the compressive response is predominant. These two theoretic walls are working mostly in compression.

By comparing the cases with one or two fibre grids inside one mortar layer in the tensile side (so the TRM thickness is the same), it is observed that the response is almost the same. However, the cases with two fibre grids (HS12S and MS12S) show a slightly higher load-bearing capacity than the comparable walls with only one fibre grid (HS11S and MS11S). Analysing the graphs of Figure 4.12, it is noticed that the influence of doubling the amount of fibre inside a fixed mortar layer is small and it only becomes evident when analysing the vertical displacement of the wall's top.

The differences in the structural response are more evident when the thickness of the mortar layer of the TRM is increased. Thus, by comparing the results for wall HS11S, or even HS12S, with the results of HS14S (which considered a double mortar thickness), a significant load-bearing capacity increase is noticed. In addition, the lateral response is also stiffer for the cases with greater mortar thickness (see the graphs in the left position in Figure 4.12). However, the vertical deformability seems to be maintained when the TRM thickness is increased. In fact, the vertical response follows the same slope for the unreinforced walls and the walls strengthened at the tensile side although the maximum capacity is different (see the graphs in the right in Figure 4.12).

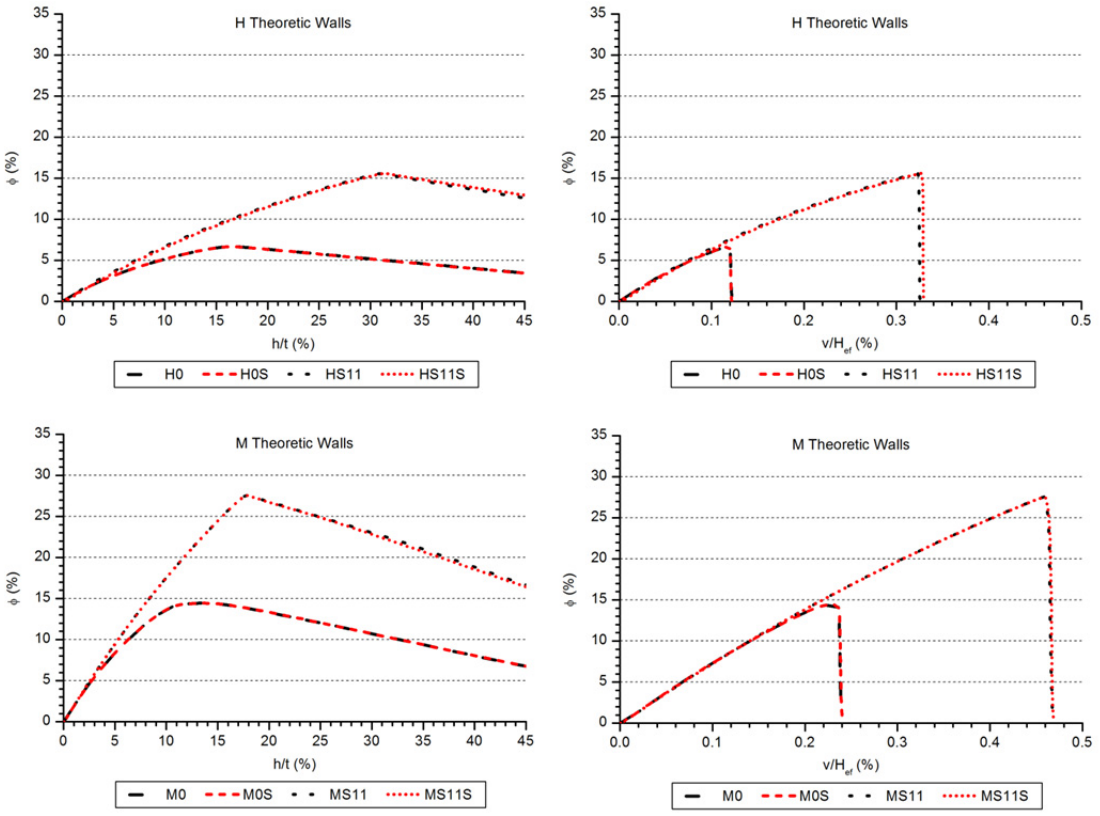

Figure 4.11 Comparison between models with and without inclined contacts near the wall's ends

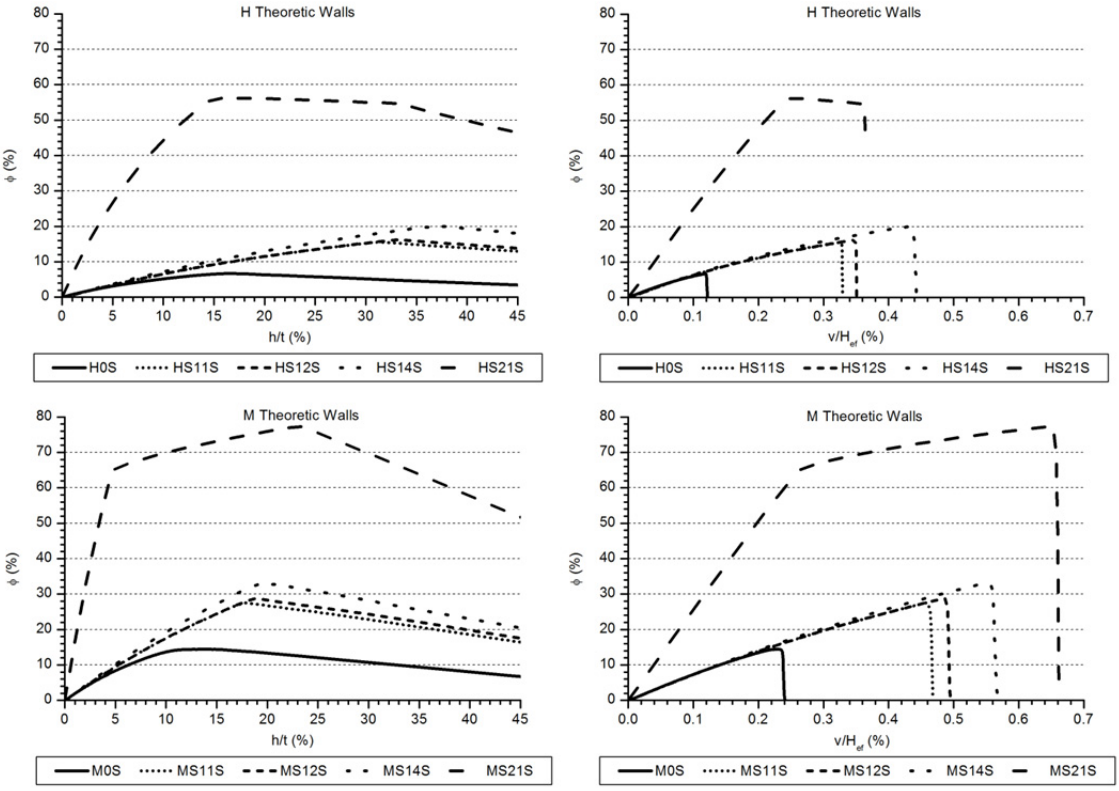

Figure 4.12 Comparison between the theoretic walls considering different strengthening variations

All these comments are valid for slenderness, H and M walls, which correspond with the upper and lower graphs in Figure 4.12 respectively. Comparing these two geometries, it is observed (Table 4.5) that the effect of the TRM strengthening is always greater for the most slender walls, which are more likely to fail due to tensile stress in the masonry or in the TRM.

Wall	***Load-bearing capacity * (kN)***	***Inclined contact effect ** (%)***	***Strengthening effect *** (%)***	***Strengthening configuration effect **** (%)***
H0	85.9			
H0S	85.9	0.00		
HS11	199.8			
HS11S	200.0	0.11	132.8	
HS12S	207.9		142.1	4.0
HS14S	257.8		200.1	28.9
HS21S	725.7		745.0	262.9
M0	185.4			
M0S	185.4	-0.03		
MS11	355.4			
MS11S	355.4	0.01	91.7	
MS12S	370.7		100.0	4.3
MS14S	425.8		129.7	19.8
MS21S	999.6		439.2	181.2

* For 1m width walls

** Comparison of cases with the same strengthening configuration with and without inclined contacts. H0S is compared with H0, HS11S is compared with HS11, M0S is compared with M0 and MS11S is compared with MS11.

*** Comparison with respect to the non-strengthened case. All analysed cases consider the inclined contact in the masonry. HS11S, HS12S, HS14S and HAS21S are compared with H0S and MS11S, MS12S, MS14S and MS21S are compared with M0S.

**** Comparison with respect to the cases strengthened with one fibre grid embedded into one mortar layer applied on one side of the wall. HS12S, HS14S and HS21S are compared with HS11S and MS12S, MS14S and MS21S are compared with MS11S.

Table 4.5 Load-bearing capacity of the theoretical walls

Looking at the results in Table 4.5, it is noticed that applying a simple TRM layer on the tensile side is really effective for the materials and geometries considered. However, the effectiveness of applying two fibre grids inside one mortar layer does not significantly increase the load-bearing capacity (around 4%). Moreover, placing four fibre grids inside a thicker mortar layer does not seem to bring an effectiveness increase proportional to the used material (between 20% and 30% of load-bearing capacity increase respect the simplest strengthening option). In contrast, applying a TRM layer on both sides seems really effective. In fact, the load-bearing capacity of the cases with both sides strengthened is around the double

of that for the cases with only one side strengthened. However, this occurs because of the greater stiffness of the strengthening mortar and the wall's thickness increase. This last change is related with the reduction of the eccentricity of the applied load and with the reduction of the slenderness of the structure. Thus, according with the simulation results, applying just one layer of TRM in the tensile side together with a layer of strengthening mortar in the compression side (this one with no grids) would be a good strengthening procedure.

4.4 Conclusions

A numerical model for the analysis of the structural response of brickwork walls under eccentric axial load has been proposed, described and applied. This model is based on the simplified micromodelling technique and it is aimed to be a simple calculation tool ready to be implemented in general purpose FEA software.

This model has been validated by comparing the numerical results with experiments from bibliography, which represented different structural configurations and a wide range of mechanical properties. This comparison has shown good accuracy of the proposed model, achieving predictions with a lower error than the corresponding scattering of the experimental results.

In addition, the model has been applied to simulate the experimentally tested cases (Chapter 3). Experimental and numerical results have been compared and the error obtained for the prediction of the ultimate load-bearing capacity is within the range of the scattering of the input parameters. In general, the model is applicable for both unreinforced and TRM-strengthened brickwork walls although the accuracy is better for the walls which are expected to collapse due to a mechanism formation failure.

Regarding the model definition, it can be concluded that the use of two triangular objects to model the hinges is a valid and efficient solution which has produced satisfactory results. The material used to model these hinges was much stiffer than the masonry. In addition, the use of an inclined contact, which was characterised by a cohesive zone model response, to allow simulating of the compressive-shear failure near the wall's end has accomplished its expected goal: it has no effects on the simulation of the walls which are not expected to fail in this way, but these contacts are involved in the simulated failure mode for those walls which had shown this particular collapse pattern in the experimental campaign.

The simulation of the experimental tests of the current research shows that the proposed model is better at predicting the load-bearing capacity of the most slender walls or the walls with the load applied at a greatest eccentricity. Thus, although the accuracy of the results is good and reasonable if compared with the scattering of the experimental input data, when the compressive response of the brickwork is the dominant process, the model tends to underestimate the load-bearing capacity of the wall.

On the whole, the proposed model correctly predicts the influence of the walls' slenderness and the eccentricity of the load for all series. Moreover, the influence of using different TRM systems is also correctly captured by the FEA.

Concerning the interpretation of the numerical results, it has to be said that the simplified sensibility analysis, which consisted of using extreme values for the mechanical properties of the materials, has shown that the range of possible results is wide. In addition, it has been noted that the load-bearing capacity is very sensitive to the variation of the Young's modulus of the brickwork. This parameter is the one with larger experimental scattering. Hence, the interpretation of the numerical results has to be done taking into account the uncertainties involved in input data of the numerical model.

By analysing the application of the model to simulate TRM strengthened walls, it has been noticed that the FEA's results are conservative in most of the cases, especially if the compressive response is significant or the crushing of the masonry is involved in the failure mode. However, the numerical results are comparable with the experimental ones. In fact, the achieved accuracy is good if compared with the typical scattering of the properties of the brickwork structures. In addition, the influence of placing two fibre grids or changing the TRM components on the load-bearing capacity is also correctly predicted.

Taking into account the results obtained by comparing the experimental tests with the numerical simulations of all the cases, it is concluded that the behaviour of the model might be improved by implementing a constitutive equation to account for the over-strengthening of the masonry in compression. This effect, characterised by the increase of the compressive strength for eccentric loading conditions, have been noticed by other authors as Brencich et al. The inclusion of the over-strengthening in compression would cause higher load-bearing capacity when the crushing failure process is significant. It is the case of the less slender walls subjected to concentric or moderately eccentric loads.

Looking at the application of the developed model to theoretical cases, it can be concluded that the tensile strength of the TRM's mortar is an important parameter which has to be taken into account. Thus, according with the obtained results, it is necessary to take into account the contribution of both the mortar and the fibre grid on the tensile strength of the TRM. In addition, the theoretical cases also showed that the effect of placing a mortar layer on the compression side of the walls might be a practical and effective solution to enhance the performance of TRM. This is due to the thickness increase, the eccentricity reduction and the slenderness decrease associated with the application of a mortar layer. In addition, the stiffness of this mortar contributes to the wall's load-bearing capacity.

Finally, it has been shown that the proposed numerical model correctly predicts all possible failure modes observed in the experiments. However, several causes of collapse are possible for some particular and thus, it is difficult to select the one which is going to show first.

After analysing the accuracy of the proposed numerical model, it has to be concluded that some work could be carried out to enhance its application range. Essentially, this work should be oriented to better represent the behaviour of the masonry in compression and shear. However, this aim is beyond the scope of the current research, which was oriented to the proposal of a simplified and practical numerical modelling as a secondary goal.

To sum up, the proposed numerical model has shown acceptable accuracy at predicting the load-bearing capacity of the wide range of considered experimental cases.

5

Analytical approach

5.1 Introduction

Classical scientific approach and the corresponding analytical formulations are useful to be included in regulations. However, the complex behaviour of the masonry makes it difficult to present a unique and accurate analytical approach valid for all the range of variables. Thus, several analytical approaches based on mechanical compatibility hypothesis are published in the literature (see Chapter 2) but they are only useful for specific boundary conditions or loading configuration.

In this line, two simplified analytical formulations are proposed herein. The first one is aimed to calculate unreinforced masonry walls which are supposed to fail with mechanism formation. This method uses a non-conventional hypothesis: linear stress distribution in the section (justified in section 5.2.3). Moreover, this method also considers the second order deformation reaching good accuracy in its application range. The second one is based on the current equilibrium equations for a cross section and is aimed to calculate the maximum axial-bending interaction that a TRM-strengthened masonry section can bear.

The general tendency of the analytical approaches used in the codes is to base the formulation on empirical data and adjusting the mathematical equations. For some cases, there is no direct theoretical basis of the failure phenomena (this is the case of ACI-530 [43] and EC-6 [64] when facing the case of eccentric compression). These approaches are explained and compared with the experimental evidences of the current work in this chapter.

Finally, the Southwell Plot method (see a detailed description of the method in [80]) is also used. This semi-empiric method assumes a linear elastic response of the material. Thus, it is expected to be the most suitable for the slender non-strengthened walls. However, it has been applied for all the experimental

cases to assess its accuracy. The Southwell plot method allows obtaining the load-bearing capacity of the walls from the experimental data of the loading process, usually obtained far before the collapse point.

The two main subsections of this chapter separately cover the cases of the UnReinforced Masonry Walls (URMW) and the TRM Strengthened Masonry Walls (TRMW) before presenting the conclusions in the last part. The applicable current regulations are considered and their results analysed only for the URMW whilst the results of the section strength approach and the Southwell Plot analysis are presented for both typologies of the walls.

5.2 UnReinforced Masonry Walls (URMW)

The analyses herein presented have two main aims: comparing the experimental results of the tests on unreinforced masonry walls with two of the most used current regulations (Eurocode-6 and ACI-530) and to present an analytical method for predicting the load-bearing capacity of the walls. This method is based on the hypothesis of linear elastic response of the material which is not commonly considered. However, the accuracy of the results suggest this approximation is a useful tool for calculating walls which failed by mechanism formation. Finally, the Southwell plot method is applied to predict the load-bearing capacity of the URMW.

5.2.1. Eurocode-6 formulation

Eurocode-6 (EC-6) is the current standard for masonry structures in Europe. The applicable formulation for the compressed brickwork walls is based on experimental studies on concrete walls (see [63]). The case with eccentric axial load is calculated by taking into account the eccentricity of the wall and its slenderness. The boundary conditions are considered inside the slenderness parameter by defining an effective height. The eccentricity parameter considers the eccentricity of the axial load, the geometric irregularities of the wall and the out-of-plane loading effects.

According with EC-6, the load-bearing capacity of a vertically compressed masonry wall is the minimum value between the load associated with the compressive failure of the ends of the wall (only affected by the eccentricity) and the load associated with the failure at the central fifth of the height of the wall (affected by the eccentricity and the slenderness). For the structural configuration of the walls tested, the limiting condition is always in the central fifth of the wall's height.

It is also worth mentioning that EC-6 calculates the load-bearing capacity taking into account the axial, bending and buckling phenomenon together. According with the formulation, the load-bearing capacity of tested walls (N_{Rd}) should be calculated by reducing the compressive capacity of the cross section, obtained by multiplying the thickness of the wall by the compressive strength of the masonry ($t \cdot f_k$), with a non-linear factor (ϕ_m) which depends on the eccentricity of the vertical load ($M_m/N_m = e$). This eccentricity, e, might be expressed as the ratio of the bending moment at mid-height, M_m, out of the

corresponding axial force, N_m. The factor ϕ_m also depends on the geometric irregularities, $e_a=h_{ef}/450$, which are set to be the effective height of the wall divided by 450 for the studied walls. The effective height of a wall h_{ef} depends on the boundary conditions and is defined as the distance between hinges for most of the studied cases. Moreover, ϕ_m depends on the eccentricity associated with the out-of-plane loads (e_{hm}), the slenderness, which is defined as the ratio of the effective height out of the thickness of the wall ($\lambda=h_{ef}/t$), the creep coefficient ($\phi_\infty=1$ for clay bricks) and the mechanical characteristics of the masonry (compressive strength, f_k, and Young's modulus, $E=780MPa$ according with the experimental results).

The formulae for the calculation of the load-bearing capacity of the studied brickwork walls are in the box corresponding with (Eq. 5.1).

$N_{Rd} = \phi_m t f_k$	$\phi_m = A_1 e^{-\frac{u^2}{2}}$	$A_1 = 1 - 2\frac{e_{mk}}{t}$	$u = \frac{\frac{h_{ef}}{t} \cdot \sqrt{\frac{f_k}{E}} - 0.063}{0.73 - 1.17\frac{e_{mk}}{t}}$	(Eq. 5.1)
$e_{mk} = e_m + e_k \geq 0.05t$	$e_m = \frac{M_m}{N_m} + e_{hm} \pm e_a$	$e_a \geq \frac{h_{ef}}{450}$	$e_k = 0.002\phi_\infty \frac{h_{ef}}{t}\sqrt{te_m}$	

These (Eq. 5.1) are the general equations from [64] where, $t=132mm$ is the wall's thickness. This thickness coincides with the effective thickness (t_{ef}) for the studied cases. This variable is defined as the vertical distance between the hinges' axes for all walls except for wall W#4. This particular wall shows a fixed-pinned configuration and the effective height is 0.7 times the distance between hinge's axes.

It has to be highlighted that EC-6 code does not consider the tensile strength of the masonry, which has been proved to be essential for the most slender and/or most eccentrically loaded masonry walls (see [73,87,89]), leading to conservative results (see section 5.2.5.1). The values of the particular variables (h_{ef}, f_k, e) needed to calculate the load-bearing capacity of each wall according with EC-6 are summarised in section 5.2.5.

5.2.2. ACI-530 formulation

ACI-530 [43] is the reference code for the masonry construction in the United States of America. Similarly to Eurocode-6, the formulation in based on series of empirical data obtained from experimental campaigns which have been used to adjust the mathematical formulation.

ACI-530 includes empirical coefficients in the formulation like EC-6. Nevertheless, it is worth mentioning that ACI-530 checks the three possible phenomenon (axial, bending and buckling) separately, in contrast with EC-6 which provides a unique formulation. In addition, ACI-530 considers the possibility of calculating the limit stress instead of the ultimate load. The formulation proposed in [43] for calculating the stress distribution is based on the elasticity equations (linear stress distribution) but the

limit stress is defined with an empirical criteria. The safety factors included in the code are not considered here (see equations (Eq. 5.2)) for the calculation of the load-bearing capacity of the tested walls because a direct comparison with the experimental results is required.

Phenomena	***Case***	***Calculation***
Axial	$\frac{h_{ef}}{r} \leq 99$	$N_{max} = \frac{f'_m\left(1-\left(\frac{h_{ef}}{140r}\right)^2\right)}{bt}$
	$\frac{h_{ef}}{r} > 99$	$N_{max} = \frac{f'_m\left(\frac{70r}{h_{ef}}\right)^2}{bt}$
Bending and axial	$\frac{h_{ef}}{r} \leq 99$	$\frac{\frac{M_{max}}{I}y}{f'_m} + \frac{\frac{N_{max}}{bt}}{f'_m\left(1-\left(\frac{h_{ef}}{140r}\right)^2\right)} = 1$
	$\frac{h_{ef}}{r} > 99$	$\frac{\frac{M_{max}}{I}y}{f'_m} + \frac{\frac{N_{max}}{bt}}{f'_m\left(\frac{70r}{h_{ef}}\right)^2} = 1$
Buckling	All	$N_{max} = P_e = \frac{\pi^2 E_m I}{h^2}\left(1-0{,}577\frac{e}{r}\right)^3$

(Eq. 5.2)

The formulae for calculating the load-bearing capacity according with each possible failure phenomenon are presented in (Eq. 5.2). N_{max} is the load-bearing capacity, $M_{max}=e\cdot N_{max}$ is the associated bending moment for the eccentricity in the calculus section *e*, $y=t/2$ is the distance from the neutral axis to the most compressed fibre in the pure bending configuration, f_m' is the compressive strength of the material (without any reduction as the code proposes) and E_m the corresponding Young's modulus. *b* is the width of the wall, $t=132mm$ the thickness of the wall, h_{ef} the effective height and the radius of gyration, *r*, is defined as:

$$r = \sqrt{\frac{I}{A}} \qquad \text{(Eq. 5.3)}$$

In (Eq. 5.3) *I* is the momentum of inertia of the cross section and *A* the area of the cross section.

For the tested walls, two possible failure modes were possible: the bending-axial and the buckling. Thus, both have been checked to obtain the load-bearing capacity of the wall (corresponding with the minimum of them). Observing (Eq. 5.2) it is noticed that there are two possible situations depending on the geometry of the cross section: whether *h/r* is greater or less than 99.

Like EC-6, ACI-530 does not consider the tensile strength of the masonry in the calculation of the load-bearing capacity which is expected to outcome in conservative results. The values of the particular variables (h_{ef}, f_k, b and e: eccentricity in the calculation section) which are required to calculate the load-bearing capacity of each wall according with ACI-530 are summarised in section 5.2.5. All URMW have been calculated according with the procedure proposed in ACI-530 and the results are presented in section 5.2.5.1.

5.2.3. 2nd order deformation and section strength comparison

The second order deformation of the URMW walls can be directly calculated if assuming an elastic response of the material. It has to be noted that this hypothesis is not conventional. In fact, the compression response of the masonry is usually assumed to be plastic and a rectangular stress diagram is used for most of the common calculations of masonry walls. However, these second order deformations represent the geometric non-linearity of the problem which might be more influent on the load-bearing capacity than the material non-linear response in compression for the tested unreinforced walls. Thus, assuming a linear elastic behaviour allows considering these significant second order deformations in an easy and effective way. It has to be highlighted that this proposed analytical method for the URMW is mainly oriented to calculate those walls whose failure mode is associated with a mechanism formation. The accuracy of the obtained results (see section 5.2.5.1 and 5.2.5.2) also justify this hypothesis.

The differential equation which relates the bending moment with the deflection can be specifically written for both cases of the boundary conditions studied: fixed-pinned wall corresponding with W#4 and pin ended walls for the rest of the non-strengthened walls.

The solution of this differential equation, $v(x)$, is the deformation of the wall along its height. For all walls, except W#4, the maximum deflection is located at mid-height and its value can be calculated with the expression (Eq. 5.4) according with [122]. A sketch of the calculated deformation is shown in Figure 5.1.

$$v\left(x=\frac{h_{ef}}{2}\right)=e\cdot\left(\frac{1}{cos\left(\frac{h_{ef}}{2}\cdot\sqrt{\frac{N}{EI}}\right)}-1\right) \quad \text{(Eq. 5.4)}$$

In this equation, e is the real eccentricity at mid-height at the beginning of the loading process, h_{ef} is the effective height of the wall, E and I are the Young's modulus of the masonry and the modulus of inertia of the cross section respectively, and finally, N is the applied load.

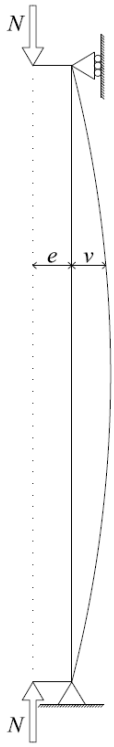

Figure 5.1 Second order deformation of an eccentrically loaded column

Using (Eq. 5.4) it is possible to obtain a theoretical evolution of the total eccentricity of the load (e_{total}). It is calculated by adding the constant value of the initial eccentricity (e) to the calculated deflection (v) for each load step along the loading process. The resulting formulation is (Eq. 5.5).

$$e_{total}\left(x = \frac{h_{ef}}{2}\right) = e \cdot \left(\frac{1}{cos\left(\frac{h_{ef}}{2} \cdot \sqrt{\frac{N}{EI}}\right)}\right) \qquad \text{(Eq. 5.5)}$$

Finally, for each load step it is possible to calculate the theoretical applied bending moment: multiplying the axial load, N, by the total eccentricity, e_{total}. Gathering the data for different load steps an axial-bending interaction curve might be drawn. This type of plot shows the theoretical evolution along a loading process. For each wall, this curve was compared with the experimental one obtained from the measured deflection at mid-height and the corresponding applied axial load.

In contrast, for wall W#4, the point with the maximum deflection depends on the applied load (see (Eq. 5.6)) and might not coincide with the mid-height.

$$v\left(x=\frac{h_{ef}}{2}\right)=e\cdot\left(tan\left(\frac{h_{ef}}{2}\cdot\sqrt{\frac{N}{EI}}\right)\cdot sin\left(\frac{h_{ef}}{2}\cdot\sqrt{\frac{N}{EI}}\right)+cos\left(\frac{h_{ef}}{2}\cdot\sqrt{\frac{N}{EI}}\right)-1+\sqrt{\frac{N}{EI}}\cdot tan\left(\frac{h_{ef}^2}{4}\cdot\sqrt{\frac{N}{EI}}\right)\right) \quad \text{(Eq. 5.6)}$$

It was decided to calculate the deflection at mid-height in order to compare these analytical results with the experimental ones (measured at mid-height). The formula to calculate the total eccentricity at mid-height is (Eq. 5.7) according with [122].

$$e_{total}\left(x=\frac{h_{ef}}{2}\right)=e\cdot\left(tan\left(\frac{h_{ef}}{2}\cdot\sqrt{\frac{N}{EI}}\right)\cdot sin\left(\frac{h_{ef}}{2}\cdot\sqrt{\frac{N}{EI}}\right)+cos\left(\frac{h_{ef}}{2}\cdot\sqrt{\frac{N}{EI}}\right)+\sqrt{\frac{N}{EI}}\cdot tan\left(\frac{h_{ef}^2}{4}\cdot\sqrt{\frac{N}{EI}}\right)\right) \quad \text{(Eq. 5.7)}$$

Identically to the rest of the non-strengthened studied walls, the bending moment at mid-height was calculated with the axial load and the total eccentricity (e_{total}). Then, the axial-bending response curve was also obtained and compared with the experimental one for the wall W#4.

The aim of calculating the axial-bending response curves was double: to compare them with the corresponding experimental curves (see Figure 5.13and Figure 5.14 later on) and to intersect them with the curves representing the axial-bending stress limit criterion. These curves associated with the stress limit criterion were calculated by assuming the following hypotheses previously justified:

- Linear strain distribution along the cross section thickness.
- Linear stress distribution in both tensile and compressed areas.
- Failure criteria when the maximum compressive stress reached the compressive strength of the masonry (f_c) or when the tensile stress reached the value of the tensile strength of the masonry joints (f_t).

The limit criteria calculated in this simple way is represented by two straight lines which depend on the geometry of the cross section (thickness, t and width, b) and on the compressive (f_c) and flexural (f_t) strength of the masonry. Thus, each wall thickness (because all the studied walls had the same theoretical width) or masonry type has a slightly different failure criterion to compare with both experimental and analytical wall response in the axial-bending interaction plane.

The maximum axial force (N) and bending moment (M) combination that a rectangular section can bear taking into account the maximum compressive strength (f_c) of the masonry is calculated, under the previous hypothesis, with the formula (Eq. 5.8):

$$M=\frac{f_c b t^2}{6}+\frac{Nt}{6} \quad \text{(Eq. 5.8)}$$

Similarly, the maximum axial force (N) and bending moment (M) combination that a rectangular section can bear taking into account the maximum tensile strength (f_t) of the masonry is calculated, under the previous hypothesis, with the formula (Eq. 5.9):

$$M = \frac{f_t b t^2}{6} - \frac{N t}{6} \qquad \text{(Eq. 5.9)}$$

5.2.4. Analysis with Southwell Plot method

The Southwell Plot method is commonly used to estimate the buckling critical load of a compressed element taking into account the load eccentricity in an implicit way. A detailed explanation of the method can be consulted in Bažant and Cedoline [80]. This semi-empiric method is useful for predicting the load-bearing capacity of structural elements which are likely to fail because of buckling process and show an elastic response. The Southwell Plot method requires measuring the response of the structural element (applied load and corresponding lateral deformation) for low or moderate loads (non-destructive). The studied structure needs eccentrically applied loads or geometric imperfections that initially cause lateral deflections in order to obtain the required data to apply the Southwell Plot method.

A direct application of the Southwell Plot method is presented in this section although other authors have dealt with the consideration of more complex hypothesis like plastic buckling [81]. Essentially, Southwell proposed that there was a relationship between the lateral deflection (h) and the applied load (N) which depends on the critical load (P_{cr}) and the initial mid-height lateral deformation (a), see (Eq. 5.10):

$$h \approx \frac{a}{\frac{P_{cr}}{N} - 1} \qquad \Longrightarrow \qquad \frac{h}{N} \approx \frac{1}{P_{cr}} h + \frac{a}{P_{cr}} \qquad \text{(Eq. 5.10)}$$

Thus, when plotting h versus $\frac{h}{N}$ in y and x axis respectively, a straight line is obtained and the slope of this line is a measure of the buckling load.

The applicability of the Southwell Plot method depends on the scattering of the measured data. For this reason, this method is not suitable for those cases with large dispersion in the measurements or inconsistent experimental data. In fact, during the current research has been observed that the points of the Southwell Plot (h versus $\frac{h}{N}$ graph) should be linear fitted with a regression coefficient greater than 0.8 to obtain reliable results when using this semi-empiric method. More scattered data results in a meaningless value of the load-bearing capacity.

5.2.5. Results and comparison

First of all, it is necessary to summarise the input data used (see Table 5.1) before presenting and analysing the results of the different analytical methods applied on the calculation of the unreinforced masonry walls. More detailed data of the experimental tests is shown in Annex 1.

Wall	*Eccentricity, e (mm)*	*Effective height, h_{ef} (mm)*	*Masonry compressive strength, f_c (MPa)*
W#1	5.6	2947	18.2
W#2	19.6	2927	12.9
W#3	1.2	2922	
W#4	3.9	1980	
W#5	7.0	2917	
W#6	33.7	2857	13.7
W#7	13.1	2872	
W#8	-7.6	2942	
W#9	21.5	2892	
W#10	0.2	1865	10.8
W#11	13.9	1892	
W#12	1.6	1841	
W#13	31.8	1861	
W#14	21.2	1861	
W#15	29.0	1845	
W#16	19.5	1860	
W#17	88.0	1905	
W#18	20.8	1197	
W#19	30.3	1220	
W#20	33.0	1221	

Table 5.1 Data for the analytical calculation of the walls

The theoretical width (90cm) and thickness (132mm) was considered for all walls, except for wall W#17 which has a thickness of 282mm.

5.2.5.1 Load-bearing capacity

The load-bearing capacity (N_{max}) of the URMW was calculated with three different methods: Eurocode-6, ACI-530 and Southwell Plot. The first two methods only require geometric data and some masonry strength parameters (listed before in sections 5.2.1 and 5.2.2) to calculate the load-bearing capacity of the walls. In contrast, the Southwell Plot method needs experimental data about the structural response of the walls to predict the ultimate load. In particular, this method requires the load versus lateral displacement data for loads far lower than the collapse one. The results of all these methods are summarised in Table 5.2. In this table the absolute values of the relative errors are also shown.

Type	*Wall*	N_{max} *(kN)*				*Error (%)*		
		EC-6	*ACI-530*	*Southwell*	*Experimental*	*EC-6*	*ACI-530*	*Southwell*
H	W#1	0.0	117.0	(*)	172.3	100.0	30.9	(*)
	W#2	0.0	53.8	63.6	68.7	100.0	18.1	3.3
	W#3	0.1	88.9	176.0	136.7	99.9	33.5	31.5
F	W#4	29.0	317.7	(*)	578.6	95.0	45.1	(*)
H	W#5	0.0	76.2	(*)	242.7	100.0	68.2	(*)
	W#6	0.0	50.8	29.0	32.8	100.0	69.4	3.3
	W#7	0.0	114.3	168.7	137.5	100.0	15.2	25.3
	W#8	0.0	150.4	152.0	132.2	100.0	16.3	17.5
	W#9	0.0	82.1	107.8	112.7	100.0	25.2	1.8
M	W#10	66.6	224.3	320.1	425.7	84.3	47.1	24.5
	W#11	13.1	96.2	319.1	372.9	96.5	74.1	14.0
	W#12	73.2	285.4	413.4	472.8	84.5	39.4	12.3
	W#13	0.2	44.5	91.9	85.4	99.8	46.9	9.7
	W#14	3.9	119.8	558.0	520.3	99.2	76.9	7.6
	W#15	0.5	53.3	260.5	238.5	99.8	77.5	10.0
	W#16	5.5	161.7	540.5	410.0	98.6	60.4	32.4
T	W#17	87.2	190.0	398.7	494.9	82.2	61.3	18.8
S	W#18	118.9	297.2	(*)	804.4	85.2	63.0	(*)
	W#19	34.6	141.0	(*)	687.1	95.0	79.4	(*)
	W#20	21.9	111.3	165.1	153.6	85.6	27.0	8.2

(*) The regression line was not representative (regression coefficient lower than 0.8). The experimental data makes it not possible to calculate the ultimate load using Southwell Plot.

Table 5.2 Results of the three analytical methods (Eurocode-6, ACI-530 and Southwell Plot) for calculating the load-bearing capacity of URMW walls.

The load-bearing capacities according with Eurocode-6 and ACI-530 were calculated as described in the sections 5.2.1 and 5.2.2 respectively.

Figures 5.2-6 show the Southwell Plot for all URMW walls. Each figure is composed of two graphs and corresponds to one wall typology according with the geometric main characteristics. The left one represents the Southwell Plot whereas the graph at the right shows the corresponding linear regressions. The values of the slope of these linear fittings are the predicted load-bearing capacities.

Because of the testing procedure most of the points plotted in the Southwell Plot correspond to the beginning of the test, when little load was applied. For this reason, the straight line resulting from fitting the first points (the only ones typically used for the Southwell Plot method) coincide with the line obtained by adjusting all the points of the test. Thus, these linear fittings were carried out using all the available experimental data.

Only the regression lines with a regression coefficient (R^2) greater than 0.8 were considered for calculating the load-bearing capacity. The other cases have no result in Table 5.2 because the experimental data showed a large scattering and the plot cannot be assumed to be linear.

The results of the calculus carried out accordingly with Eurocode-6, ACI-530 and Southwell Plot method for each URMW are presented next. These are classified by the geometric characteristics of the walls.

- H series

It is observed that the average error for walls of the H series is 100%, 34.6% and 13.8% for EC-6, ACI-530 and Southwell Plot respectively. Thus, the most accurate code is ACI-530 but Southwell Plot method provides an even most precise prediction of the load-bearing capacity. However, it has to be said that the Southwell Plot is not applicable for walls W#1 and W#5. The relative errors are 100% and 29.6% respectively, if considering the results of EC-6 and ACI-530 without walls W#1 and W#5 in order to compare the three methods with the same cases

The results in Table 5.2 point out that the results of EC-6 are always conservative for H series (this method always predicts lower load-bearing capacities than those experimentally obtained). ACI-530 provides conservative errors for most of the cases belonging to the H series. In contrast, Southwell Plot is balanced with estimated load-bearing capacities over and below the experimental ones.

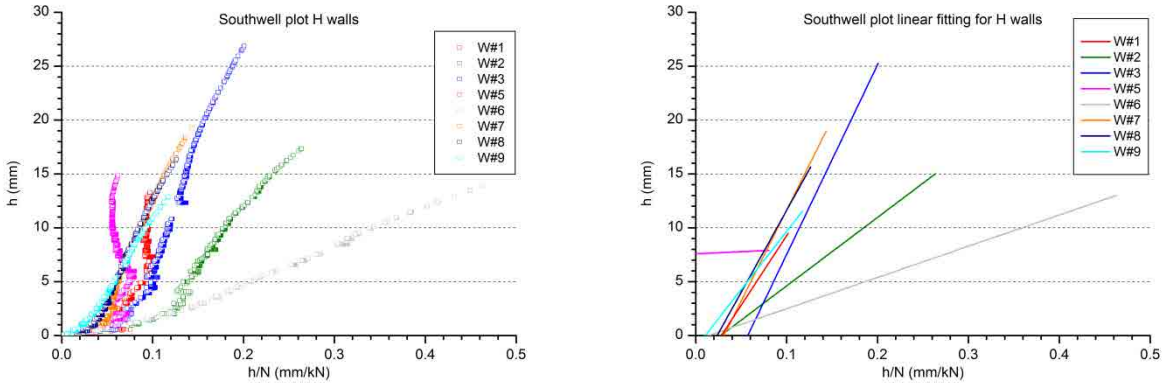

Figure 5.2 Southwell Plot for H walls (left) and the corresponding linear fitting (right)

- F series

The calculation of this wall considering EC-6 and ACI-530 was performed on the basis that the effective height of wall W#4 was 0.7 times the real height of the wall. Southwell Plot does not provide a valid value of the critical load because of the scattering of the obtained data. Finally, if comparing the two codes, ACI-530 is the most accurate one with a relative error around 45%.

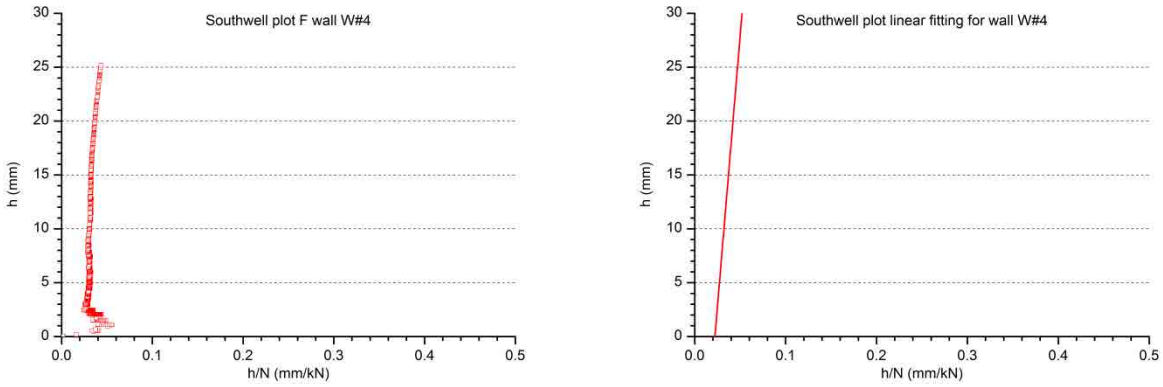

Figure 5.3 Southwell Plot for wall W#4 (left) and the corresponding linear fitting (right)

- M series

The first thing to highlight is that Southwell Plot is applicable for all the walls of this series. The relative errors of the calculation methods are 94.7%, 64.3% and 15.8% for EC-6, ACI-530 and Southwell Plot respectively. Thus, the best of the codes is ACI-530 like for the walls of the H series. In addition, the calculation method with the best accuracy among the ones tried is Southwell Plot. However, its applicability in field conditions would be restricted to those cases which could be tested by applying axial loads. Regarding the sign of the error, EC-6 and ACI-530 are always conservative whereas are Southwell Plot's results are balanced.

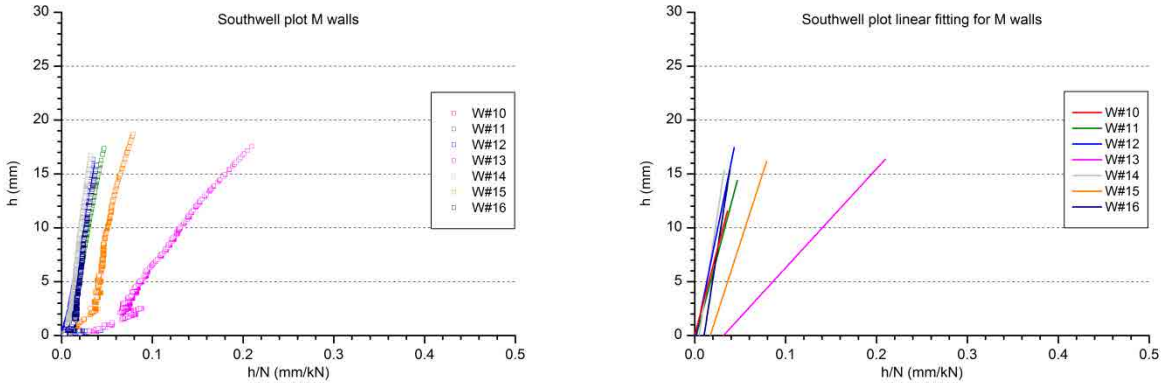

Figure 5.4 Southwell Plot for M walls (left) and the corresponding linear fitting (right)

- T series

The only wall of this series has been calculated using the three methods. All of them provide conservative results and the Southwell Plot is the most accurate one with a relative error below 20% whereas the error of the codes is far larger: 61.3% for ACI-530 and over 80% for EC-6. It has to be

noticed that the failure mode of this wall suggested not using the Southwell Plot because the failure mode was not a typical mechanism formation.

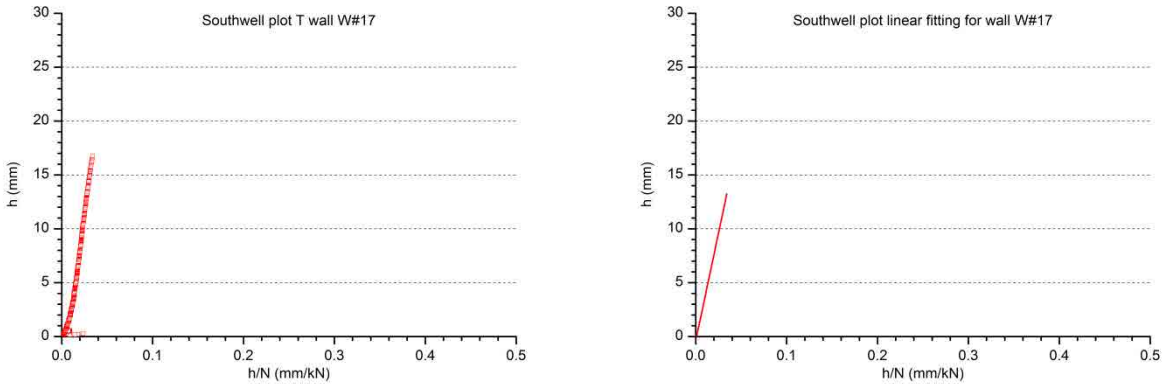

Figure 5.5 Southwell Plot for wall W#17 (left) and the corresponding linear fitting (right)

- S series

The anomalous experimental response of two of the walls of this series (see Figure 5.6) caused that the Southwell Plot method could only be used for calculating the load-bearing capacity of wall W#20. For this particular case the relative error is around 8%. Like for the T series, it has to be remarked that the experimentally observed failure mode for the S series walls (not corresponding with a simple mechanism formation) suggested that the Southwell Plot method was not suitable for these cases. The two analysed standardised methods, which are valid for all walls, have an error of 56.5% and 61% respectively for EC-6 and ACI-530 calculations.

Thus, EC-6 is better than ACI-530 at predicting the ultimate strength of the less slender walls but ACI-530 show better agreement with the experimental data for the most slender and most eccentrically loaded walls.

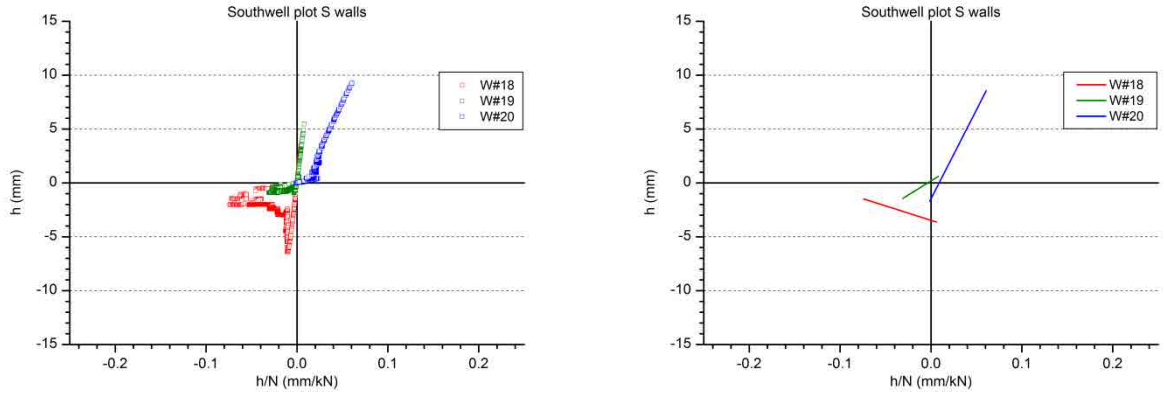

Figure 5.6 Southwell Plot for S walls (left) and the corresponding linear fitting (right)

5.2.5.2 Structural response

The theoretical bending moment versus axial load curve is compared with the experimental one for each wall. The theoretical bending moment is calculated multiplying the theoretical lateral deflection (Eq. 5.7) by the associated axial load, *N*. Then, the theoretical response is intersected with the section strength criteria, (Eq. 5.8) and (Eq. 5.9), to obtain the corresponding load-bearing capacity which is compared with the experimental one in Table 5.3.

Type	***Wall***	***Theoretical maximum load (kN)***	***Experimental maximum load (kN)***	***Error (%)***	***Average error no sign (%)***
H	W#1	115.5	172.3	-33.0	27.0
	W#2	63.7	68.7	-7.2	
	W#3	142.4	136.7	4.1	
	W#5	113.2	242.7	-53.3	
	W#6	37.2	32.8	13.4	
	W#7	86.1	137.5	-37.4	
	W#8	106.0	132.2	-19.8	
	W#9	58.8	112.7	-47.8	
F	W#4	72.9	578.6	-87.4	87.4
M	W#10	373.0	425.7	-12.4	49.8
	W#11	159.4	372.9	-57.2	
	W#12	352.4	472.8	-25.5	
	W#13	60.4	85.4	-29.3	
	W#14	104.3	520.3	-80.0	
	W#15	65.3	238.5	-72.6	
	W#16	115.2	410.0	-71.9	
T	W#17	96.8	494.9	-80.4	80.4
S	W#18	238.0	804.4	-70.4	77.5
	W#19	59.2	687.1	-91.4	
	W#20	44.9	153.6	-70.8	

Table 5.3. Load-bearing capacity calculated with the theoretical deflection considering the second order effects on URMW.

First of all, it has to be reminded that the maximum load-bearing capacity of the wall W#4 (F series) is calculated by comparing the moment at mid-height with the section strength although the maximum moment should be placed in an upper location of the wall. That means that the theoretical maximum load-bearing capacity for wall W#4 is supposed to be lower than the presented one. However, in order to compare the experimental response (measured at mid-height) with the theoretical one, the mid-height reference has been chosen.

Observing the Table 5.3 it is noticed that the best accuracy is obtained for the most slender walls (H series) which agrees with the fact that these are the cases with the greatest effect of the second order. In contrast, this calculation method does not reach good accuracy for the less slender walls (S and T series) and the wall with fixed endings (W#4). These results might be also explained by the initial hypothesis of

considering a linear stress distribution instead of a rectangular one for the calculation of the strength criteria. This alternative stress distribution would bring higher values of the load-bearing capacity of the walls of the S, T and F series. This response confirms the orientation of the proposed analytical method which was aimed to accurately predict the cases of the walls which are most likely to fail by a mechanism formation.

Analysing the results, it might be concluded that the proposed method consisting of calculating the second order deflection and comparing the associated bending moment with a simple section strength criteria works correctly for the cases which show a more linear response and a larger lateral deflection (the most slender ones). This agrees with the initial hypotheses of the method.

Finally, it has to be highlighted that the average error of the proposed analytical method for the H series (27%) is within the range of the scattering of the input data, so this is a suitable method for calculating these cases. Moreover, this method underestimates the load-bearing capacity of the walls for all cases except walls W#3 and W#6. This underestimation tendency grows when the slenderness decreases and the second order effects are less important and the material behaves mainly in a non-linear way in compression.

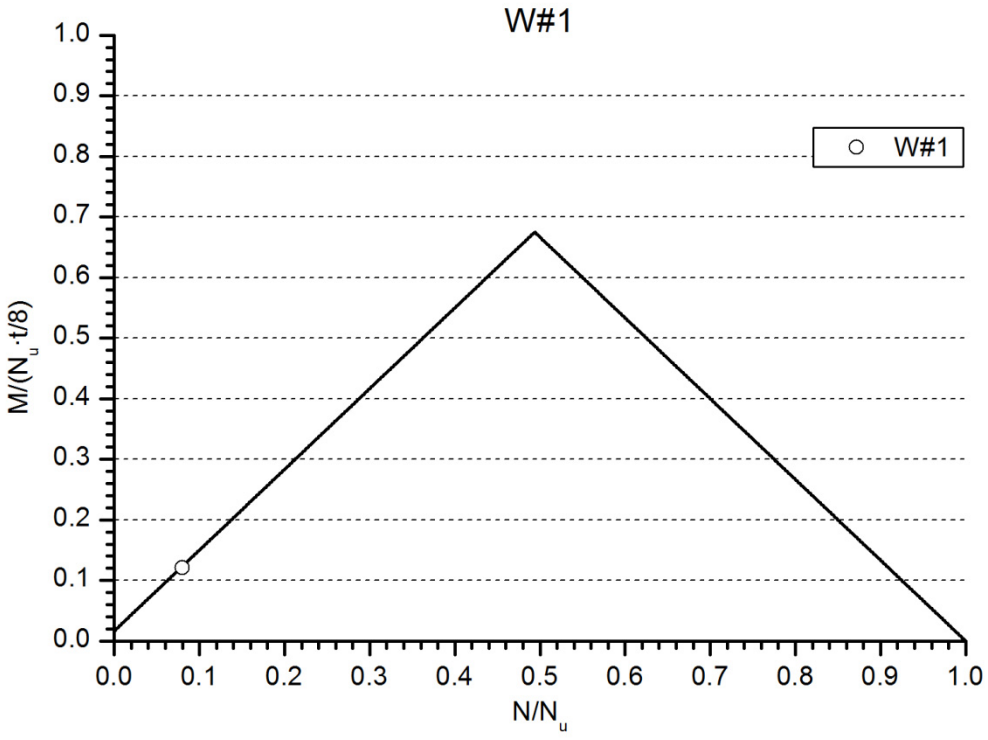

Figure 5.7 Section strength failure criteria and axial-bending load-bearing capacity for wall W#1

The section strength failure criteria for each wall typology – assuming the theoretical width and calculated with (Eq. 5.8) and (Eq. 5.9) – is represented and compared with the experimental axial force-bending moment pairs in graphs corresponding to Figures 5.7-12. The axial force variable is presented in a dimensionless form by dividing the axial force (*N*) by the maximum compressive strength of the wall's

section assuming a uniform stress distribution ($N_u=btf_k$). Similarly, the bending moment is presented in a dimensionless form by dividing its value by the moment $M_u=N_ut/8$.

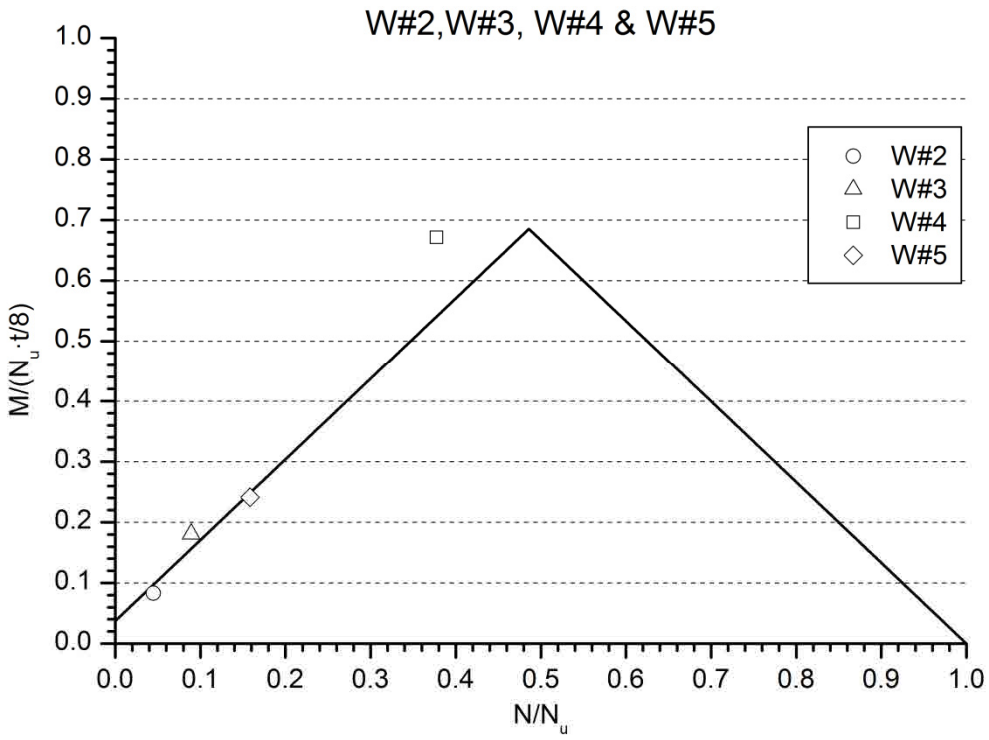

Figure 5.8 Section strength failure criteria and axial-bending load-bearing capacity for walls W#2-5

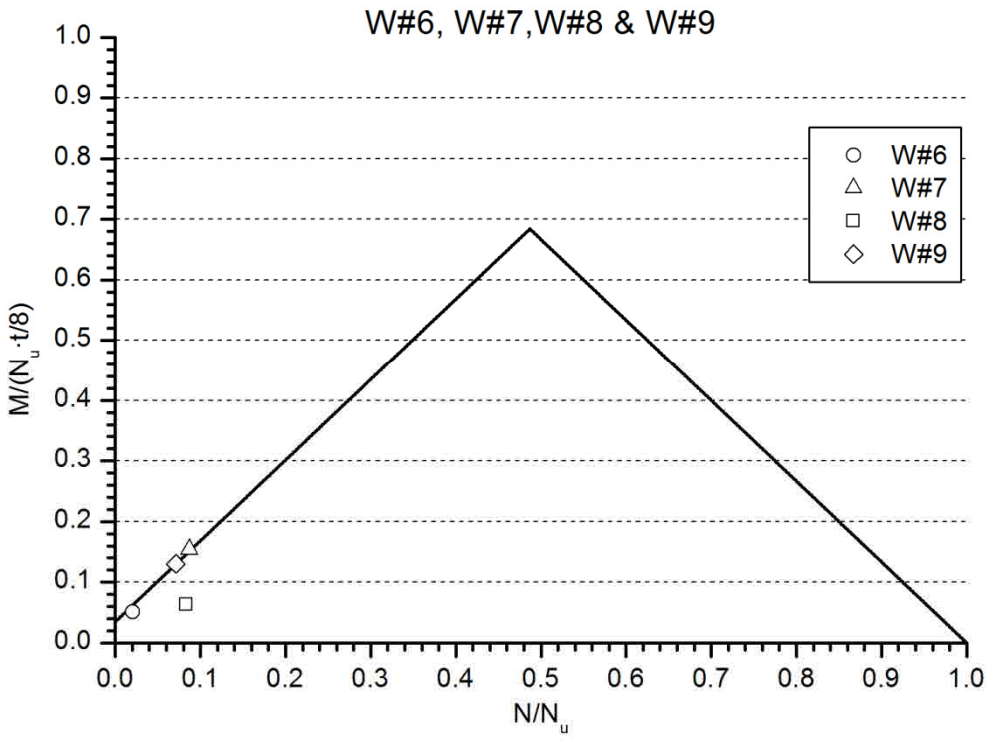

Figure 5.9 Section strength failure criteria and axial-bending load-bearing capacity for walls W#6-9

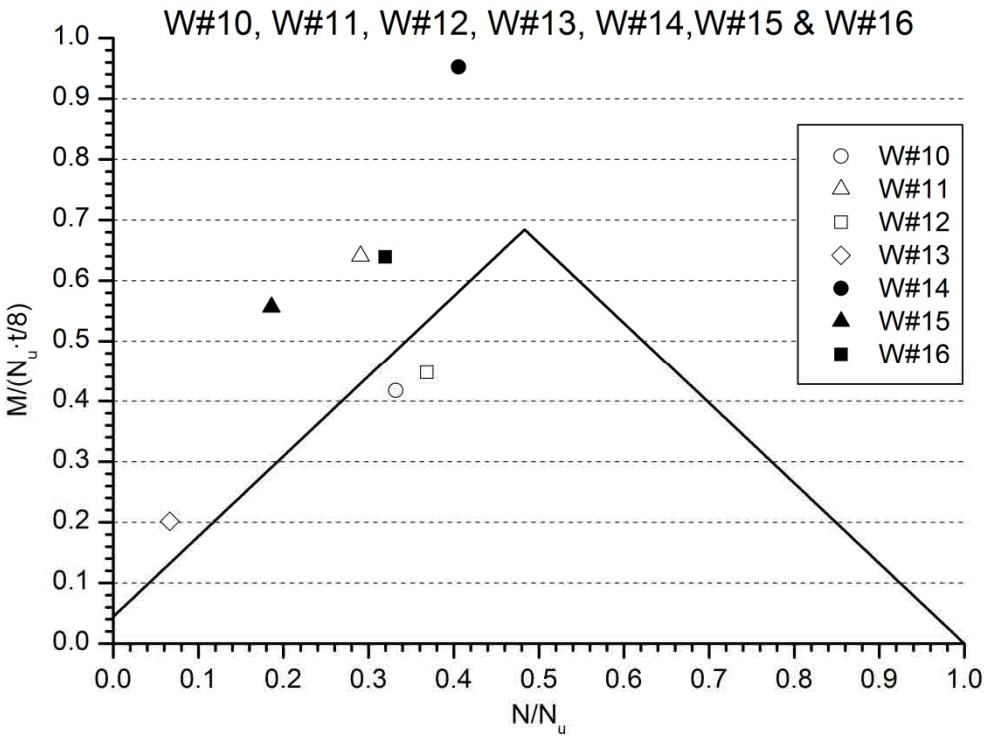

Figure 5.10 Section strength failure criteria and axial-bending load-bearing capacity for walls W#10-16

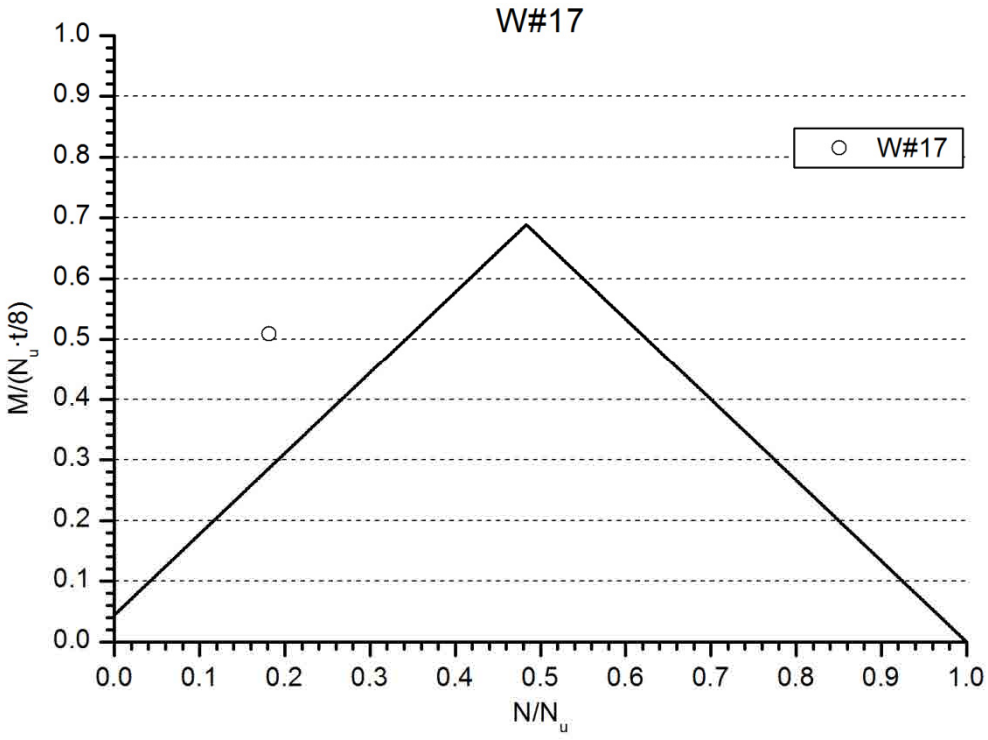

Figure 5.11 Section strength failure criteria and axial-bending load-bearing capacity for wall W#17

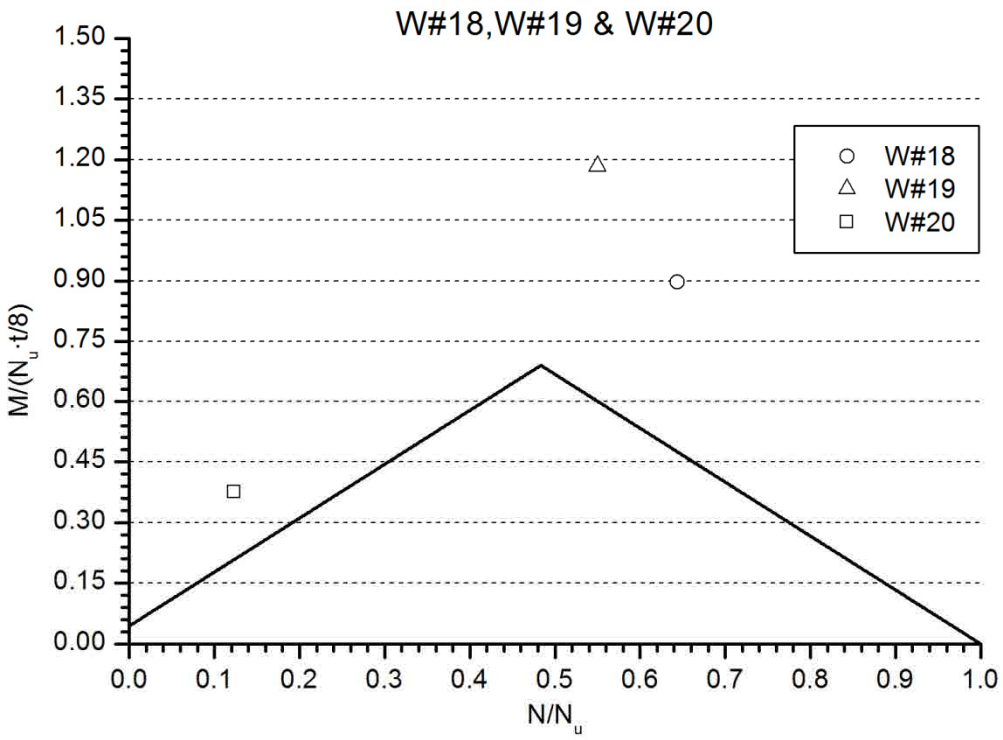

Figure 5.12 Section strength failure criteria and axial-bending load-bearing capacity for walls W#18-20

Observing the graphs in Figures 5.7-12 the first thing that should be highlighted is that the tensile strength of the masonry is taken into account in the cross section failure criteria. This is the reason why the line with positive slope does not start in the origin. In fact, it represents that the section can bear a little bending moment with no axial force associated.

The graphs in Figures 5.7-12 show that the best accuracy is obtained for the most slender walls (H series, W#1-3 and W#5-9). For these cases, the experimental ultimate axial-bending pairs (the points in the graphs) are close to the failure criteria (lines). In particular, all of them are near the line with positive slope which corresponds to the tensile failure of the section. Thus, the proposed section strength failure criterion is suitable to predict the ultimate load in these cases. In conclusion, it means that the main failure cause for the most slender walls is reaching the tensile strength (left ramp of the graphs in Figures 5.7-12).

In contrast, this failure criterion seems to show discrepancy with the experimental results of the less slender unreinforced walls (W#17-20) which are out of the intended applicability range of the proposed method. Thus, as it was expected, when the compression response is significant, the linear stress distribution assumption might not provide accurate results. In addition, some of these differences between the experimental evidence and the theoretical calculation might be also caused by the scattering of the material's properties, especially of the compressive and tensile strengths.

All walls of the M series (except W#14 and W#15) failed with experimental axial-bending moment pairs near the line which represents the tensile strength criterion of the cross section. Although the accuracy is not as good as for the H series, it is within the scattering range. The obtained results over and underestimate the load-bearing capacity of the walls, so the method is balanced. Moreover, the most probable failure criterion for all them, according with the experimental observation, is reaching the tensile strength of the masonry as the analytical method suggest.

Figure 5.13 shows the comparison between: (a) the theoretical axial force versus bending moment curve calculated using the second order deflection method and represented with a red line, and (b) the experimental response represented with scatter points. The maximum buckling load of concentrically loaded wall, calculated with elastic theory (Euler, (Eq. 5.11)) is also presented with a black horizontal solid straight line to fix a theoretical threshold value. In (Eq. 5.11), *E* is the Young's modulus and *I* is the modulus of inertia of the cross section.

$$P_{cr} = \frac{\pi^2 EI}{h_{ef}^2} \qquad \text{(Eq. 5.11)}$$

For wall W#4, the formula to calculate the Euler's critical load according with its boundary conditions is (Eq. 5.12):

$$P_{cr} = 2.046\frac{\pi^2 EI}{h_{ef}^2} \qquad \text{(Eq. 5.12)}$$

The theoretical response plotted in all graphs gathered in Figures 5.13-16 is drawn up to the maximum bending moment that the cross section can bear according with the failure criterion presented in equations (Eq. 5.8-9).

In Figure 5.13 it is observed that the theoretical 2nd order response calculated with the classical stability formulation, (Eq. 5.4-7), tends to reach the Euler maximum load. Thus, the buckling phenomena – understood as the final instability due to the deflection growing associated with the eccentricity and the second order effects – seems to be the theoretical failure process for the H walls. However, the experimental response does not perfectly match with the theoretical one for all walls. In some cases, the experimental data show a stiffer behaviour (walls W#7-9) than the theoretically expected. In other cases (W#3) a softer response was measured but for most of them (W#1,2,5,6) the theoretical response is really close to the calculated one. Thus, the presented calculation method is suitable for predicting the lateral deformation and the ultimate load of the most slender walls (H series) although the scattering of the materials properties and the geometric irregularities suggest considering its results carefully.

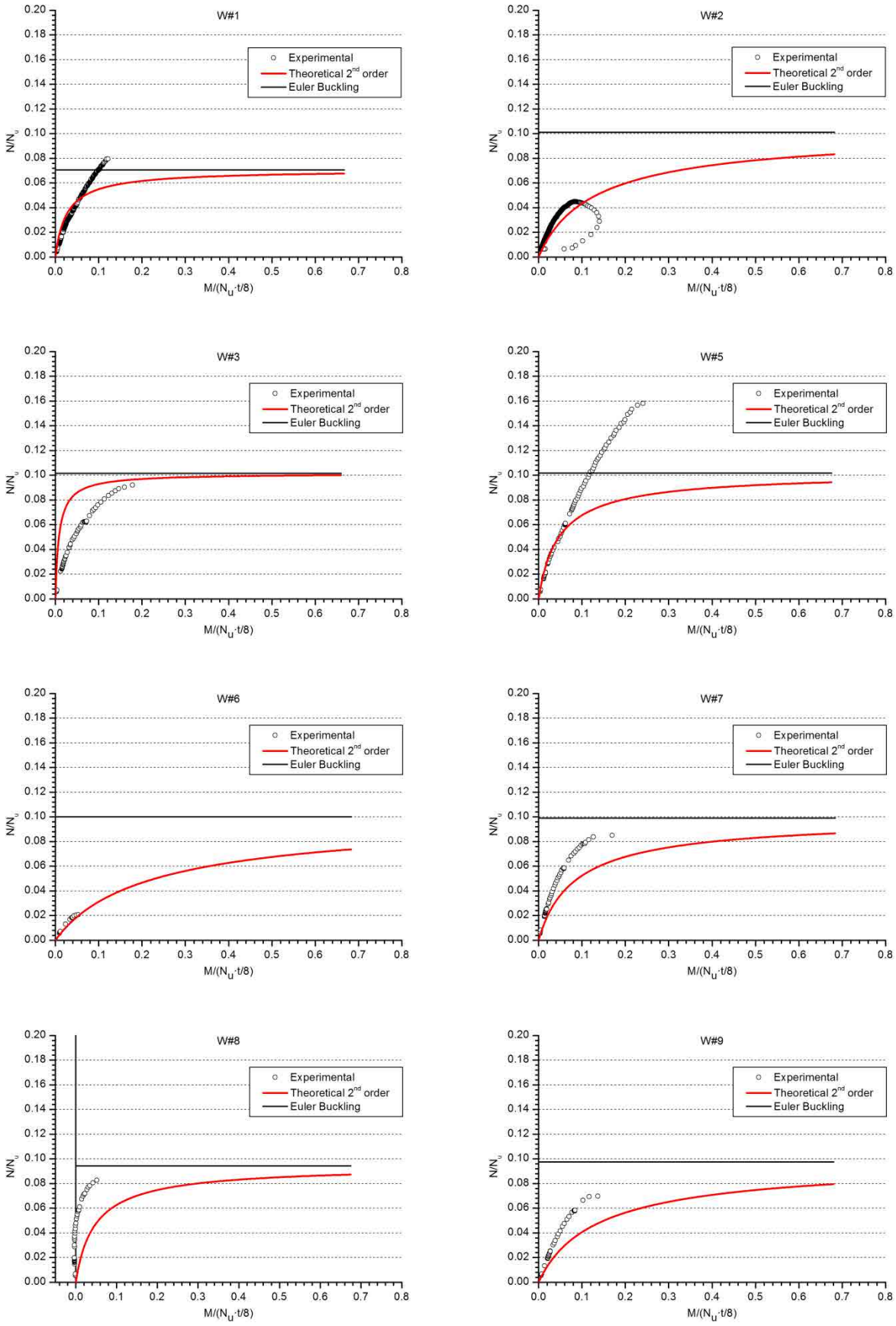

Figure 5.13 Theoretical and experimental axial-bending response of the H series walls.

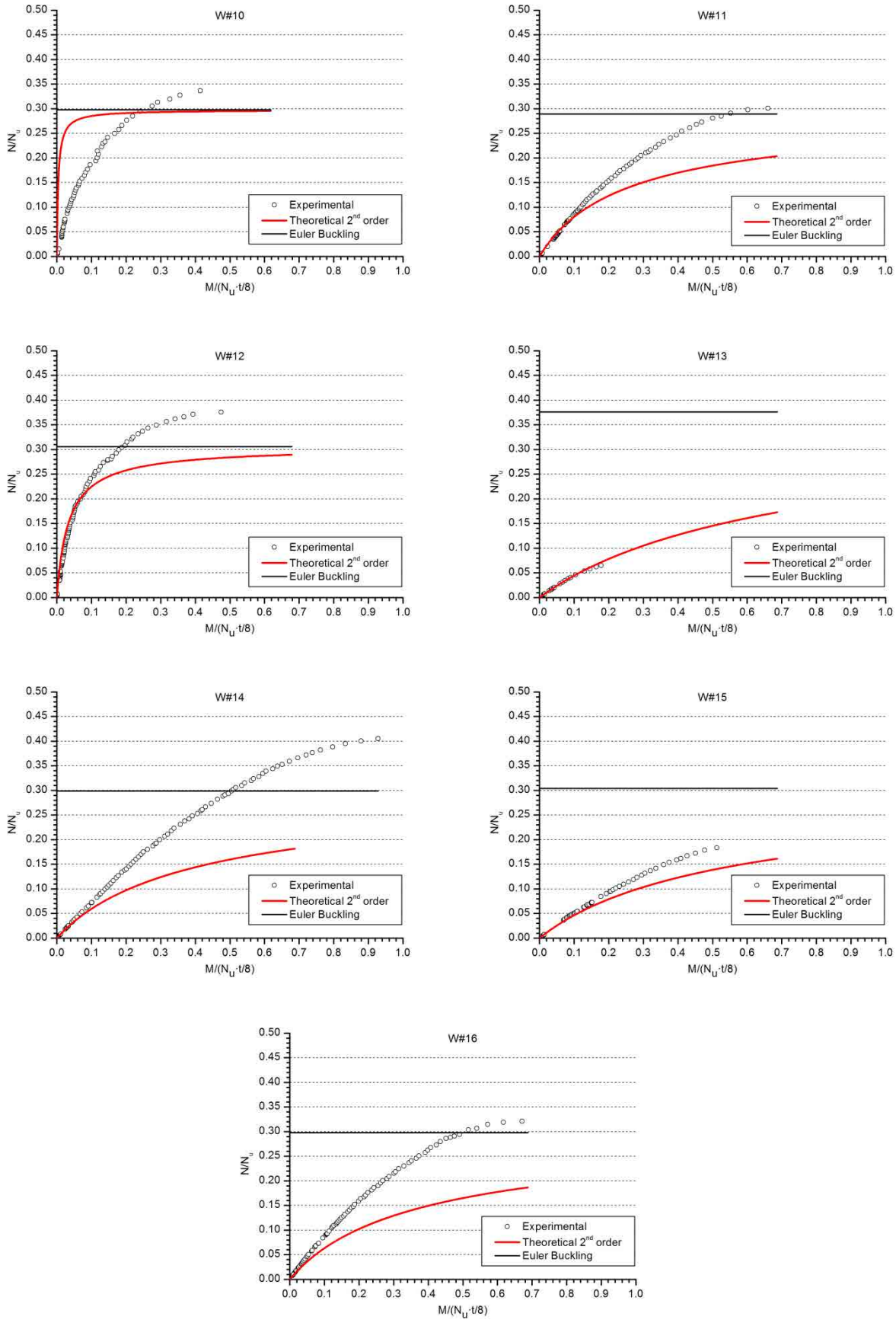

Figure 5.14 Theoretical and experimental axial-bending response of the M series walls.

For the walls of the M series (Figure 5.14) the comparison between the experimental and theoretical lateral deflection response is similar to the H series and the proposed method has reached good accuracy. However, the theoretical response tends to predict larger deflection (and, thus, larger bending moments) than the experimentally measured for these cases. It is observed by comparing the experimental and theoretical dimensionless axial-bending curves for the walls W#11, W#14-16. In fact, the calculation method underestimates the load-bearing capacity for these particular cases the ones with the stiffest lateral response of the M series. As the lateral deflection grew slower than predicted, the associated bending moment was lower and the load-bearing capacity (of considering the cross section failure) was larger for the laboratory test than the obtained with the presented formulation. In addition, for walls W#10, W#11, W#12, W#14 and W#16, the experimental maximum axial load was larger than the Euler's critical load indicating a possible non-linear response of the material combined with the likely fact that the Young's modulus could have been larger than the obtained in the average testing of the material corresponding with this walls' series.

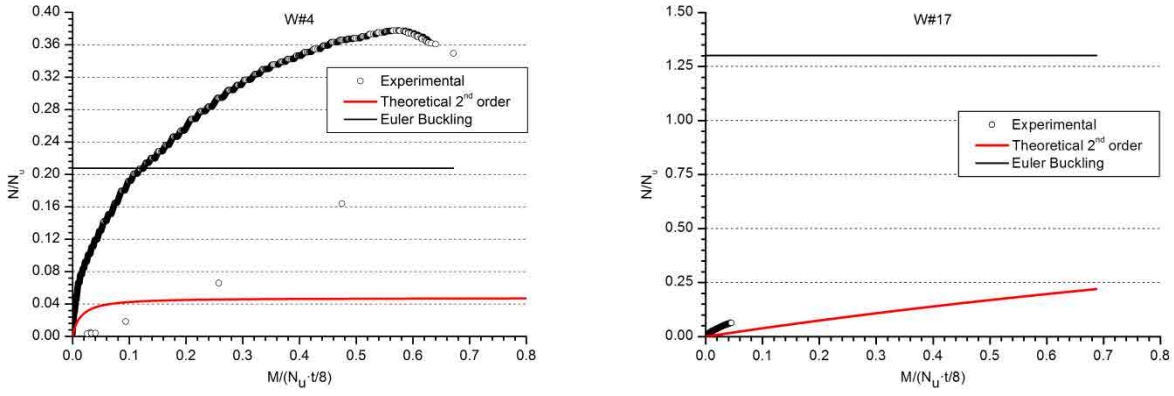

Figure 5.15 Theoretical and experimental axial-bending response of the F and T series walls.

For the walls of the F and T series (W#4 and W#17 respectively), it is observed (Figure 5.15) that the theoretical lateral deflection response differs significantly from the experimental data. For both cases, the deflection measured in the laboratory was lower than the calculated one. In addition, reaching the cross section strength, probably in compression, is the most likely failure criterion because the theoretical curves are associated with lower loads than the buckling theoretical maximum load. This is even more evident for wall W#17 whose Euler's critical load is larger than the cross section uniform compression capacity (N/N_u values over 1). Thus, the buckling phenomenon was not possible, and, in fact, it was not observed in these cases during the experimental campaign. In conclusion, the second order effects are not significant for the lateral deflection response of the less slender walls, which are controlled by the compressive response of the material. Thus, these cases are out of the intended applicability range of the proposed method.

The general tendency of the walls of the S series is the same than for the F and T series ones. The second order calculation method tends to overestimate the lateral deflection, and thus, underestimate the load-bearing capacity. In Figure 5.16 it is observed that the experimental response of walls W#18 and W#19 was stiffer than the calculated one. In contrast, W#20 theoretical and experimental responses almost coincide in the dimensionless axial-bending moment graphs. In fact, W#20 is the one whose theoretical results are closer to the section strength criterion (see Figure 5.12). The second order effects are not significant for the walls of the S series (except for W#20) and their most likely failure mode would be associated with the compressive strength of the masonry. For these cases, the linear stress distribution hypothesis used seems not to be representative enough of the behaviour of the masonry (see Figure 5.12).

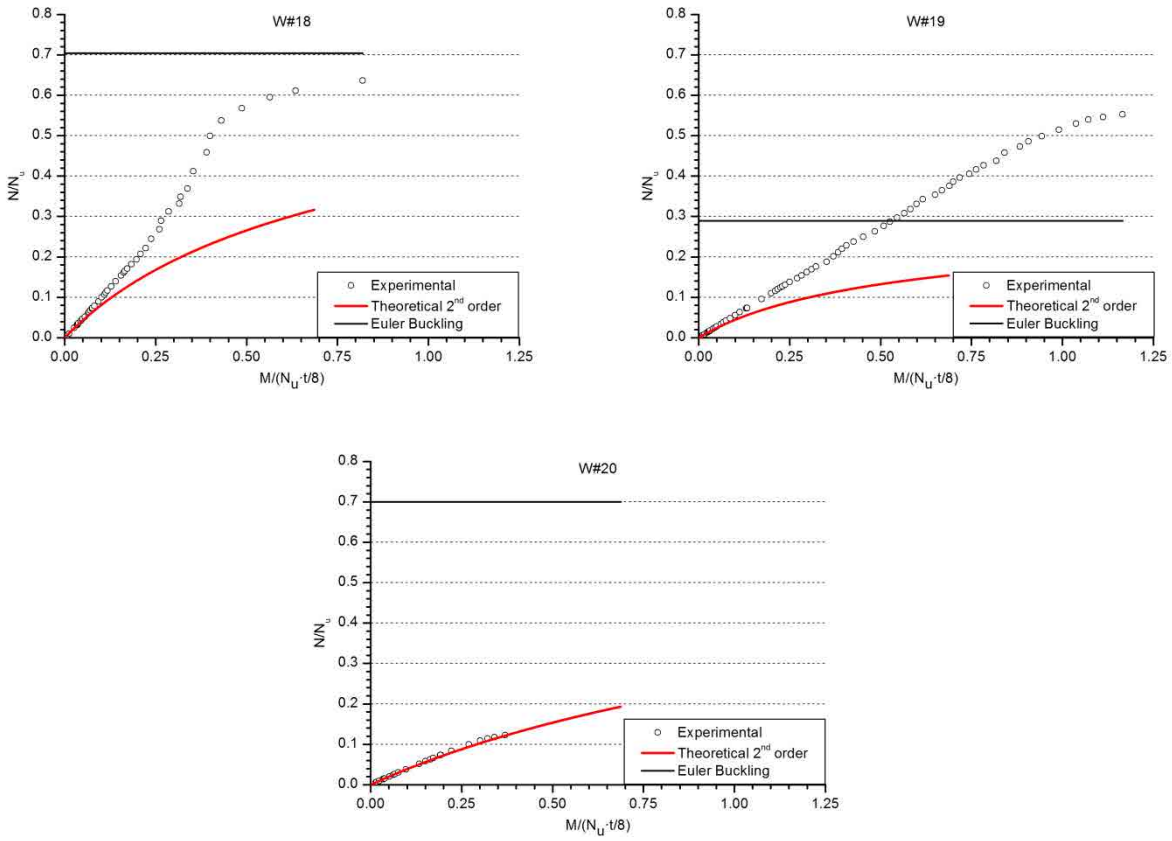

Figure 5.16 Theoretical and experimental axial-bending response of the S series walls.

5.3 TRM Strengthened Masonry Walls (TRMW)

In contrast with the unreinforced masonry walls (URMW), for the case of the TRM strengthened brickwork walls (TRMW) there are no standards to compare the experimental information with. Thus, in this subsection only two analytical approaches are presented. The first one is oriented to compare the

maximum axial and bending moment of each wall with a simple cross section strength criterion. The second approach is the Southwell Plot, and its use is aimed to assess its applicability on the TRMW.

5.3.1. Section strength comparison

A simplified method based on section equilibrium and strain compatibility equations is herein proposed. It assumes that walls failed when the stresses reach the strength or the strain reach the maximum elongation of any of the component materials. Three more hypothesis are: (a) that it is supposed that the TRM prevents the mechanism formation failure and that this strengthening system limits the second order effects turning the problem under study into a simple section resistance analysis. This hypothesis is supported by the obtained results (see section 5.3.3) which accurately associate the experimental axial-bending combination with the strength limit criterion of the cross section, indicating that the most likely failure mode was associated with reaching the component material's strength. In addition, the measured lateral deformations were far littler than the ones obtained for the corresponding unreinforced walls. (b) A linear strain distribution in the wall's thickness is assumed. Any plane section remains plane and small deformations are supposed. This hypothesis is related with limiting the influence of the second order effects included in the previous hypothesis. (c) Finally, linear stress-strain relationships for all materials are assumed for the presented analytical method.

The calculation procedure consists of obtaining the envelope of the axial (N) – bending (M) interaction curves for the two failure modes: reaching the tensile strength of TRM and reaching the compressive strength of masonry. The most restrictive condition (compression or tension) is considered for each axial load to draw the limit curve. This curve distinguishes the safe *N-M* states from those above the materials' strength possibilities. Thus, the presented formulation is analogue to the one conventionally used for reinforced concrete bending strength calculation.

Step by step, the procedure to calculate the *N-M* dimensionless interaction curve, and the values of the required variables (see Chapter 3 for the justification of these values), under the hypothesis of reaching the tensile strength of the fibre grid is:

a) Fixing a value of the depth of neutral axis, c, which is the distance between the most compressed point in a section and that point with no normal strain;

b) Obtaining the deformation of the most compressed point in the section, ε^c, by applying the strain compatibility equation (Eq. 5.13) and assuming the fibre grid would reach the fibre maximum elongation, $\varepsilon_{ult}^{fibre}$, which was 3% for the glass fibre grid cases and 2.1% for the carbon fibre grid cases. The total thickness from the most compressed point to the fibre grid (d) is also an input variable (see Figure 5.17) and there was set a unique value – the average – for each strengthening pattern. d was also used as the reference thickness for the calculation of the maximum axial load, N_u, necessary to obtain the dimensionless value of the axial load, N/N_u. d was 138.6mm, 136.9mm and 136.6mm for the cases

strengthened with one glass fibre grid (W#21-24), two glass fibre grids (W#25-26) and one carbon fibre grid (W#27-29)respectively;

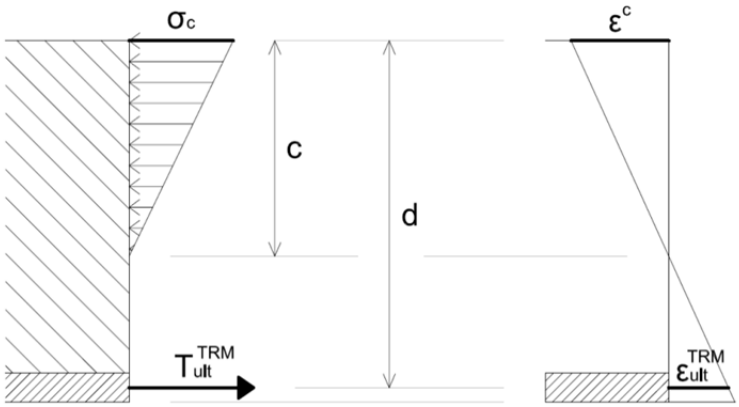

Figure 5.17 Stress (left) and strain (right) distribution in the section under the hypothesis of failure caused by reaching the fibre tensile strength

$$\varepsilon^c = \frac{c \cdot \varepsilon_{ult}^{TRM}}{(d-c)} \quad \text{(Eq. 5.13)}$$

c) According with the hypothesis of linear stress-strain relationship (Eq. 5.14), the stress of the most compressed point in the masonry, σ_c, is calculated with the masonry Young's modulus (E_c=780MPa, experimentally obtained);

$$\sigma_c = E_c \cdot \varepsilon^c \quad \text{(Eq. 5.14)}$$

d) The value of σ_c is compared with the masonry compressive strength, f_c=10.8MPa for the TRMW walls, to assure all mechanical conditions are fulfilled;

e) Calculating the axial load, *N*, using (Eq. 5.15), assuming the TRM has reached its maximum resistance $\left(T_{ult}^{TRM}\right)$ and supposing a linear stress distribution on the compressed depth. The maximum resistance of the TRM, T_{ult}^{TRM}, was calculated by reducing the value given by fibre grid producer per 1 meter width considering the width of the tested walls (0.9m) and the effectiveness ratio of the TRM, *ER*, calculated with (Eq. 3.1) from the experimental data, as described in Chapter 3. For the glass fibre cases a unique value – average of the experimental results – was used. Thus, T_{ult}^{TRM} is 39.4kN for the cases with one glass fibre grid, 78.8kN for the cases with two glass fibre grids installed and 39.0kN for the cases with one carbon fibre grid;

$$N = \frac{\sigma_c \cdot b \cdot c}{2} - T_{ult}^{TRM} \quad \text{(Eq. 5.15)}$$

f) Calculating (Eq. 5.16) the maximum moment, *M*, corresponding with the calculated situation at the failure moment. Thus, this simplification assumes that the fibre of the grid reaches its maximum elongation when the TRM system reaches its maximum tensile strength implying that there is a perfect bonding between the masonry and the TRM and between the components of the TRM. This is valid as a first approach to the calculus of the TRM strengthened masonry and meets the experimental observations.

$$M = T_{ult}^{TRM} \cdot \frac{d}{2} + \frac{\sigma_c \cdot b \cdot c}{2} \cdot \left(\frac{d}{2} - \frac{c}{3}\right) \quad \text{(Eq. 5.16)}$$

g) Calculation the dimensionless values of the axial load by dividing its value, *N*, by the maximum compressive strength of the wall's section assuming a uniform stress distribution ($N_u=bdf_k$) on the thickness of the strengthened section. Similarly, the bending moment is presented in a dimensionless form by dividing its value by the moment $M_u=N_ud/8$. These dimensionless variables are plotted later on in a curve that sets the failure criterion.

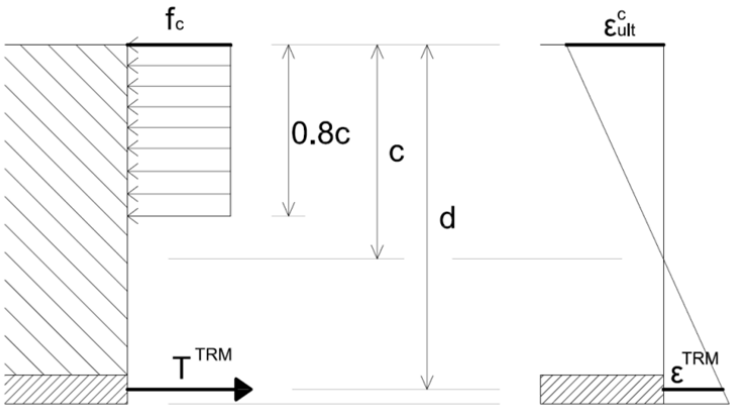

Figure 5.18 Stress (left) and strain (right) distribution in the section under the hypothesis of failure caused by reaching the masonry compressive strength

Step by step, the procedure to calculate the *N-M* dimensionless interaction curve, and the values of the required variables (see Chapter 3 for the justification of these values), under the hypothesis of reaching the masonry's compressive strength (see Figure 5.18) is:

a) Fixing a value of the axial load, N that now is an arbitrary input variable;

b) Calculating the strain in the fibre grid ($\varepsilon^{\text{fibre}}$) using (Eq. 5.17) which is obtained from the combination of the force equilibrium equation with the strain compatibility equations. The ultimate compressive strain of masonry, $\varepsilon_{\text{ult}}^{\text{c}} = 0.0035$, is an input value in this step; c) checking the value of $\varepsilon^{\text{fibre}}$ to ensure it is below its tensile limit elongation presented before (3% for the glass fibre grid cases and 2.1% for the carbon fibre grid cases);

$$\frac{T_{ult}^{TRM}}{\varepsilon_{ult}^{fibre}} \cdot \left(\varepsilon^{fibre}\right)^2 + \left(N + \frac{T_{ult}^{TRM}}{\varepsilon_{ult}^{fibre}} \cdot \varepsilon_{ult}^{c}\right) \cdot \varepsilon^{fibre} + (N \cdot \varepsilon_{ult}^{c} - 0.8 \cdot b \cdot d \cdot f_c \cdot \varepsilon_{ult}^{c}) = 0 \quad \text{(Eq. 5.17)}$$

d) Calculating the depth of the neutral axis, c, using the strain compatibility equation (Eq. 5.18);

$$c = \frac{\varepsilon_{ult}^{c} \cdot d}{\varepsilon^{fibre} + \varepsilon_{ult}^{c}} \quad \text{(Eq. 5.18)}$$

e) Calculating the corresponding bending moment taking into account a rectangular compressive stress distribution on the 80% of the compressed depth (Eq. 5.19). The Young's modulus of the TRM is not required but it is indirectly represented by assuming that the TRM reaches is maximum strength (T_{ult}^{TRM}) when the fibre of the grid reaches the maximum elongation ($\varepsilon_{ult}^{fibre}$). This simplification assumes a perfect connection between the components of the TRM which is a first approach to the modelling of the structural problem.

$$M = \varepsilon^{fibre} \cdot \frac{T_{ult}^{TRM}}{\varepsilon_{ult}^{fibre}} \cdot \frac{d}{2} + 0.8 \cdot b \cdot c \cdot f_c \cdot \left(\frac{d}{2} - 0.4 \cdot c\right) \quad \text{(Eq. 5.19)}$$

Finally, the two calculated dimensionless curves are compared with the experimentally measured pairs of axial load and bending moment in order to draw conclusions.

5.3.2. Analysis with Southwell Plot method

The analysis carried out with the Southwell Plot is the same than for the URMW. However, it was expected that the Southwell Plot did not provide accurate results for these walls because the TRM strengthening limits the lateral deformation and the buckling failure is not likely. Confirming that these TRM-strengthened walls are out of the range of application of the Southwell Plot method is an indirect supporting evidence of the hypothesis that this strengthening system limits the second order effects turning the problem under study into a simple section resistance analysis.

The applicable formulation and procedure have been already presented in the subsection 5.2.4. Briefly, this approach can be described as a semi empirical method because its main aim is to predict the load-bearing capacity of a column/wall from the experimental load and lateral deflection data measured at loads lower than the wall's capacity.

5.3.3. Results and comparison

The theoretical curves calculated according with the procedure presented in section 5.3.1 are compared with the experimental results in Figures 5.19-21. These curves representing the section strength failure criteria have two different parts. At the beginning of the curve, for the lower axial loads, the tensile

strength of the TRM is the dominant failure mode and the representation follows approximately a straight line. After that, the section strength criterion is controlled by the compression of the masonry and the plot is parabolic. These curves for the TRMW walls are comparable to those presented in Figures 5.7-12 for the URMW walls.

All experimental points corresponding with the ultimate state of the TRMW walls are near the failure criterion. In general, there is a slight tendency to underestimate the load-bearing capacity of these walls. This is noticed because two out of three points in Figures 5.19-21 are placed below the lines which separate the "safe" states (under the curve) from the axial-bending combinations which were, theoretically, above the resistance capacities of the cross section of the walls (over the curve).

It is also worth mentioning that all experimental points are placed near the right part of the curves. Thus, the theoretical failure cause would be always reaching the compression strength of the masonry. This partially agrees with the experimental results: seven out of nine walls collapsed because of the compression-shear combination near one ending of the wall and only two collapses might be associated with the TRM tensile failure. This qualitative prediction is less accurate for the cases with a single fibre grid. The proposed analytic approach seems to be more conservative in these cases.

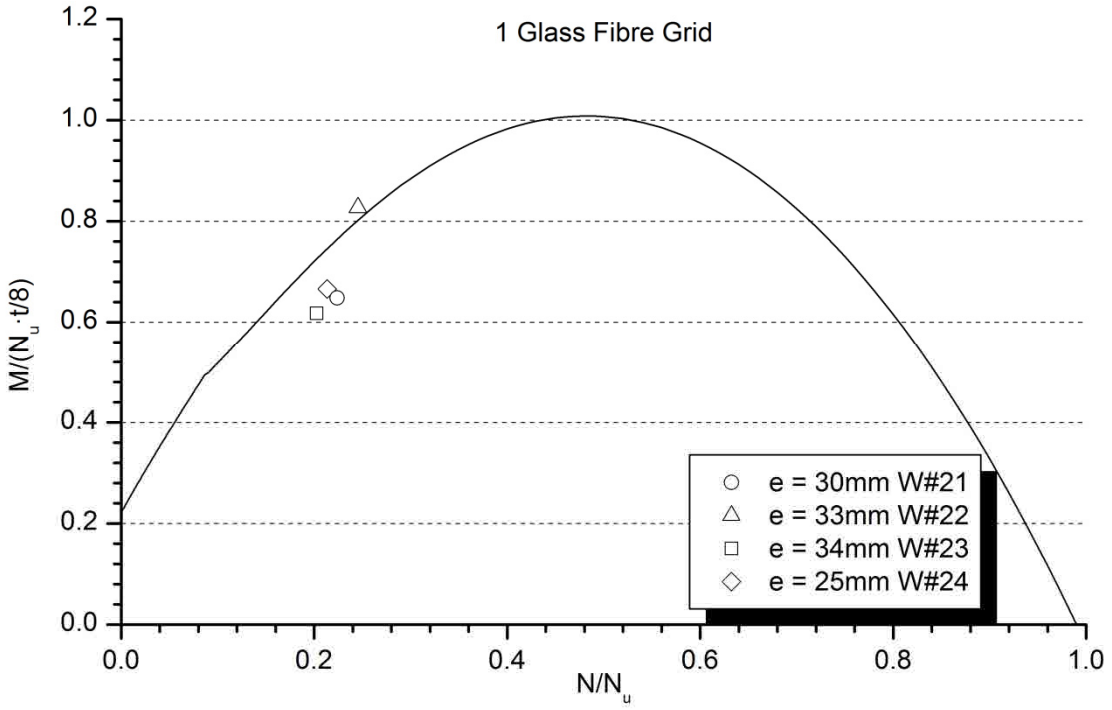

Figure 5.19 Section strength failure criteria and axial-bending load-bearing capacity for the walls strengthened with one glass fibre grid

In addition, the experimentally observed cracking pattern (see Chapter 3) of most of the walls suggested an important influence of the shear response. The combination of normal and tangential stresses near the

ends of the walls might explain the slight differences between the analytic failure criteria and the measured axial-bending combination at the collapse of the walls. Considering the shear phenomena may improve the analysis presented in section 5.3.1. Overall, these particularities might explain the little tendency of this method to underestimate the load-bearing capacity of the TRMW walls.

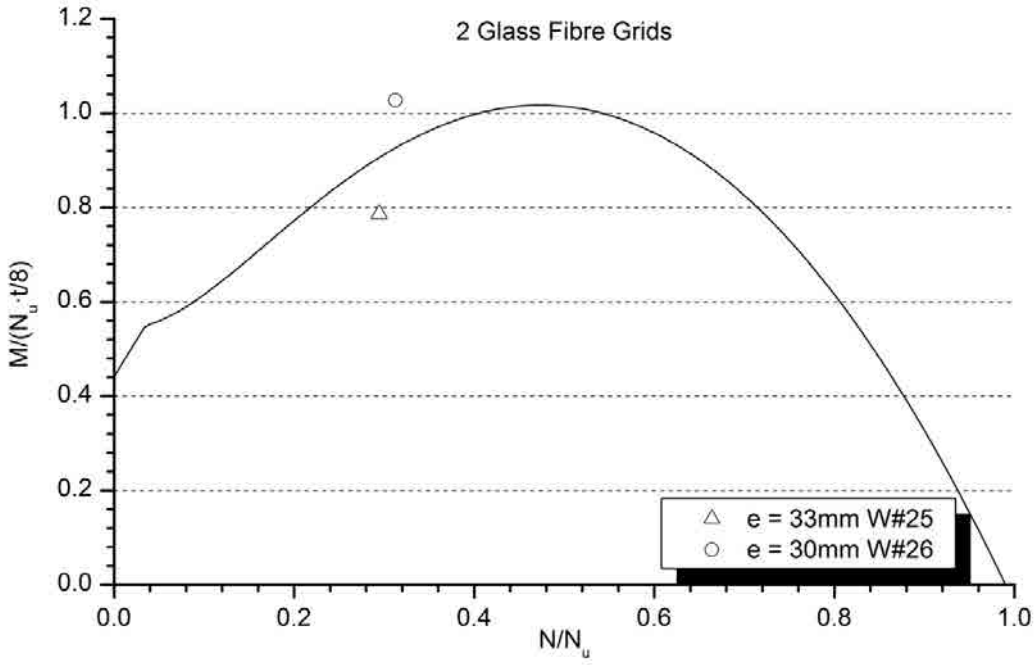

Figure 5.20 Section strength failure criteria and axial-bending load-bearing capacity for the walls strengthened with two glass fibre grid

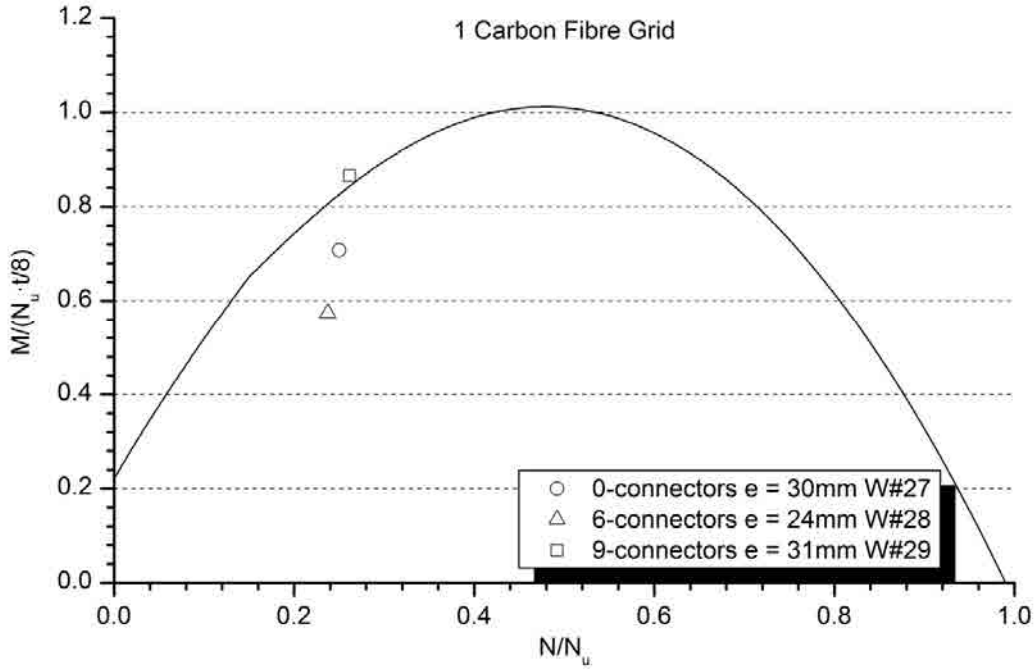

Figure 5.21 Section strength failure criteria and axial-bending load-bearing capacity for the walls strengthened with one carbon fibre grid

Wall	*Grid*	N^{exp}/N_u	$M^{exp}/(N_u \cdot t/8)$	$M^{analytic}/(N_u \cdot t/8)$ [(1)]	*Error (%)*
W#21	1 Glass	0.224	0.648	0.765	18.1
W#22		0.245	0.828	0.841	1.6
W#23		0.202	0.618	0.725	17.3
W#24		0.213	0.667	0.746	11.8
W#25	2 Glass	0.295	0.787	0.906	15.1
W#26		0.312	1.027	0.926	-9.8
W#27	1 Carbon	0.250	0.708	0.826	16.7
W#28		0.237	0.575	0.806	40.2
W#29		0.262	0.865	0.844	-2.4

[(1)] Corresponding to the maximum experimental axial force and according to the analytical formulation

Table 5.4. Experimental and analytical results (section strength criterion) for the TRMW walls

Dimensionless maximum analytic bending moments corresponding with the experimental maximum axial loads have been calculated for all walls assuming the failure criterion represented by the curves in Figures 5.19-21. These theoretical maximum bending moments are compared with the experimental ones in Table 5.4 to quantitatively asses the proximity of the experimental points to the failure criteria lines in Figures 5.19-21. The average relative error (considering no sign) is 14.8% which is less than the scattering of the input variables indicating that the proposed method accurately predicts the maximum bending moment associated with the experimentally determined maximum axial load. This fact proves that the problem of calculating the load-bearing capacity of these TRM-strengthened walls can be studied as a simple section strength analysis case, confirming the hypothesis.

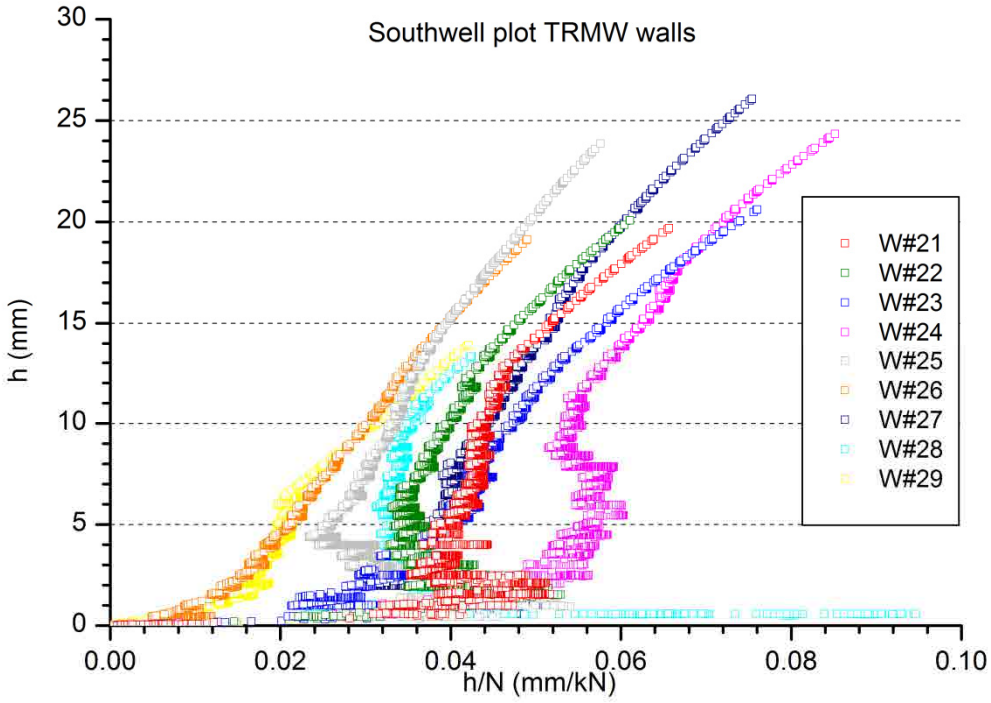

Figure 5.22 Southwell Plot for TRMW walls

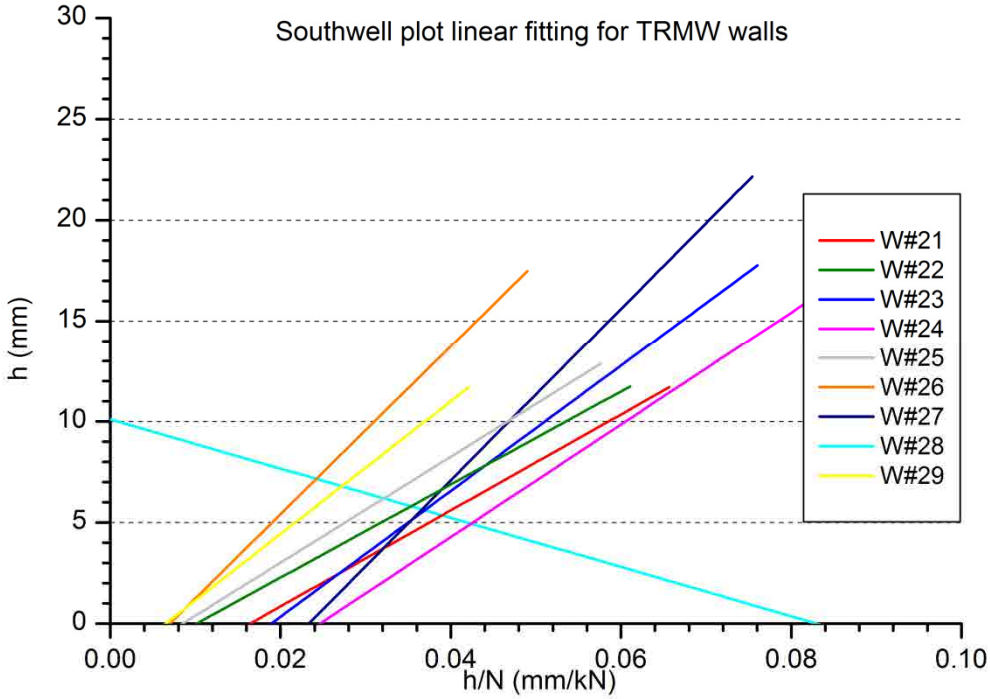

Figure 5.23 Linear fitting of the Southwell Plot for TRMW walls

In reference with the Southwell Plot method, it has to be said that the non-linear lateral deflection response of the TRMW walls (see Figure 5.22) makes it difficult to perform the linear fitting (see Figure 5.23) which is required to obtain the load-bearing capacity prediction. In fact, the regression wellness measure (R^2) is above 0.8 for only two of the walls (W#23 with R^2=0.87 and W#26 with R^2=0.95), and for these two cases the load prediction has an average relative error of 10.7% which is within the scattering range of the masonry properties. Thus, when the Southwell method is applicable, the obtained results show good accuracy but the main drawback is that for the herein presented tests, this approach was suitable only for two out of nine TRMW walls. This fact proves that the second order effects are very limited by the TRM strengthening and the buckling failure is not likely in these cases.

5.4 Conclusions

After performing calculations with different analytical approaches it has been observed that there is not a unique method which works accurately for all the cases considered. Thus, the method to be applied must be carefully selected depending on the application range of each of the proposed alternatives.

Regarding the unreinforced walls (URMW) and focusing on the codes considered, it has to be mentioned that ACI-530 achieves more accurate results than Eurocode-6 in the prediction of the experimental ones. In addition, it has been observed that the codes tend to underestimate the load-bearing capacity of the tested walls.

Regarding the Southwell Plot method, it is the one which shows better accuracy among all the methods tested in the current research. However, it can only be applied to the cases for which there is sufficient experimental information as to describe consistently a load-displacement curve and it is linear. Hence, it cannot be presented as a general purpose method. In the case of the tested walls, it has only been applicable to less than 60% of them. Confirming that the tested TRM-strengthened walls are out of the application range of the Southwell Plot method supports the idea that this strengthening system actually limits the second order effects, reduces the lateral displacements, makes it less likely the buckling failure of the walls and shifts the material performance towards non-linear.

The analytical approach used for URMW, consisting of calculating the second order lateral deflections and obtaining the load-bearing capacity by imposing a cross section failure criterion has reached the best results among the methods which were always applicable for the walls of the H, M and F series. However, it is also shown to be a poor method for the walls of the T and S series. On the whole, this proposed analytical method seems to be suitable for predicting the most slender wall's response and their failure cause which is strongly influenced by the second order effects. This agrees with the hypothesis of linear stress distribution oriented to be applied on cases for which the compressive response was not significant. Finally, the application of this calculation method has pointed out that the walls of the M and H series actually collapsed at reaching the tensile strength of the masonry. By comparison, this method underestimates the strength of the walls with less slenderness, which are not actually affected by the second order deformations.

By analysing the results of the analytical method proposed to obtain the axial-bending limit interaction curve for the TRMW walls, it can be concluded that this procedure fulfils its main aim by providing an easy tool for calculating the ultimate capacity of TRM strengthened masonry walls subjected to axial loading conditions. Although the results are conservative, they are satisfactorily close to the experimental values, especially if, the scattering of the input data is taken into account. Hence, it can be concluded that the proposed calculation method can be used for designing TRM strengthening systems of load-bearing masonry walls. However, the experimentally observed failure pattern, together with the analytical results, suggests that it would be interesting to enhance the presented analytical method with the inclusion of the effect of the shear forces.

6

Conclusions and further research

6.1 Conclusions

The experimental campaigns, numerical simulations and analytical calculations carried out in the present research have contributed to enhance the understanding of the structural response of the unreinforced and TRM-strengthened load-bearing masonry walls subjected to eccentric compressive loading conditions. The following sections summarize the main particular conclusions obtained for each of the different tasks of the present research.

6.1.1. Particular conclusions

6.1.1.1 Conclusions about the state of the art

The review of the experimental investigations carried out to date about the structural response of unreinforced and strengthened masonry load-bearing walls, about the corresponding analytical formulations to calculate these structural cases, and about the numerical approaches to model them has allowed to draw the following conclusions.

- Masonry is a building material used worldwide and the load-bearing wall is the most common structural element in existing buildings still in service. However, the research effort aimed to mechanically characterise this material has been so far very limited compared to that devoted to more modern materials such as steel or concrete. In addition, the manual production of historical masonry (as in the case of many existing buildings) causes large scattering in the experimental results, which suggests that a larger experimental effort may be necessary. This only fact justifies by itself the need for additional experimental characterisation of the masonry.
- Among the possible failure patterns of the eccentrically loaded structural unreinforced masonry walls, the mechanism formation due to lateral deflections associated with second order bending effect is

common and represents a hazard because of its brittle response. However, the bibliographic research reveals that this phenomenon has not been deeply studied. Thus, an experimental campaign on full-scale masonry walls to study this case is necessary.

- The most comprehensive consulted papers, thesis and journals which included experimental information about load-bearing unreinforced masonry walls eccentrically loaded are from before 1980 and the data summarised in them is incomplete. The boundary conditions and the data about the measuring equipment are usually missing and just a few of these documents bring information about the lateral deflection associated with the second order bending. For this reason, it may be controversial to use this old data for the validation of the newest numerical models. In conclusion, it would be interesting to carry out new tests in order to acquire more detailed and comprehensive data using the possibilities of modern experimental equipment.
- The recent bibliographic review suggests that strengthening procedures are going to be generally applied in the near future to upgrade the existing structures or preserve their conservation. Among them, the Textile Reinforced Mortar (TRM) is the most promising one to be applied on masonry structures and particularly in load-bearing walls because of its mechanical, chemical and physical compatibility with the masonry. However, there are no regulations about the application of TRM and the influence of the TRM at strengthening load-bearing masonry walls against the mechanism formation collapse mode has not been widely studied. Thus, it is concluded that research on this topic is needed.
- The analytical formulations presented over the years to calculate the structural response of compressed load-bearing masonry walls were limited to simple constitutive laws (material behaviour) or particular boundary conditions. Only a few complex formulations have a wider range of application. However, using them requires the aid of a computer and it is considered that nowadays using a numerical model might be more efficient in this context. Thus, it is noticed that the analytical formulations, which are actually aimed to be applied with no computer aid in an early design stage, have to be oriented to bring a first estimation of the load-bearing capacity of the masonry walls.
- The newest research on the numerical analysis of load-bearing unreinforced masonry walls suggest that there is a growing tendency to use general purpose finite element software to implement simplified numerical models instead of using specific software and complex material definitions. However, the interface elements to model the contact phenomena are required to accurately represent the masonry response in tensile or bending conditions. Thus, it is considered that a simple and reliable model which can be used for a wide range of finite elements packages is required.
- There is little research about modelling TRM-strengthened masonry walls with finite element analysis. Therefore, implementing a reliable partial model describing the response of the TRM reinforcement itself is required to correctly model the TRM-strengthened masonry.

6.1.1.2 Conclusions about the experimental campaign

The main conclusion of the experimental campaign is that the proposed objective of obtaining relevant data to study the structural response of unreinforced and TRM-strengthened walls under eccentric compressive loading conditions has been achieved. The acquired data is complete and precise enough to be used as validation information for the development of numerical tools. In addition, more specific conclusions have been obtained:

- Regarding the testing procedures it can be concluded that the test setup used for testing the full-scale walls is suitable and reaches the proposed goals of easily setting the eccentricity of the load and allowing free rotation conditions at the endings of the walls.
- Regarding the practical application of TRM strengthening system it is concluded that this system can be applied by current brick layering professionals with almost any extra formation. However, the use of connectors poses some difficulties and requires extra application time that should be considered in the planning tasks.
- Regarding the material characterisation, it is concluded that the scattering of the mechanical properties of the masonry is significant and has to be taken into account in the calculation procedures or in the interpretation of the results. The larger scattering is observed for the Young's modulus.
- The bonding strength between the solid clay bricks and the mortar of the masonry highly depends on the type of mortar used and has a significant scattering (as shown in the experimental results) that has to be considered in the analysis.
- Regarding the tests on full-scale unreinforced walls it is concluded that the geometric parameters (geometric imperfections, eccentricity of the load and slenderness) are the ones that most influence on the load-bearing capacity and the structural response during the test.
- By observing the failure patterns of the unreinforced walls it is concluded that the most likely failure mode is the mechanism formation after the opening of one or more mortar joints at a position near mid-height of the wall. In the case of the lesser slenderness walls or the case with centred load, crushing of the masonry is observed together with mechanism formation.
- The initial experimental research about the performance of different TRM solutions concluded that the combination of carbon fibre grids and pozzolanic mortar did not fulfil the provider's specifications. The observed response points out that the most probable cause was adherence problems between the mortar and the fibre because the other tested solutions (using different fibre grids and mortars) correctly reached the expected strength.
- The tests on TRM-strengthened walls showed that different failure modes are possible: the joint opening together with the TRM tensile failure and the corresponding mechanism formation, the masonry crushing in compression which usually appears together with a tensile failure of the reinforcement and the shear-compressive masonry failure near the wall's ends which is the most common failure mode observed. Thus, it is concluded that the performance of the TRM-strengthening system is enough as to

change the failure mode of the walls from the mechanism formation typical of the unreinforced ones to the compressive/shear failure of masonry when strengthened.

- From the results of the tests on full-scale walls it is concluded that the load-bearing capacity of the strengthened walls is less dependent on slenderness and eccentricity than for the unreinforced ones. In addition, using the TRM strengthening system tends to make more uniform the wall's behaviour (in the sense of reducing the scattering) and to reduce the out-of-plane non-linear response. Finally, it is remarkable that the TRM is an effective strengthening method which can achieve more than 100% of load-bearing capacity increase.
- By comparing the TRM-strengthened walls between them it is observed that it is possible to use two overlapped fibre grids embedded into a single mortar layer if the grid spacing is large enough for the mortar to penetrate. However, this solution provides just a slight increase of load-bearing capacity. Similarly, it was observed that using connectors makes no difference in the load-bearing capacity.
- A significant conclusion regarding the use of the mortars distributed as part of the TRM is that the adherence of these mortars has proved to be enough to prevent the debonding failure for all analysed cases. Thus, using connectors for strengthening masonry walls is not necessary.
- Regarding the structural response of the walls strengthened with different TRM solutions, it has to be highlighted that they all behave similarly up to loads close to the failure one. Thus, the strain on the strengthened face depends on the TRM system only for loads near the collapse. The experimental results show that the failure mode might be related with the measured strains at low loads (under 50% of the collapse load for each wall) but not with the TRM strengthening system. Thus, the failure mode detection might be possible.

6.1.1.3 Conclusions about the numerical analysis

The proposed numerical model has shown good accuracy at predicting the load-bearing capacity of the wide range of considered experimental cases. In addition it achieves the requirements of being simple enough to be implemented in almost all general purpose finite element packages.

In particular, the proposed model is a bidimensional, plain-strain simplified micromodel characterised by the use of contact elements to represent the tensile and shear response of the masonry and the TRM. This response, defined with a cohesive zone model, is linear up to the maximum strength and after that the joint opens or slides with a linear descending stress. The masonry-TRM contact is perfectly bonded for all cases. In compression, the masonry is set to be elastic-perfect plastic and modelled as a single material (without distinguishing between the brick and the mortar). Triangular objects are used to model the real hinges at the ends of the walls. The numerical model calculation has large deformation capabilities and the load is indirectly applied through an increasingly vertical displacement of the top of the wall.

The analysis of the results of the numerical simulation allows some more specific conclusions.

- Firstly, which has to be mentioned before presenting other conclusions based on the numerical simulation, is that the prediction of the load-bearing capacity is very sensitive to the variation of the Young's modulus of the masonry. In addition, the determination of this parameter shows large scattering which causes uncertainty in the value of this variable. Thus, the uncertainty of E might influence on the results of the numerical model.
- Regarding the model definition, it should be concluded that using two triangular objects to model the hinges is a valid and easy solution which provides good results.
- Moreover, defining an inclined contact to make it possible the compressive-shear failure near the wall's endings for the TRM-strengthened walls has proved to be an efficient solution to capture this failure pattern for the walls which failed in this way. Furthermore, it is concluded that considering the contact has no effects on the results when modelling walls which are not expected to fail in this way.
- The proposed equation (Eq. 4.1), which was aimed to calculate the first mode fracture energy, has brought suitable input data according with the accuracy of the obtained results for the particular analysed cases. Thus, it is considered that (Eq. 4.1) might be an acceptable approach to calculate this required parameter although further research is needed.
- The model has achieved results with a lower error than the corresponding scattering of the experimental results for the validation cases (as can be seen in the scientific literature on the subject) of the unreinforced walls. This makes it possible to conclude that the accuracy of the model at predicting the load-bearing capacity of unreinforced walls with compressive loads eccentrically applied permits its use as a design tool.
- In addition, this model has also achieved results with an error which is within the range of the scattering of the input parameters for the tests of unreinforced walls presented in this thesis.
- Being more precise, it might be concluded that the proposed model is better at predicting the load-bearing capacity of the most slender walls or the walls with the load applied with larger eccentricity for the unreinforced cases.
- On the contrary, it might be concluded that the model tends to underestimate the load-bearing capacity of the wall when the compressive response of the brickwork is the dominant process.
- The proposed model correctly predicts the influence of the walls' slenderness and the load eccentricity in all cases. Thus, it may be concluded that the model correctly predicts the structural response of the walls and can represent the real behaviour of this type of structures.
- It has to be mentioned that the influence of using different TRM systems or placing two fibre grids is correctly captured by the proposed numerical model.
- In addition, the results of modelling the TRM-strengthened walls indicate that the proposed model is conservative in most of the cases, especially if the compressive strength or the crushing of the masonry is involved in the failure mode.

- The tensile strength of the TRM's mortar is an important parameter which has to be taken into account in order to obtain accurate results on the wall capacity. This is observed by comparing the theoretical simulated cases among them and analysing the influence of this variable.
- The application of the model to theoretical cases proved that considering that the fibre grid is the only component that resists the tensile forces is not the best approximation to the problem because the strength and stiffness of the mortar has significant effect on the calculated response.
- The same application showed that the geometric effect (thickness increase) of placing a mortar layer in the compression side of the walls provides a practical and effective solution to enhance their performance.
- The same theoretical simulations show that the TRM effectiveness is greater for the most slender walls.
- Finally, it has to be noticed that distinguishing the failure mode for some simulations is difficult. This situation is explained because the loads associated to different calculated collapse modes are close.

6.1.1.4 Conclusions about the analytical approach

Two proposed analytical approaches aimed to calculate the load-bearing capacity of unreinforced and TRM-strengthened masonry walls have been used and compared with the Southwell Plot method. For the unreinforced walls the comparison with Eurocode-6 and ACI-530 was also performed. After carrying out all these calculations and comparison it has been obtained that there is not a unique methodology which works accurately for all the cases considered. Therefore the application range of each of the proposed analytical approaches must be clearly indicated.

The proposed analytical method for unreinforced masonry walls (URMW) consisted on calculating the second order deflection which allows calculating the corresponding bending moment associated to the axial load. Then the maximum tensile and compressive stress due to the axial-bending combination is compared with the corresponding strengths. In contrast, the proposed analytical method for TRM-strengthened masonry walls is based on equilibrium and strain compatibility equations in the cross section to calculate the axial-bending limit combinations.

Some particular conclusions can be proposed regarding the analytical approaches and their range of application.

There is a general tendency of the codes (Eurocode-6 and ACi-530) to underestimate the load-bearing capacity of the tested unreinforced walls.

- ACI-530 achieves more accurate results than Eurocode-6 for the tested unreinforced masonry walls subject to eccentrically applied compressive load.

- The analytical approach consisting of calculating the second order lateral deflections and obtaining the load-bearing capacity by imposing a cross section failure criterion used for the URMW is always applicable and shows accurate results for the most slender walls and the cases with large load eccentricity. Thus, it is concluded that this method is the most suitable one for cases with application range corresponding to slenderness over 12 and load eccentricity over 1/6 of the thickness, accordingly with the comparison with the experimental results.
- The proposed analytical approach for unreinforced walls is able to predict the failure mode of the cases within its application range.
- However, this analytical method is not suitable for calculating the load-bearing capacity of the walls with lesser slenderness, which are not really affected by the second order deformations. It can be concluded that the method is extremely conservative for these cases and is out of its application range.
- The Southwell Plot method is the most accurate one but this is not reliable because of its limited applicability. This method requires experimental data which is not always available or might not be consistent enough to be processed in order to predict the collapse load. So, the applicability range of Southwell Plot method is not defined and depends on the experimental results. In addition, this method could not be directly applied on walls with fixed-fixed configuration.
- The analytical method proposed for calculating the TRM-strengthened walls fulfils the objective of providing an easy tool to obtain the ultimate capacity of TRM strengthened masonry walls subjected to axial loading. Although it is slightly conservative, this method is satisfactory if compared with the scattering of the input data.

6.2 Further research

The present research has allowed the identification of some knowledge gaps in need of additional investigation. A proposal of the main topics to be included in a further research is presented in the following paragraphs.

Firstly, it would be interesting to carry out more tests for the characterisation of the masonry strengthened with TRM because it has been observed that the effectiveness of this strengthening system depends on the loading conditions, several installation variables or the component materials. Thus, more research is required to comprehensibly characterise this composite material.

The value of the variables which define the mechanical performance of the TRM systems highly depends on the testing setup. Thus, it would be suitable to develop a standardised uniform testing procedure in order to homogenise the information provided with the TRM systems.

The experimental campaign on full-scale walls developed in the present work could be completed with additional experiments on TRM-strengthened walls subjected to different slenderness and load eccentricities. It would be interesting to carry out this additional research in order to analyse the influence of these parameters on strengthened walls. Similarly, it would be necessary to test full-scale walls which consider other typologies of masonry: stone masonry, block masonry, different mortars in the masonry joints or different masonry patterns. Taking into account the numerical results on theoretical cases, it would be interesting to test masonry walls strengthened with TRM applied at both sides to check if the predicted large load-bearing capacity increase meets with experimental evidence.

A relationship between the strain at the TRM surface and the failure mode of the full-scale walls was noticed in the experimental campaign. This relationship is limited to the first loading steps and it is independent from the applied TRM system. Further research to confirm this relationship would be interesting in order to plan the development of a tool for the early prediction of the failure mode.

Regarding the proposed numeric model, it would be interesting to expand its applicability range. Particularly, the response for compression and shear loading conditions might be improved while keeping the model as simple as possible. Using comparatively simple models which could be easily implemented in general purpose finite element software has been one of the main aims of the present thesis. One clear research line in this way might be taking into account the over-strengthening of masonry for eccentric compression which might lead to higher load-bearing capacities when the crushing failure process is significant, as in the case of the less slender walls subjected to concentric or moderately eccentric loads.

Finally, another future research line might consist of developing an analytical formulation for calculating the deflection of TRM-strengthened walls. Alternatively, the existing equations for elastic homogeneous materials might be adapted in order to take into account the non-linear response of the masonry in tension.

References

[1] H. Gallegos, O. Ramírez, Chapter 1: Las estructuras de mampostería, in: Edif. Mampostería Para La Vivienda, 2nd ed., Fundación ICA, A.C, Mexico D.F., 2003: pp. 1–21.

[2] A.W. Page, A study of the brick size on the compressive strength, Newcastle, 1984.

[3] P.B. Lourenço, J. Barros, Size effect on masonry subjected to out-of-plane loading, in: 12 Th Int. Brick/Block Mason. Conf. Proc., 2000: pp. 1085–1098.

[4] P.B. Lourenço, J. Barros, J.C. Almeida, Characterization of masonry under uniaxial tension, Guimarães, 2002.

[5] B. Sinha, C. Ng, R. Pedreschi, Failure criterion and behavior of brickwork in biaxial bending, J. Mater. Civ. Eng. 9 (1997) 70–75.

[6] R. Van der Pluijm, Out-of-plane bending of masonry. Behaviour and strength, Eindhoven University of Technology, 1999.

[7] R. Pluijm, Material properties of masonry and its components under tension and shear, in: V.V. Neis (Ed.), 6th Can. Mason. Symp., Saskatoon, Saskatchewan, Canada, 1992: pp. 675–686.

[8] E.A. Gazzola, R.G. Drysdale, A.S. Essawy, Bending of concrete masonry wallettes at different angles to the bed joints, in: Proc. Third North Am. Mason. Conf., Construction Research Center Civile Engineering Department University of Texas, Arlington, Texas, 1985: p. 15.

[9] E. Reyes, M. Casati, J. Gálvez, Experimental scale model study of cracking in brick masonry under tensile and shear stress, Mater. Constr. 58 (2008) 69–83.

[10] A.H.P. Maurenbrecher, Effect of the test procedures on compressive strength of masonry prisms, in: 2nd Can. Mason. Symp., National Research Council Canada, Ottawa, 1980: pp. 119–132.

[11] A.H.P. Maurenbrecher, Compressive Strength of eccentrally loaded masonry prisms, in: NRCC (Ed.), Third Can. Mason. Symp., National Research Council Canada, Edmonton, 1983.

[12] A.H.P. Maurenbrecher, Axial Compression Tests on Masonry Walls and Prisms, in: Third North Am. Mason. Conf., National Research Council Canada, Arlington, Texas, 1985: p. 17.

[13] P. Roca, J.C. Ablanque, Investigación experimental y numérica sobre el comportamiento mecanico de la obra de fábrica, in: CSIC (Ed.), I Jornadas Investig. En Construcción, 2005: pp. 261–276.

[14] T. Tassios, Meccanica delle Murature, Liguori Editori, Napoli, 1988.

[15] C. Molins, Characterization of the mechanical behaviour of masonry, in: P. Roca (Ed.), Struct. Anal. Hist. Constr., CIMNE, Barcelona, 1996.

[16] F.Y. Yokel, Strength of load bearing masonry walls, J. Struct. Div. 97 (1971) 1593–1609.

[17] A. De Falco, M. Lucchesi, Stability of columns with no tension strength and bounded compressive strength and deformability. Part I: large eccentricity, Int. J. Solids Struct. 39 (2002) 6191–6210.

[18] A. Defalco, M. Lucchesi, No tension beam-columns with bounded compressive strength and deformability undergoing eccentric vertical loads, Int. J. Mech. Sci. 49 (2007) 54–74.

[19] I. Mura, Stability of nonlinear masonry members under combined load, Comput. Struct. 86 (2008) 1579–1593.

[20] Y. Chen, a. F. Ashour, S.W. Garrity, Moment/thrust interaction diagrams for reinforced masonry sections, Constr. Build. Mater. 22 (2008) 763–770.

[21] W. Samarashinge et al., A finite element model for the in-plane behavior of brickwork, Proc. Inst. Civ. Eng. 71 (1982) 171–178.

[22] M. Dhanasekar, A.W. Page, The influence of brick masonry infill properties on the behavior of infilled frames, Proc. Inst. Civ. Eng. 81 (1986) 593–605.

[23] J.G. Rots, Numerical simulation of cracking in structural masonry, Heron. 36 (1991) 49–63.

[24] G.N. Pande, J.X. Liang, J. Middleton, Equivalent elastic moduli for brick masonry, Comput. Geotech. 8 (1989) 243–265.

[25] P.B. Lourenço, An orthotropic continuum model for the analysis of masonry structures, 1995.

[26] P.B. Lourenço, J.G. Rots, Multisurface interface model for analysis of masonry structures, J. Eng. Mech. 123 (1997) 660–668.

[27] P. Roca, J. González, E. Oñate, P.B. Lourenço, Experimental and numerical issues in the modelling of the mechanical behaviour of masonry, Struct. Anal. Hist. Constr. II. (1998) 1–35.

[28] P. Roca, F. Lopezalmansa, J. Miquel, a Hanganu, Limit analysis of reinforced masonry vaults, Eng. Struct. 29 (2007) 431–439.

[29] U. Andreaus, Failure criteria for masonry panels under in-plane loading, J. Struct. Eng. 122 (1996) 37–46.

[30] A. Zucchini, P.B. Lourenço, Mechanics of masonry in compression: Results from a homogenisation approach, Comput. Struct. 85 (2007) 193–204.

[31] M. Mistler, a Anthoine, C. Butenweg, In-plane and out-of-plane homogenisation of masonry, Comput. Struct. 85 (2007) 1321–1330.

[32] A. Cecchi, K. Sab, A homogenized Reissner–Mindlin model for orthotropic periodic plates: Application to brickwork panels, Int. J. Solids Struct. 44 (2007) 6055–6079.

[33] A. Cecchi, G. Milani, A kinematic FE limit analysis model for thick English bond masonry walls, Int. J. Solids Struct. 45 (2008) 1302–1331.

[34] G. Salerno, G. de Felice, Continuum modeling of periodic brickwork, Int. J. Solids Struct. 46 (2009) 1251–1267.

[35] E. Sacco, A nonlinear homogenization procedure for periodic masonry, Eur. J. Mech. - A/Solids. 28 (2009) 209–222.

[36] A.W. Page, FINITE ELEMENT MODEL FOR MASONRY, ASCE J Struct Div. 104 (1978) 1267–1285.

[37] S. Ali, A.W. Page, CONCENTRATED LOADS ON SOLID MASONRY WALLS-A PARAMETRIC STUDY AND DESIGN RECOMMENDATIONS., Proc. Inst. Civ. Eng. 85 (1988) 271–289.

[38] P.B. Lourenço, Analysis of masonry structures with interface elements. Theory and applications, 1994.

[39] M. Ainsworth, L.A. Mihai, An adaptive multi-scale approach to the modelling of masonry structures, Int. J. Numer. Methods Eng. 78 (2009) 1135–1163.

[40] A. Orduña, P.B. Lourenço, Three-dimensional limit analysis of rigid blocks assemblages. Part II: Load-path following solution procedure and validation, Int. J. Solids Struct. 42 (2005) 5161–5180.

[41] A.J. Aref, K.M. Dolatshahi, A three-dimensional cyclic meso-scale numerical procedure for simulation of unreinforced masonry structures, Comput. Struct. 120 (2013) 9–23.

[42] A.J. Mas Guindal, J.M. Adell, Eladio Dieste y la cerámica estructural en Uruguay, Inf. La Construcción. 56 (2007) 13–23.

[43] Masonry Standards Joint Committee, Building Code Requirements for Masonry Structures. ACI 530-05, (2005).

[44] Gobierno del Distrito Federal, Normas técnicas complementarias para diseño y ocnstrucción de estructuras de mampostería, in: Gac. Of. Del Dist. Fed., Mexico D.F:, 2004.

[45] N. Sathipara, P. Mayorca, K. Nesheli, R. Guragain, K. Meguro, Experimental study on in-plane and out-of-plane behavior of masonry wallettes retrofitted by PP-band meshes, SEISAN KENKYU. 57 (2005) 530–533.

[46] M. Maalej, V.W.J. Lin, M.P. Nguyen, S.T. Quek, Engineered cementitious composites for effective strengthening of unreinforced masonry walls, Eng. Struct. 32 (2010) 2432–2439.

[47] T. Blanksvärd, B. Täljsten, Strengthening of concrete structures with cement based bonded composites, J. Nord. Concr. Res. 38 (2008) 133–154.

[48] C.G. Papanicolaou, T.C. Triantafillou, M. Papathanasiou, K. Karlos, Textile reinforced mortar (TRM) versus FRP as strengthening material of URM walls: out-of-plane cyclic loading, Mater. Struct. 41 (2007) 143–157.

[49] E. Hamed, O. Rabinovitch, Lateral out-of-plane strengthening of masonry walls with composite materials, J. Compos. Constr. 14 (2010) 376.

[50] a Baratta, O. Corbi, Stress analysis of masonry vaults and static efficacy of FRP repairs, Int. J. Solids Struct. 44 (2007) 8028–8056.

[51] L. Delorenzis, R. Dimitri, a Lategola, Reduction of the lateral thrust of masonry arches and vaults with FRP composites, Constr. Build. Mater. 21 (2007) 1415–1430.

[52] P. Foraboschi, Strengthening of Masonry Arches with Fiber-Reinforced Polymer Strips, J. Compos. Constr. 8 (2004) 191.

[53] N. Shrive, The use of fibre reinforced polymers to improve seismic resistance of masonry, Constr. Build. Mater. 20 (2006) 269–277.

[54] A. Wiberg, Strengthening of Concrete Beams Using Cementitious Carbon Fibre Composites, Royal Institute of Technology of Sweden, 2003.

[55] S. Holler, C. Butenweg, S. Noh, K. Meskouris, Computational model of textile-reinforced concrete structures, Comput. Struct. 82 (2004) 1971–1979.

[56] R. Ortlepp, U. Hampel, M. Curbach, A new approach for evaluating bond capacity of TRC strengthening, Cem. Concr. Compos. 28 (2006) 589–597.

[57] L. Garmendia, J.T. San-José, D. García, P. Larrinaga, Rehabilitation of masonry arches with compatible advanced composite material, Constr. Build. Mater. 25 (2011) 4374–4385.

[58] N. Augenti, F. Parisi, A. Prota, G. Manfredi, In-Plane Lateral Response of a Full-Scale Masonry Subassemblage with and without an Inorganic Matrix-Grid Strengthening System, J. Compos. Constr. 15 (2011) 578.

[59] C. Papanicolaou, T. Triantafillou, M. Lekka, Externally bonded grids as strengthening and seismic retrofitting materials of masonry panels, Constr. Build. Mater. 25 (2011) 504–514.

[60] C.G. Papanicolaou, T.C. Triantafillou, K. Karlos, M. Papathanasiou, Textile-reinforced mortar (TRM) versus FRP as strengthening material of URM walls: in-plane cyclic loading, Mater. Struct. 40 (2006) 1081–1097.

[61] J. Velazquez-Dimas, M. Ehsani, Modeling out-of-plane behavior of URM walls retrofitted with fiber composites, J. Compos. Constr. 4 (2000) 172–181.

[62] B. Lewicki, W. Kukulski, J. Mathez, J. Lugez, Rapports concernant les propiétés fondamentales des matériaux et les méthodes d'essai, les méthodes de calcul des murs, Paris, 1952.

[63] J. Kukulski, W. and Lugez, Résistance des murs en béton non-armé soumis a des charges verticales, Cah. Du Cent. Sci. Tech. Du Bâtiment. 79 (1966).

[64] European Committee for Standardization, Eurocode 6: Design of masonry structures. Part 1-1: General rules for buildings. Rules for reinforced and unreinforced masonry., Versión en, AENOR, Madrid, 1997.

[65] J.G. Gross, R.D. Dikkers, J.C. Grogen, Recommended practice for engineered brick masonry, Mc Lenon, 1969.

[66] F. Cassinello, Muros de carga de fábrica de ladrillo, Madrid, n.d.

[67] D. Watstein, M.H. Allen, Structural performance of clay masonry assemblages built with high-bond organic-modified mortars, in: Second Int. Brick Mason. Conf., Structural Clay Products Institute, 1970: pp. 99–112.

[68] A. de Grave, H. Motteu, Testing and calculation of masonry: Recommendations based on research in Belgium, in: SIBMAC Proc., 1970: pp. 266–272.

[69] K. Kirtschig, W. Asntötz, Buckling tests on masonry, in: Proc. 9th Int. Brick/Block Mason. Conf., IBMAC, Berlin, 1991: pp. 202–209.

[70] R.G. Drysdale, A.A. Hamid, Effect of eccentricity on the compressive strength of brickwork, Hournal Br. Ceram. Soc. 30 (1982) 102–108.

[71] S.S. Hasan, A.W. Hendry, Effect of slenderness and eccentricity on the compressive strength of walls, in: 4th Int. Brick Mason. Conf., Brugge, 1976: p. Paper 4.d.3.

[72] C. Murthy, a Hendry, Model experiments in load bearing brickwork, Build. Sci. 1 (1966) 289–298.

[73] C. Sandoval, P. Roca, E. Bernat, L. Gil, Testing and numerical modelling of buckling failure of masonry walls, Constr. Build. Mater. 25 (2011) 4394–4402.

[74] J.R. Rosell Amigó, J. Leiva Navarro, Comportament experimental de la fàbrica de maó: campanya d'assaigs per determinar alguns aspectes de la fàbrica de maó., Barcelona, 1999.

[75] D. García, Experimental and numerical analysis of stone masonry walls strengthened with advanced composite materials, Escuela de Ingenieria de Bilbao, 2009.

[76] J. Harajli, M.H., ELKhatib, H., Tomas San-Jose, Masonry Walls Strengthened Using Fibre Textile-Mortar System: Experimental Evaluation of Out-of-Plane Cyclic Response, in: CSHM-3, Ottawa-Gatineau, Canada, 2010: pp. 19–32.

[77] G. Magenes, Comportamento delle strutture murarie sotto carichi verticali. Corso di dottorato sulle Costruzioni in Muratura., (2009).

[78] P. Haller, Die knickfestigkeit von Mauerwerk aus künstlichen Steinen, Schweizerische Bauzeitung. 67 (1949).

[79] K. Angervo, Úber der Knickung und Tragfähigkeit eines gedrückten Pfeilers ohne Zugfestigkeit, Helsinki, 1954.

[80] Z.P. Bažant, L. Cedolin, Stability of structures: elastic, inelastic, fracture and damage theories, World Scientific, 2010.

[81] J. Singer, On the applicability of the Southwell plot to plastic buckling, Exp. Mech. 29 (1989) 205–208.

[82] F.Y. Yokel, Stability and load capacity of members with no tensile strength, J. Struct. Div. 97 (1971) 1913–1926.

[83] M. Hatzinikolas, J. Longworth, J. Warwaruk, Concrete masonry walls, Edmonton, Alberta, 1978.

[84] H. Knutsson, Vertical load bearing masonry - The danish approach, Mason. Int. 5 (1991) 23–26.

[85] F. Romano, S. Ganduscio, G. Zingone, Cracked nonlinear masonry stability under vertical and lateral loads, J. Struct. Eng. 119 (1993) 69–87.

[86] J.L. Dawe, Y. Liu, Analytical modeling of masonry load-bearing walls, Can. J. Civ. Eng. 30 (2003) 795–806.

[87] M. Lu, A. Schultz, H. Stolarski, Analysis of the Influence of Tensile Strength on the Stability of Eccentrically Compressed Slender Unreinforced Masonry Walls Under Lateral Loads, J. Struct. Eng. 130 (2004) 921.

[88] Masonry Standards Joint Committee, Building Code Requirements for Masonry Structures ACI530-05, American Concrete Institute, Farmington Hills, 2005.

[89] A. Brencich, C. Corradi, L. Gambarotta, G. Mantegazza, E. Sterpi, Compressive strength of solid clay brick masonry under eccentric loading, in: Proc. Br. Mason. Soc., 2002: pp. 37–46.

[90] K. Martini, Finite element studies in the two-way out-of-plane failure of unreinforced masonry, in: Earthquake Engineering Research Institute (Ed.), Proc. 6th Natl. Conf. Earthq. Eng., Seattle, 1998: pp. 1–12.

[91] A. Brencich, L. Gambarotta, Mechanical response of solid clay brickwork under eccentric loading. Part I: Unreinforced masonry, Mater. Struct. 38 (2005) 257–266.

[92] A. Orduña, Seismic assessment of ancient masonry structures by rigid blocks limit analysis, PhD Thesis 2003. University of Minho, Portugal. Available at www. civil. uminho. pt/masonry, 2003.

[93] J. Lopez, S. Oller, E. On, J. Lubliner, A homogeneous constitutive model for masonry, Int. J. Numer. Methods Eng. 46 (1999) 1651–1671.

[94] G. Milani, P.B. Lourenço, A. Tralli, Homogenised limit analysis of masonry walls, Part I: Failure surfaces, Comput. Struct. 84 (2006) 166–180.

[95] G. Milani, P.B. Lourenço, A. Tralli, Homogenised limit analysis of masonry walls, Part II: Structural examples, Comput. Struct. 84 (2006) 181–195.

[96] J. Dallot, K. Sab, O. Godet, Experimental validation of a homogenized plate model for the yield design of masonry walls, Comptes Rendus Mécanique. 336 (2008) 487–492.

[97] B.C.N. Mercatoris, P. Bouillard, T.J. Massart, Multi-scale detection of failure in planar masonry thin shells using computational homogenisation, Eng. Fract. Mech. 76 (2009) 479–499.

[98] P.B. Lourenço, J.G. Rots, J. Blaauwendraad, Continuum model for masonry: Parameter estimation and validation, J. Struct. Eng. 124 (1998) 642–652.

[99] S. Chen, F. Moon, T. Yi, A macroelement for the nonlinear analysis of in-plane unreinforced masonry piers, Eng. Struct. 30 (2008) 2242–2252.

[100] M. Ramalho, A. Taliercio, A. Anzani, L. Binda, E. Papa, A numerical model for the description of the nonlinear behaviour of multi-leaf masonry walls, Adv. Eng. Softw. 39 (2008) 249–257.

[101] A. Mohebkhah, a. a. Tasnimi, H. a. Moghadam, Nonlinear analysis of masonry-infilled steel frames with openings using discrete element method, J. Constr. Steel Res. 64 (2008) 1463–1472.

[102] G. Milani, Kinematic FE limit analysis homogenization model for masonry walls reinforced with continuous FRP grids, Int. J. Solids Struct. 48 (2011) 326–345.

[103] A. Cecchi, G. Milani, A. Tralli, In-plane loaded CFRP reinforced masonry walls: mechanical characteristics by homogenisation procedures, Compos. Sci. Technol. 64 (2004) 2097–2112.

[104] M.R. Valluzzi, Mechanical behaviour of historic masonry structures strengthened by bed joints structural repointing, Constr. Build. Mater. 19 (2005) 63–73.

[105] R.B. Petersen, In-plane Shear Behaviour of Unreinforced Masonry Panels Strengthened with Fibre Reinforced Polymer Strips, University of Newcastle Australia, 2009.

[106] F. a. Zuccarello, G. Milani, R.S. Olivito, A. Tralli, A numerical and experimental analysis of unbonded brickwork panels laterally loaded, Constr. Build. Mater. 23 (2009) 2093–2106.

[107] G. Drosopoulos, G. Stavroulakis, C. Massalas, FRP reinforcement of stone arch bridges: Unilateral contact models and limit analysis, Compos. Part B Eng. 38 (2007) 144–151.

[108] Y. Zheng, S. Taylor, D. Robinson, Nonlinear finite element analysis of masonry arch bridges reinforced with FRP, in: 6th Int. Conf. Arch Bridg., Fuzhou, China, 2010: pp. 838–845.

[109] S.S. Mahini, a. Eslami, H.R. Ronagh, Lateral performance and load carrying capacity of an unreinforced, CFRP-retrofitted historical masonry vault – A case study, Constr. Build. Mater. 28 (2012) 146–156.

[110] F. Schladitz, M. Frenzel, D. Ehlig, M. Curbach, Bending load capacity of reinforced concrete slabs strengthened with textile reinforced concrete, Eng. Struct. 40 (2012) 317–326.

[111] A. Si Larbi, A. Agbossou, P. Hamelin, Experimental and numerical investigations about textile-reinforced concrete and hybrid solutions for repairing and/or strengthening reinforced concrete beams, Compos. Struct. 99 (2013) 152–162.

[112] H.M. Elsanadedy, T.H. Almusallam, S.H. Alsayed, Y. a. Al-Salloum, Flexural strengthening of RC beams using textile reinforced mortar – Experimental and numerical study, Compos. Struct. 97 (2013) 40–55.

[113] Committee AEN/CTN 83, UNE-EN 1015-11:2000/A1:2007. Métodos de ensayo de los morteros para albañilería. Parte 11: Determinación de la resistencia a flexión y a compresión del mortero endurecido., (2007).

[114] Ministerio de Fomento. Comisión Permanente del Hormigón, EHE-08. Instrucción de Hormigón Estructural, (2008).

[115] J. Charry, Estudio experimental del comportamiento de paredes de obra de fábrica de ladrillo ante la acción de cargas laerales, Universitat Politècnica de Catalunya, 2010.

[116] Committee AEN/CTN 41, UNE-EN 772-1:2002. Métodos de ensayo de piezas para fábrica de albañilería. Parte 1: Determinación de la resistencia a compresión., (2002).

[117] Committee AEN/CTN 41, UNE-EN 772-11:2001/A1:2006. Métodos de ensayo de piezas para fábrica de albañilería. Parte 11: Determinación de la absorción de agua por capilaridad de piezas para fábrica de albañilería, en hormigón, piedra natural y artificial, y de la tas, (2006).

[118] A. Brencich, C. Corradi, L. Gambarotta, Eccentrically loaded brickwork: Theoretical and experimental results, Eng. Struct. 30 (2008) 3629–3643.

[119] A. Brencich, G. De Felice, Brickwork under eccentric compression: Experimental results and macroscopic models, Constr. Build. Mater. 23 (2009) 1935–1946.

[120] V.Z. Bosiljkov, Y.Z. Totoev, J.M. Nichols, Shear modulus and stiffness of brickwork masonry: An experimental perspective, Struct. Eng. Mech. 20 (2005) 21–44.

[121] G. Alfano, M.A. Crisfield, Finite Element Interface Models for the Delamination Anaylsis of Laminated Composites: Mechanical and Computational Issues, Int. J. Numer. Methods Eng. 50 (2001) 1701–1736.

[122] J. Monty, Mechanincs course material. Lecture notes. Chapter 6, (n.d.) 32–49.

[123] ASTM, C 1072 Standard Test Method for Measurement of Masonry Flexural Bond Strength, Methods. (2001) 1–13.

[124] Committee AEN/CTN 41, Métodos de ensayo para fábricas de albañilería. Parte 2: Determinación de la resistencia a la flexión. EN 1052-2:1999, (1999).